



UNIVERSITÀ DEGLI STUDI DI MILANO

FACOLTÀ DI SCIENZE AGRARIE E ALIMENTARI

Department of Food, Environmental and Nutritional Sciences (DeFENS)

**Graduate School in Molecular Sciences and Plant, Food and
Environmental Biotechnology**

PhD programme in Food Science, Technology and Biotechnology

XXV Cycle

Development of Nano-material for Food Packaging

Scientific field AGR/15

FEI LI

Tutor: Prof. Luciano Piergiovanni

Co-tutor: Prof. Saverio Mannino

PhD Coordinator: Prof. Maria Grazia Fortina

2011/2012

CONTENTS

ABSTRACT	IV
RIASSUNTO	VI
ACKNOWLEDGEMENTS	VIII
0 PREFACE	1
1 STATE OF THE ART	2
1.1 Nano-cellulose	2
1.1.1 Nano-cellulose structure	3
1.1.2 Nano-cellulose classifications	4
1.1.3 Nano-cellulose preparations	4
1.1.4 Morphology of CNs	5
1.2 CNs applications	8
1.2.1 Barrier properties	8
1.2.2 Mechanical properties	10
1.2.3 Thermal properties	13
1.3 References	19
2 AIM OF STUDY	27
3 RESULTS AND DISCUSSION	28
3.1 Topic/theme 1: The process, structure, morphology of different-form cellulose nanocrystals (CNs)	28
3.2 Materials and methods 1	30
3.2.1 CNs extraction process	30
3.2.2 Freeze-dried powder	30
3.2.3 CNs gel	30
3.2.4 Fourier transform infrared spectroscopy (FTIR)	31
3.2.5 Solid-state nuclear magnetic resonance (NMR) spectroscopy	31
3.2.6 XPS (X-ray photoelectron spectroscopy)	31
3.2.7 Transmission electronic microscopy (TEM)	31
3.2.8 Scanning electronic microscopy (SEM)	31
3.2.9 Atomic force microscopy (AFM)	32
3.2.10 Size distribution	32
3.3 Results and discussion 1	33
3.3.1 Modified process and different forms of CNs	33
3.3.2 Structure of CNs	34
3.4 Conclusions 1	46

3.5 References.....	47
3.6 Topic/theme 2: Multi-functional green coating of cellulose nanocrystals (CNs) on conventional films for food packaging applications.....	51
3.7 Materials and methods 2	53
3.7.1 Materials.	53
3.7.2 CNs producing process.	53
3.7.3 Preparation of Coating Dispersion.	53
3.7.4 Coated Film Preparation.	54
3.7.5 Thickness measurement	54
3.7.6 Transmission Electron Microscopy.....	55
3.7.7 Atomic force microscopy	55
3.7.8 Transparency measurements	55
3.7.9 Haze	55
3.7.10 Oxygen Transmission Rate (OTR), oxygen permeability (P_{O_2}) and Water Vapor Transmission Rate (WVTR) measurements.....	55
3.7.11 Contact angle measurements	56
3.7.12 Coefficient of friction.....	57
3.8 Results and discussion 2	58
3.8.1 Morphology of CNs and CNs on different substrates	58
3.8.2 Coefficient of friction of bare and coated substrates.....	59
3.8.3 Optical properties.....	61
3.8.4 Anti-fog property	61
3.8.5 Barrier properties.	65
3.9 Conclusions 2.....	67
3.10 References.....	68
3.11 Topic/theme 3 Tunable Green Oxygen Barrier through Layer by Layer Self-assembly of Chitosan (CS) and Cellulose Nanocrystals (CNs)	71
3.12 Materials and methods 3	73
3.12.1 Materials	73
3.12.2 Preparation of biopolymer dispersions for layer-by-layer coating.....	73
3.12.3 Surface charge density measurements.....	73
3.12.4 Layer-by-Layer assembly	74
3.12.5 Transparency measurements	74
3.12.6 Fourier transform infrared spectroscopy (FTIR).....	74
3.12.7 XPS (X-ray photoelectron spectroscopy).....	74
3.12.8 Atomic Force Microscopy.....	75
3.12.9 Ellipsometry.....	75

3.12.10 Field-Emission Scanning Electron Microscopy	76
3.12.11 Oxygen barrier properties	76
3.13 Results and discussion 3	77
3.13.1 Layer-by-layer assembly	77
3.13.2 Structure of CS/CNs nanocomposite	79
3.13.3 Thickness of CS/CNs nanocomposite coating	83
3.13.4 Oxygen permeability of CS/CNs nanocomposite coating	86
3.14 Conclusions 3.....	90
3.15 References.....	91
APPENDIX 1.....	94
Gas and water vapor permeability coefficient summary.....	94
Chitosan XPS plots comparison between the 30 and 60 min	95
APPENDIX 2.....	97
Publications	97
Posters.....	99

ABSTRACT

Being cellulose the most abundant natural polymer in biosphere, more and more attention has been paid on its new functionalities, sustainability, and renewability. Meanwhile, food packaging materials is one of the largest products we are using in daily life, but most of conventional materials are still oil-based due to their low cost and good performances. Therefore, in order to improve the sustainability and renewability of food packaging materials, this PhD dissertation focuses on development new nano-material (cellulose nanocrystals, CNs) for food packaging and includes mainly four sections.

In the first section of this PhD dissertation, we reviewed the progress in knowledge on nano-cellulose first and then, specifically, on CNs. In this section the structure and classifications of various nano-cellulose preparations are included, as well as the preparation, the morphologies, and applications of CNs. In CNs applications, we reviewed that it exhibits excellent barrier, mechanical, and thermal properties itself or combined with other polymers. Particularly, the barrier properties refer to oxygen, water vapor, and migration barrier; mechanical properties are related with tensile strength, Young's modulus, and strain percentage; the thermal properties include glass transition and melting or decomposition temperature, heat flow, and thermal mechanical parameters.

In the second section of this PhD dissertation, to better understand the structure and status of CNs itself or in other polymers, we have used different powerful analytical tools for qualification and quantification. Firstly, we have obtained the relatively precise dimensions of CNs and observe its redispersability in different solvents, mainly water solutions. In the following, we could gain the information of the CNs status in other polymers in order to interpret the final performance efficiently. Finally, we preliminarily concluded that TEM, SEM, and AFM are suitable tools for observing individual crystals, estimating the roughness, and learning the morphology in different scale, respectively. As for the size distribution, functional groups, and interactions between the atoms of CNs, the particle size distributor, FTIR, XPS, and NMR are used for determinations, respectively.

In the third section of this PhD dissertation, we have systematically investigated the properties of conventional films coated with CNs. In particular, we have analyzed their optical properties (transparency and haze), mechanical properties (static and dynamic coefficient of friction), anti-fog (contact angle and surface energy) and barrier properties (oxygen and water vapor transmission rates). In doing this, we have demonstrated that CNs coatings mainly lead to a

reduction of friction, a premium feature for industrial applications, and that their influence on the optical properties of the packaging is not significant. Excellent anti-fog property guarantees customers more conveniently to evaluate the product inside the packages easily. At last but not the least, CNs coatings dramatically improve not only the oxygen barrier properties of conventional flexible food packaging, but also lead to a certain reduction in the water vapor transmission rate. The perspective use of CNs as multi-functional coatings favors a reduction of the required thickness for plastic films, towards a more environmentally-friendly and sustainable approach to packaging.

In the last section of this PhD dissertation, we demonstrated the use of chitosan (CS)/CNs nanocomposites realized by layer-by-layer (LbL) self-assembly as oxygen barrier under different pH combinations. The oxygen permeability coefficient of CS/CNs nanocomposites is as low as $0.02 \text{ cm}^3 \mu\text{m m}^{-2} 24\text{h}^{-1} \text{ kPa}^{-1}$, close to EVOH co-polymers, under dry conditions. Meanwhile, we consider that CNs has no potential risks for human beings and the renewable origin of the carbohydrate polymers as significant added values that justify a deeper investigation. Finally, it deserves to be underlined also the chance of finely tuning the oxygen permeability by means of the pH values and the sharp control of the thickness associated with this process. Therefore, based on the advantages outlined above, the LbL CS/CNs nanocomposite represents a promising oxygen barrier component in transparent flexible packaging materials and semi rigid tridimensional objects (bottles, trays, boxes and etc.).

Based on our researches, we conclude that CNs leads to very promising applications in food packaging field and deserves to be further investigated in the future.

RIASSUNTO

La cellulosa è il polimero naturale più abbondante sulla terra, una risorsa rinnovabile che ogni anno viene prodotta in miliardi di tonnellate da molti organismi vegetali. Per questa ragione, su di essa si sta concentrando una crescente attenzione nell'ipotesi di una sua sempre maggiore applicazione nei più diversi campi. Quello del food packaging, che è ancora fortemente dipendente da materiali di sintesi e provenienti da risorse non rinnovabili, è particolarmente interessato ad un suo più ampio impiego, anche con il fine di aumentare la sostenibilità dei suoi prodotti e di ridurre l'impatto ambientale. Con questa tesi di dottorato si è inteso mettere a fuoco le potenzialità di impiego della nano cellulosa (cellulose nanocrystals, CNs), sperimentare la produzione e valutare le proprietà di alcune lacche a base di CNs, destinate a ricoprire convenzionali materiali flessibili per il confezionamento alimentare. La tesi si compone di quattro parti distinte.

Nella prima parte si è inteso rappresentare lo stato dell'arte delle conoscenze e delle applicazioni della nanocellulosa, attraverso un ampio lavoro di documentazione bibliografica. Dapprima si è voluto mettere a fuoco quanto noto sulla struttura e la classificazione delle varie forme di nanocellulosa che è oggi possibile produrre e, a proposito della cellulosa nanocristallina in particolare, si è fatto il punto sulle tecniche di preparazione, la morfologia e le principali applicazioni. Da questo lavoro di documentazione sono emerse le notevoli proprietà di barriera ai gas ed a potenziali migranti, le eccellenti proprietà meccaniche (resistenza alla rottura, massima elongazione tensile, modulo di Young) e le interessanti caratteristiche termiche (transizione vetrosa, punto di fusione e di decomposizione) della CNs da sola ed in combinazione con altri materiali.

Nella seconda sezione della tesi, al fine di comprendere meglio la struttura e la morfologia dei nanocristalli di cellulosa ottenuti attraverso un processo di idrolisi acida di linter di cotone, sono state utilizzate diverse tecniche analitiche avanzate, sia per la caratterizzazione qualitativa che quantitativa. È stato così possibile ottenere informazioni precise sulle dimensioni dei nano cristalli, il rapporto di forma, la solubilità e numerose altre loro importanti proprietà. In particolare le tecniche di TEM, SEM, e AFM sono apparse come le più adatte per osservare la morfologia dei cristalli, studiare le caratteristiche e la rugosità delle superfici trattate con lacche a base di CNs. Si è inoltre indagato sulla distribuzione delle dimensioni dei cristalli ottenuti e, grazie all'uso di FTIR, XPS e NMR, sulla natura dei gruppi funzionali disponibili e sulle loro interazioni.

La terza parte della tesi è dedicata ad uno studio delle proprietà di alcuni differenti film, largamente impiegati per il food packaging (PET, OPP, OPA e cellophane), rivestiti con uno strato sottile di CNs. In particolare, è stato messo a punto il processo di laccatura e sono state misurate le proprietà ottiche (la trasparenza, l'opacità e le proprietà anti-fog), il coefficiente di frizione statico e dinamico, le energie superficiali e gli angoli di contatto, le proprietà di barriera all'ossigeno ed al vapor d'acqua. Da questo lavoro è emerso come sia effettivamente possibile rivestire di uno strato sottile (intorno ad un micron di spessore), omogeneo e continuo, film plastici differenti e che attraverso questo processo di laccatura, si riduce significativamente il coefficiente di frizione, si incrementano le proprietà anti-fog, si aumenta decisamente la barriera all'ossigeno, senza pregiudicare la trasparenza dei film di supporto. La prospettiva molto concreta è quella di costituire, in un modestissimo spessore, un coating multifunzionale con spiccate caratteristiche di sostenibilità e di sicurezza alimentare.

L'ultima sezione della tesi è dedicata al lavoro fatto per sperimentare la possibile applicazione di una tecnica di rivestimento molto moderna (*layer-by-layer coating*, LbL) che sfrutta la formazione di legami elettrostatici tra biopolimeri caricati diversamente. In particolare si è dimostrata la possibilità di costituire lacche di un composito ottenuto mediante la sovrapposizione alternata di sottilissimi strati (da 6 a circa 30 nm) di chitosano e cellulosa nanocristallina. Il diverso pH delle soluzioni in cui vengono dispersi i due biopolimeri determina un diverso grado di ionizzazione delle cariche, rispettivamente positive del chitosano e negative della cellulosa, e di conseguenza diversi spessori e proporzioni relative dei due biopolimeri nel coating composito che si realizza. Ciò, evidentemente, permette di modulare in un ampio intervallo di valori, la permeabilità del film ricoperto. Il coefficiente di permeabilità del composito giunge a valori pari $0.02 \text{ cm}^3 \mu\text{m m}^{-2} 24\text{h}^{-1} \text{ kPa}^{-1}$, molto simili a quelli espressi da copolimeri a base di EVOH, in condizioni anidre. I vantaggi di un simile rivestimento sono comunque fondamentalmente legati alla sicurezza e non tossicità dei biopolimeri impiegati, dalla loro sostenibilità e dall'ampio grado di libertà disponibile nel modulare le caratteristiche finali di barriera, secondo le esigenze del prodotto da confezionare. Lo strato di lacca LbL così costituita rappresenta, in definitiva, una barriera all'ossigeno particolarmente promettente negli impieghi reali più critici anche per la concreta possibilità di realizzarla convenientemente su oggetti tridimensionali come bottiglie, vassoi e altri imballaggi finiti.

In conclusione, le ricerche condotte rappresentano una base di partenza molto promettente per un'innovazione di sostenibilità e di prestazioni nel campo dell'imballaggio flessibile e meritano ulteriori approfondimenti ed applicazioni.

ACKNOWLEDGEMENTS

Firstly, I would like to thank my supervisor, **Prof. Luciano PIERGIOVANNI**, for helping and guiding me on every aspect, including daily life and academic research. Without him, I could not have done my research smoothly and obtained my PhD degree. Also, I would like to thank **Dr. Paolo BIAGIONI** for helping me on academic research and scientific publications.

Secondly, I would like to thank my co-supervisor, Prof. Saverio MANNINO, and Prof. Matteo SCAMPICCHIO, who guided and taught me electrospinning and electrochemical applications which lead to my first publication during first-year of my PhD, Prof. Enzo RAGG who has been helping determining and interpreting CNs structures by NMR, Dr. Silvia TAVAZZI who manipulated and interpreted ellipsometry data, Prof. Franco FAORO who helped in TEM observations, and Dr. Giorgio Capretti who helped in the surface charge density measurements.

Thirdly, I would like to thank my girlfriend (Dandan LV), parents (Mr. Nan LI and Ms Mengtao HAO) and relatives for mentally supporting me.

Fourthly, I would thank Dr. Sara LIMBO who is always helping me to solve practical problems during the experiments, PhD coordinator, Prof Maria Grazia FORTINA who was informing us related academic activities, and Dr. Chiara FERRARIO who translated everything especially for foreign students. Also, thank my colleagues in PACKLAB or those from other labs who helped me.

Finally, I would like to thank Dr. Carmen ROVEDA, Cesare PONTIERI and Dario DAINELLI, from Sealed Air (Passirana di Rho, Italy), who carried out most of oxygen permeability measurements, Dr. Gero BONGIORNO, from Fondazione Filarete (Milano, Italy), who helped in SEM observations, Dr. Graziano BIAGIONI, from ILPA (Bazzano, Italy), who provided A-PET sheets, and Alessandro BORGHESI for his help during the ellipsometry measurements, Dr. Maccagnan ANDREA and Roberto GALBASINI, from Goglio (Daverio, Italy), who carried out the permeability tests.

0 PREFACE

The requirement of sustainability and safety of products and processes are increasing due to the progressive reduction in un-renewable resources and to the environment deterioration. A sustainable green economy needs a revolutionary change to overcome today's dependency on fossil fuels and bring about a shift towards products based on natural resources. Within the energy supply sector, the change will be solar and wind power; within the materials sector, it is renewable materials, bio-based plastics and composites.

Food packaging, as one of the largest markets all over the world, accounts for about 500 billion euro and uses approximately 250 million tons of different materials each year. Packaging, however, is not only about holding foods but also to prolong shelf-life and extend quality maintenance of foods in order to distribute them in long term, and where they are most needed. Therefore, a special attention to packaging materials performance has to be paid together with the evaluation of their sustainability. Conventional food packaging materials have limited sustainability but exhibit many advantages so as to be very difficult to substitute them by new materials in short term.

Cellulose has been used for thousands of years in many different fields and is an annual renewable resource; thus, its safety and sustainability are beyond debate. However, the present utilization of cellulose limits on conventional way. After many years' development, cellulose nanocrystals (CNs) come into our views and recently have been paid more and more attention.

Based on above situations, we did some investigations on basic structure, morphology, and different properties of CNs in order to better understand it and attempt to develop new applications of CNs on high performing food packaging materials.

1 STATE OF THE ART

1.1 Nano-cellulose

Cellulose is the most abundant natural material biopolymer in the biosphere. Its production is estimated to be over seventy-five billion tons annually (Habibi et al., 2010), we therefore could consider cellulose as the most abundant sustainable and renewable material biopolymer. Paper, furniture, floor etc. all origin from cellulose, which indicates that human beings have been realizing and using cellulose almost everywhere in our daily life for thousands of years. However, since the computers emerged, the use for one of the largest cellulose-based products, paper, has been reducing all the time. Facing huge quantity of cellulose, we therefore have to rethink about how to utilize it more efficiently and develop more functions from it. Based on above situation, nano-cellulose therefore is paid more attention once again recently.

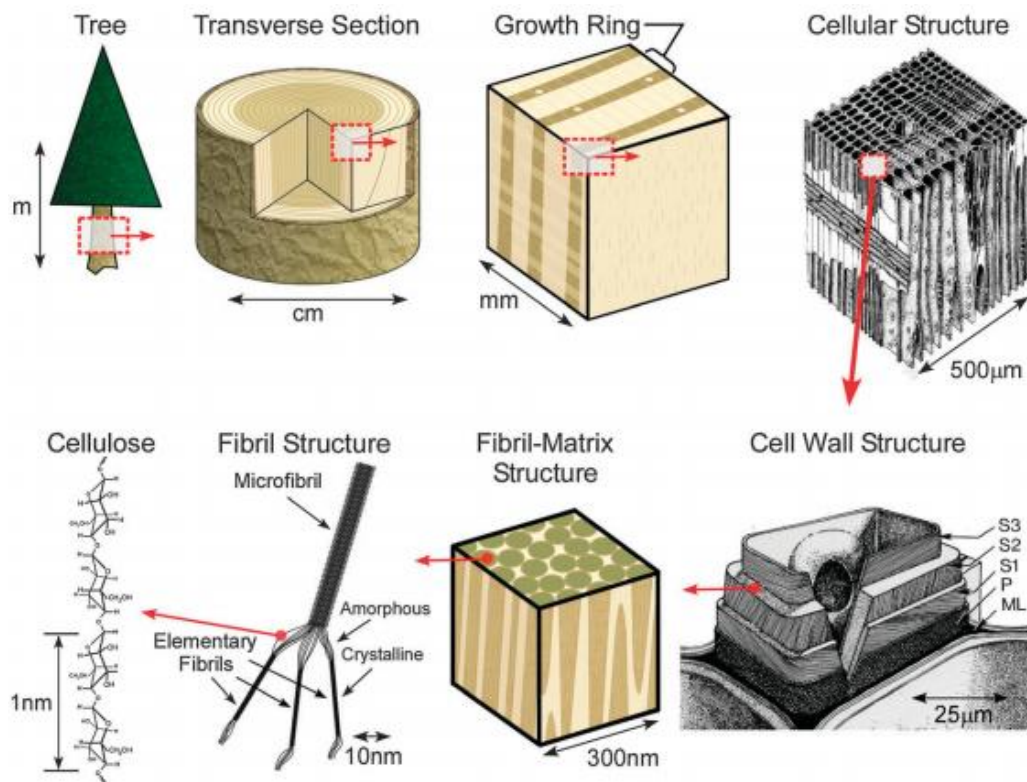


Figure 1 Schematic of the tree hierarchical structure (Postek et al., 2011).

In our daily life, the use of cellulose only could be classified into the first generation, which took advantages of hierarchical structure design. Natural materials develop functionality,

flexibility and high mechanical strength/weight performance by exploiting hierarchical structure design that spans nanoscale to macroscopic dimensions (Figure 1). However, the first generation cellulose products are insufficient to meet the demands of modern society for high performance materials, which is another reason for compelling scientists to further investigate the fundamental reinforcement unit, cellulose nanoparticles, in our case, cellulose nanocrystals (CNs).

1.1.1 Nano-cellulose structure

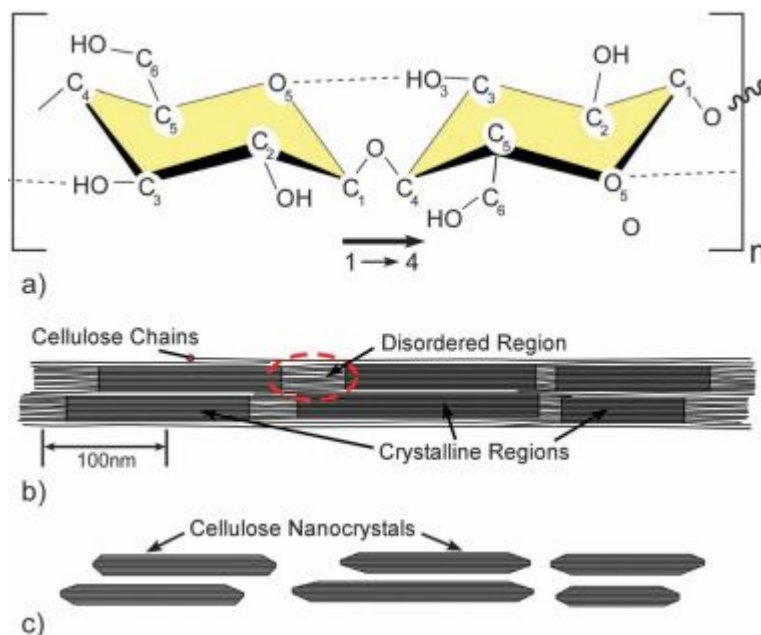


Figure 2 Schematics of (a) single cellulose chain repeat unit, showing the directionality of the 1→4 linkage and intrachain hydrogen bonds (dotted line), (b) idealized cellulose microfibril showing one of the suggested configurations of the crystalline and amorphous regions, and (c) cellulose nanocrystals after acid hydrolysis dissolved the disordered regions (Moon et al., 2011).

Cellulose is a linear chain of ringed glucose molecules and has a flat ribbon-like conformation. The repeat unit (Figure 2a) is comprised of two anhydroglucose rings ($(C_6H_{10}O_5)_n$); $n = 10000$ to 15000, where n is depended on the cellulose source material) linked together through an oxygen covalently bonded to C1 of one glucose ring and C4 of the adjoining ring (1→4 linkage) and so called the 1–4 glucosidic bond (Azizi Samir et al., 2005; Moon et al., 2011). The intra- and inter-chain hydrogen bonds network between hydroxyl groups and oxygen of the adjoining ring molecules stabilizes the linkage, and makes cellulose having linear chain thereby be a

relatively stable polymer, and gives the cellulose fibrils high axial stiffness. These cellulose fibrils are the main reinforcement phase for trees, plants, some marine creatures (tunicates), algae, and bacteria. Within these cellulose fibrils there are highly ordered (crystalline) regions and disordered (amorphous-like) regions, but the structure and distribution of these crystalline and amorphous domains within cellulose fibrils have yet to be rectified (Figure 2b) (Moon et al., 2011; Nishiyama, 2009). However, it is these crystalline regions contained within the cellulose microfibrils that are extracted, resulting in cellulose nanocrystals (CNs) (Figure 2c).

1.1.2 Nano-cellulose classifications

The term nano-cellulose generally includes cellulose nanocrystals, nanowhisker, or nanocrystalline (CNs, CNW, or CNC), micro- or nano-fibrillated cellulose (MFC or NFC), TEMPO-oxidized cellulose nanofibre (TOCN), and bacterial cellulose (BC). Herein, although we classify nano-cellulose into four groups by preparation methods, there yet should be some overlapped parts among them. In the literature CNs are also referred as CNW or CNC, when they are stiff and rod like or as MFC, NFC, or cellulose microcrystals, or microcrystallites when they are longer and more flexible consisting of alternating crystalline and amorphous domains. The latter are usually prepared by combining mild hydrolysis (acidic or enzymatic) and mechanical defibrillation treatments (ultra-blender, grinder, homogenizer and so on). In the PhD dissertation, we focus on the CNs and its characterizations, morphology, and applications.

1.1.3 Nano-cellulose preparations

Chemical and physical treatments are two ways for preparing nano-cellulose. A huge number of scientific articles appeared during recent years, describing possible procedures to obtain cellulose at nanoscale. Few of them led to industrial applications but all are good descriptions of main principles behind nano cellulose obtainment. In this PhD project we used the method most useful and suitable for our lab's facilities but literature is easily available for accurate reports about the different ways of preparing nano cellulose; in this paragraph, these different methods are just shortly mentioned with references to the main papers published as follows: chemical ways: acidic (Habibi et al., 2010; Moon et al., 2011) and enzymatic hydrolysis (Ahola et al., 2008; Filson et al., 2009; Meyabadi & Dadashian, 2012; Paakko et al., 2007; Siro & Plackett, 2010) and TEMPO-oxidized processes (Fujisawa et al., 2011; Fukuzumi et al., 2009; Isogai et al., 2011; Okita et al., 2011; Saito et al., 2007; Saito et al., 2006; Saito et al., 2005; Shinoda et al., 2012); physical ways: refining and high-pressure homogenization (López-Rubio et al., 2007; Nakagaito et al., 2005; Paakko et al., 2007; Stenstad et al., 2008; Zimmermann et al., 2004), cryocrushing (Alemdar & Sain, 2008; Chakraborty et al., 2007; Wang & Sain, 2007a, b) and grinding (Iwamoto et al., 2007; Iwamoto et al., 2005).

In the PhD dissertation, we are specifically studying on CNs. The main process of CNs preparation from cellulose fibers is acidic hydrolysis. During the hydrolysis, the disordered (amorphous) or para-crystalline regions of cellulose are preferentially hydrolyzed, but the crystalline parts remain intact due to its higher resistance to acid attack (Anglès & Dufresne, 2001).

The sulfuric and hydrochloric acids have been extensively utilized as well as the phosphoric and hydrobromic acids (Habibi et al., 2010; Johansson et al., 2012). Moreover, different acids, H_2SO_4 and HCl for hydrolysis lead to distinct properties of CNs: Colloidal dispersion of the HCl-treated sample was obtained by more thorough removal of acid from the hydrolysate than in the case of H_2SO_4 treatment (Araki et al., 1998). In other words, the dispersed ability of HCl-treated sample is limited and their aqueous suspensions tend to flocculate, whereas during hydrolysis of H_2SO_4 the cellulose grafts several charged sulfate ester group on the surface, which results in improving the dispersion of CNs in aqueous solutions and polar solvents, and hence induces crucial characters. It was reported that the optimized processes of extracting CNs from plant resource, for instance cotton, were grinding and 64% (w/w) sulfuric acid, following with neutralization by dilution and dialysis, ultrasonic treatment, filtration and removing excess ions from suspension (Dong et al., 1998). To obtain the CNs from different origins, the processes are similar, but the conditions (Elazzouzi-Hafraoui et al., 2007) varied according to different measurements and requirements. Likewise, Bondeson et al prepared the CNs from Microcrystalline cellulose (MCC) by 63.5% (w/w) H_2SO_4 , sequentially obtaining CNs with a length between 200 and 400 nm and a width less than 10 nm in approximately 2 h with a yield of 30% (of initial weight) (Bondeson et al., 2006). The investigation of Håkansson & Ahlgren found that dilute acids (HCl and H_2SO_4) hydrolysis of pulp led to the same leveling-off degree of polymerization (LODP) (Håkansson & Ahlgren, 2005), but a longer time was needed under the milder conditions. Meanwhile, they reported that distinguished intrinsic viscosities of birch prehydrolysed kraft pulp and a mixed hardwood prehydrolysed kraft pulp, after hydrolysis, only had a small difference (10%) in LODP. Beck-Candanedo demonstrated that longer hydrolysis times and increasing acid-to-pulp ratio produced shorter CNs, less polydisperse black spruce CNs and slightly increased the critical concentration for anisotropic phase formation and the biphasic range became narrower (Beck-Candanedo et al., 2005).

1.1.4 Morphology of CNs

The acidic hydrolysis methods (Araki et al., 1998; Beck-Candanedo et al., 2005; Bondeson et al., 2006; de Souza Lima & Borsali, 2002; Dong et al., 1998; Elazzouzi-Hafraoui et al., 2007; Favier et al., 1995; Håkansson & Ahlgren, 2005; Marchessault et al., 1961; Nickerson & Habrle, 1947; Roman & Winter, 2004) were commonly used for extracting the CNs from natural origins,

which brings on producing varieties of CNs and observed by transmission electronic microscopy (TEM). TEM figures of CNs are presented in Figure 3 and show rod-like morphology with dimensions dependent on the source of the native cellulose, including cotton, Valonia algae, bacterial cellulose, tunicates, and wood pulps. The concentrated acid firstly attacks and hydrolyzes the hemi- and amorphous (defects) parts of native cellulose. After the hydrolysis, the high crystallinity regions remain intact (Anglès & Dufresne, 2001), which show rod-like nanocrystals with different morphologies in Figure 3 due to the source of native cellulose, including cotton (Dong et al., 1998), wood pulp (Elazzouzi-Hafraoui et al., 2007), ramie (Habibi et al., 2008), tunicate (Elazzouzi-Hafraoui et al., 2007), Valonia (Imai et al., 1998) and, bacterial cellulose (Grunert & Winter, 2002). Furthermore, different sources lead to various CNs dimension, including heterogeneous cross-sections and lengths, which result in the differences in their aspect ratio (ratio of length to width) (Moon et al., 2011). Diverse aspect ratio exhibits distinct CNs mechanical properties and capabilities of reinforcement (Eichhorn et al., 2010), which is also presented by models in Figure 4.

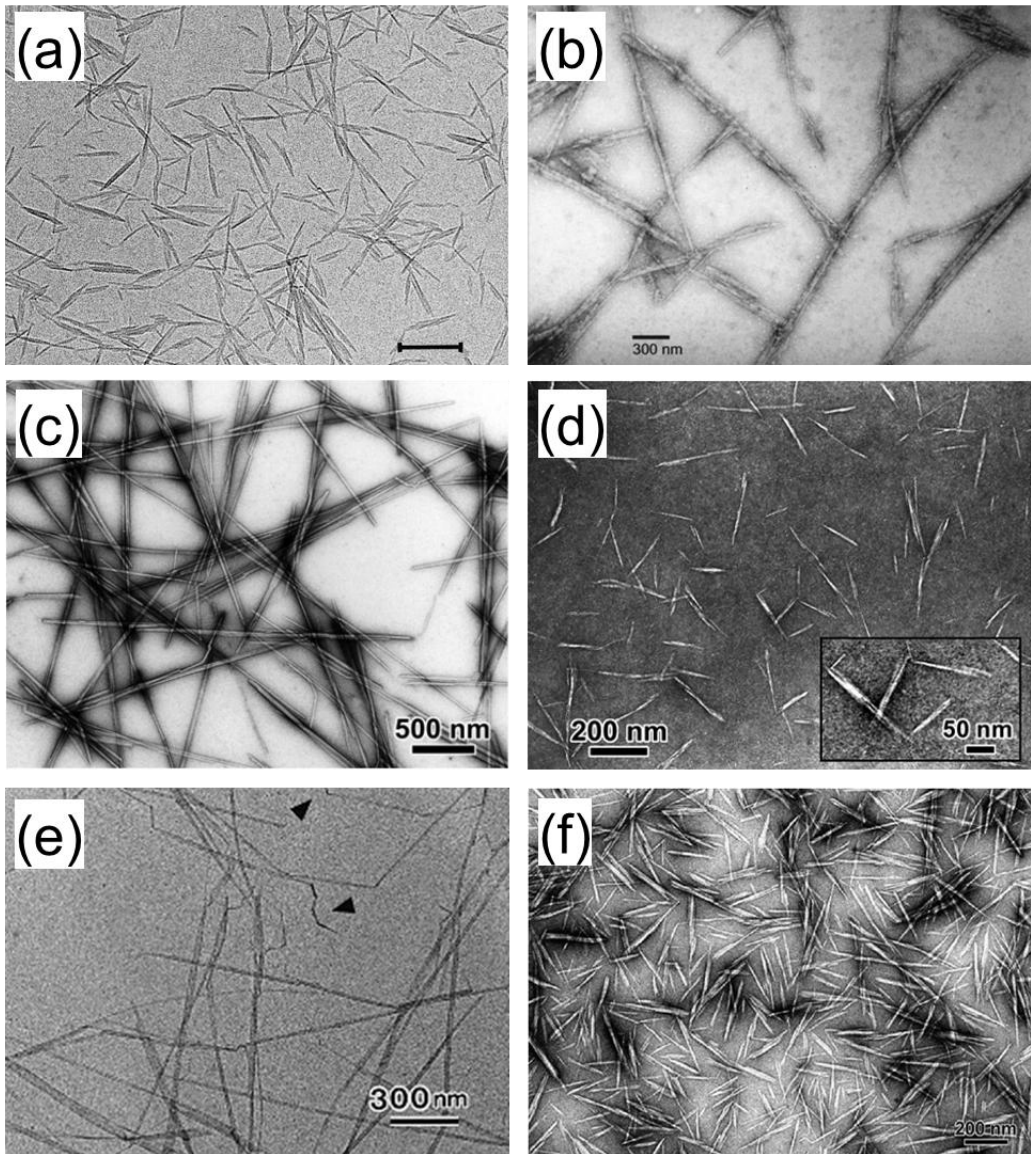


Figure 3 TEM images of dried dispersion of cellulose nanocrystals derived from (a) cotton (Dong et al., 1998), (b) bacterial cellulose (Grunert & Winter, 2002), (c) Tunicate (Elazzouzi-Hafraoui et al., 2007), (d) wood pulp (Elazzouzi-Hafraoui et al., 2007), (e) Valonia (Imai et al., 1998), and (f) ramie (Habibi et al., 2008).

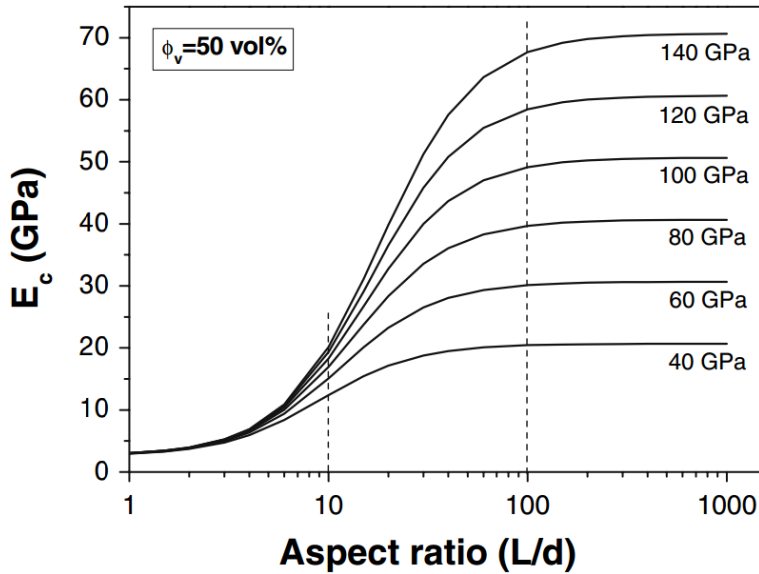


Figure 4 Model plots of the Halpin-Tsai equation for a range of fiber moduli showing the predicted composite modulus (E_c) as a function of the aspect ratio of the fiber reinforcement. The model assumes a unidirectional composite sample, with no fiber-fiber interactions and a polypropylene matrix (Eichhorn et al., 2010).

1.2 CNs applications

1.2.1 Barrier properties

Barrier properties are among the most important aspects in packaging applications. We are always attempting to find new materials which are more sustainable and have premium properties. Nano-cellulose is one of the materials who fulfill all of above requirements and has been paid more and more attention globally. As we known, conventional cellulose-based materials have excellent gas barrier properties due to their intrinsic structures (strong hydrogen bonds) (Habibi et al., 2010). According to above views, nano-cellulose is considered as a highly competitive candidate for barrier applications, whereas MFC/NFC and TEMPO-oxidized cellulose nanofibers (TOCN) have been utilized as a barrier but not the CNs. CNs has short length and narrow diameter, it thus has been supposed that CNs is only suitable for using as a filler into other polymers but not for a barrier as a coating or self-standing film (Isogai et al., 2011). We summarize the limited numbers of publications as follows. Moreover, we provide all collected permeability values from literatures in the Appendix 1 (Gas and water vapor permeability coefficient summary).

(1) Oxygen barrier

Martinez-Sanz et al. introduced the bacterial cellulose nanocrystals (BCNs) into poly (lactic

acid) (PLA) by electrospinning and melt mixing systems and all nanocomposites presented significant increases in the oxygen barrier at 0% RH (34 % reduction). Nevertheless, the oxygen barrier at 80% RH was only improved for BCNs loadings as low as 1 wt % (26 % reduction) (Martinez-Sanz et al., 2012). From another PLA reinforced by CNs report, similar improvement of oxygen barrier was presented reduction of 26 and 48% in oxygen permeability were obtained for the cast film containing 1 and 5% of surfactant modified CNs (Fortunati et al., 2012).

As for CNs coating, only a few reports were related with CNs coating for improving barrier properties. Our group recently demonstrated that CNs combing with chitosan were used as layer-by-layer coating materials to significantly improve oxygen barrier (>94% oxygen permeability reduction) (Li et al., 2013). Also, in the topic 2 of this PhD dissertation, we prepared and investigated CNs coating on different substrates which revealed excellent oxygen barrier (>99% oxygen permeability reduction). These results exhibited the similar barrier capabilities with TOCN coating which is chemically modified.

Oxygen permeability of self-standing CNs films were only reported once by Belbekhouche et al. (Belbekhouche et al., 2011). It was surprising that they demonstrated that MFC film's oxygen permeability displayed 2-order magnitudes lower than CNs film due to CNs being lower aspect ratio and the lower packing of the particles in films characterized by a large extent of porosity and MFC being entangled and high aspect ratio. This explanation however showed opposite views from other group who interpreted that smaller widths and aspect ratio TOCN had denser structures leading to excellent oxygen barrier properties (Fukuzumi et al., 2011). To better understand the relationship between the aspect ratios and oxygen barriers, further investigations are needed in the future.

(2) Water vapor barrier

The researches on water vapor permeability (P_{H_2O}) of CNs or CNs composites were relatively more than oxygen permeability in that cellulose is a hydrophilic material which is one of the most main its drawbacks. Fortunati et al. created PLA/surfactant-CNs nanocomposites by solvent casting and its P_{H_2O} was reduced by 34 and 15% at 1 and 5wt% CNs addition (Fortunati et al., 2012). CNs is evaluated as low risk potential for human beings (Kovacs et al., 2010), George and Siddaramaiah thus attempted to produce edible films by gelatin and BCNs whose WVP was reduced by ~24% at 4% BCNs addition in comparison with neat gelation films (George & Siddaramaiah, 2012). While Sanchez-Garcia et al. also produce nanocomposite combining carrageenan matrix/CNs and the largest reduction (71%) in P_{H_2O} was exhibited at 3 wt% CNs addition (Sanchez-Garcia et al., 2010a). The P_{H_2O} of CNs-reinforced methycellulose was significantly decreased and obtained a further decrease after 50 kGy γ irradiation at films

containing 0.25% CNs. Poly(vinyl alcohol)/CNs' P_{H_2O} was improved by crosslinking with poly(acrylic acid) (PAA). The 10% CNs/10% PAA/80% PVOH composition showed the best performance and P_{H_2O} reduction by 76% (Paralikara et al., 2008).

(3) Migration barrier

Nano-cellulose is becoming more and more popular in recent years and is considered as a safe and sustainable new nano-material, it therefore might have a huge potential to be applied into food related fields. Meanwhile, to migration from food packaging materials has been paid more and more attentions, since varieties of migrating substances has come into being a risk to human health for their toxicity or allergenicity. Based on above concerns, CNs as a functional barrier to limit or avoid mass transfer is emerging and so far there was only very a few related reports. After general overall migration test, Fortunati et al. reported that the migration level of the studied bio-nanocomposites (PLA/CNs) was below the overall migration limits required by the current normative for food packaging materials in both non-polar and polar simulants (Fortunati et al., 2012).

1.2.2 Mechanical properties

(1) Poly lactic acid (PLA) reinforcement

Oksman group firstly reported that 5% CNs dispersion with PLA improved the tensile strength and elongation at break, compared to its unreinforced counterpart (Bondeson & Oksman, 2007a) and that in PLA feeding with dry and wet CNs+PVOH extrusion system, the relative small improvements in tensile modulus (increase by 12%), tensile strength, and elongation to break for the nanocomposites indicated that it was principally the polyvinyl alcohol phase that was reinforced with whiskers but PLA phase (Bondeson & Oksman, 2007b). Regarding the silylated CNs, Pei et al. demonstrated that it was used to reinforce PLLA and the tensile modulus (1.4 GPa) and tensile strength (58.6 MPa) of the nanocomposite films were more than 20% higher than for pure PLLA with only 1 wt% silylated CNs, due to crystallinity effects and fine dispersion (Pei et al., 2010). In order to improve the affinity between the polymers and CNs, Goffin et al. found by dynamic mechanical thermal analysis (DMTA) that PLA-g(grafted)-CNs only induced a limited reinforcing effect below T_g , because of a plasticization effect of the grafted PLA chains on the polymer matrix, whereas above T_g the presence of nanofiller increases the stiffness of the material (Goffin et al., 2011a).

Concerning the electrospun system, Martinez-Sanz et al. reported that the percolation-threshold concentration of electrospun reinforced by BC-CNs is 2-3 wt %. Under this condition, The elastic modulus (2.16 GPa) and tensile strength (61.36 MPa) of nanocomposites increase ca. 17 and 14 %, respectively, as compared to neat PLA, without significantly decreasing the ductility

of the material (Martinez-Sanz et al., 2012).

(2) Polyurethanes (PU) reinforcement

Cao et al. orderly reported that the Young's modulus and tensile strength of nanocomposites (polycaprolactone (PCL)-based water-borne polyurethane (WPU) reinforced by flax/hemp CNs) were 201 and 2.5 times, respectively, when the filler amount was increased from 0 to 30 wt%. The elongation is however reduced at break over the range from 1100 to 200% (Cao et al., 2007; Cao et al., 2011). With regard to the shape memory material (segmented PU, SPU), different concentration CNs additions into SPU after polymerization led to a increase in dynamic storage and tensile modulus and a decrease in deformation at break. Addition of the cellulose nanocrystals during the synthesis increased modulus, reduced deformability and erased the shape memory behavior of the SPU's (Auad et al., 2010). Wik et al. found that castor oil-based polyurethanes reinforced by 1% CNs addition showed a significant increase of tensile modulus (682.9 MPa), compared to the unfilled solid PU (497.5 MPa) due to the incorporation of the rigid particle reinforcement and the interfacial bonding (Wik et al., 2011). It was reported that the segmented thermo-plastic polyurethane elastomers (STPUE) reinforced by 1.5% modified CNs showed a much more pronounced increase in tensile modulus (21 MPa) compared to the neat one 9.2 (MPa) (Rueda et al., 2011). Mendez et al. demonstrated that the nanocomposite with the highest CNs content investigated (20% v/v) showed Young's modulus of 1076 MPa, which represents a stiffness increase of almost 2 orders of magnitude than the one of neat PU, which was ascribed to interfacial interactions (hydrogen bonding) between the polyurethane and CNs (Mendez et al., 2011).

(3) Polyvinyl alcohol (PVOH) reinforcement

For cast films, first George reported that 10% cross-linked PVOH filled with BC-CNs, which resulted in an improved tensile strength from 62.5 MPa to 128 MPa (increase by 105%), by the addition of just 4 wt% of BC-CNs by casting method. Furthermore, the elastic modulus was found to increase from 2 GPa to 3.4 GPa (increase by 70%) (George et al., 2011). Sequentially, Pakzad reported that in PVOH/PAA/CNs (80%:0%:15%) cast film system, the PAA functioned to reduce the agglomerate of CNs and its highest elastic modulus reached to ~7.6 GPa by AFM nano-indentation. This value is, however, different from the elastic modulus (1.4 GPa) result from tensile test due to the high degree of local heterogeneity of CNC distribution (Pakzad et al., 2012).

Regarding electrospun system, Peresin et al., demonstrated that the effect moisture on electrospun nanofiber of PVOH (7%) and CNs was investigated and it was found that the plasticizing and anti-plasticizing effect of water and CNs, respectively. It was interesting that

the CNs-loaded PVA fiber mats showed a reversible recovery in mechanical strength after cycling the relative humidity (Peresin et al., 2010). Afterward, Lee and Deng demonstrated that aligned electrospun webs of PVOH (8%) reinforced by CNs showed 87.4 MPa modulus, which increased by 35% comparing to the isotropic PVOH electrospun webs (Lee & Deng, 2012).

(4) Polycaprolactone (PCL) reinforcement

In modified CNs (PCL-g-CN) and CNs with PCL nanocomposite systems, Habibi et al. reported that the addition of PCL-g-CN into PCL proved to improve considerably the Young's modulus, which increases from 230.7 MPa for unfilled PCL to 582.0 MPa for nanocomposites containing 40% of PCL-grafted CNs. The elongation at break decreases drastically, but the values remain mostly better than compositions filled with unmodified CNs (Habibi et al., 2008). Then, Goffin reported that the Young's modulus of 8wt% PCL-g-CN nanocomposites reached to 1500 MPa, 255% and 132% higher than the ones of neat matrix and 8wt% unmodified CNs nanocomposites (Goffin et al., 2011b).

In the electrospun PCL system, electrospun fiber webs from PCL reinforced with 2.5% unmodified CNs showed ca. 1.5-fold increase in Young's modulus (reach 6.54 MPa) and the ultimate strength (1.51 MPa) compared to PCL webs (Zoppe et al., 2009).

(5) Others reinforcement

Poly(ethylene oxide)(PEO): in PEO/pentaerythritol triacrylate (PETA) reinforced by CNs system, the maximum tensile stress (14.22 MPa) and Young's modulus (39.8 MPa) of the crosslinked PEO/ 10%CNs composite fibrous mats increased by 377.5 and 190.5% than those of uncrosslinked PEO mats, and 76.5 and 127.4% than those of crosslinked PEO mats, respectively (Zhou et al., 2012). As for the PEO/CNs electrospun system, the electrospun heterogeneous mats are stronger than their homogeneous counterparts for all compositions (Zhou et al., 2011) and the storage moduli of aligned electrospun PEO/CNs nanocomposite fibers (324 MPa) are 1.5-2 times greater than those of the neat PEO counterparts (Changsarn et al., 2011).

Natural rubber (NR): Siqueira et al. reported that, compared with neat natural rubber, Young's modulus and tensile strength of 10% CNs/NR were increased by 257 and 11 times (Siqueira et al., 2010). Afterward, Visakh demonstrated that the tensile strength (17.3 MPa) and storage modulus (3.8 MPa) of NR+CNs nanocomposite at 25 °C was about 88% and 124% in comparison with neat NR (Visakh et al., 2012).

Starch: For plasticized starch (PS) reinforced by hemp/flax CNs system, Cao et al. found

significant increases in the tensile strength and Young's modulus, from 3.9 to 11.9 MPa and from 31.9 to 498.2 MPa, respectively, with increasing FCN content from 0 to 30wt% (Cao et al., 2008b; Cao et al., 2007). Considering the relative humidity (RH) effects, for all RH levels, the modulus increased gradually with filler load, and above ~5% whiskers, a significant improvement is observed. The tensile strength and Young's modulus are high at lower RH levels, and elongation at break remains constant, irrespective of RH and filler content. With sorbitol, the final composite has better thermal mechanical properties than the one with glycerol due to glycerol functioning for transcrystallization which effectively decreases fiber matrix adhesion, but sorbitol which shows that a good fiber-matrix adhesion is present in the system favoring effective stress-transfer at the fiber/matrix interface (Mathew et al., 2008).

Besides above, CNs was also used for reinforcement filler into varieties of polymers which include biopolymers (carboxymethyl cellulose (CMC) (Choi & Simonsen, 2006), chotisan (Sui et al., 2010), methylcellulose (MC) (Khan et al., 2010), cellulose acetate butyrate (Ayuk et al., 2009; Siqueira et al., 2011), alginate (Urena-Benavides et al., 2010; Urena-Benavides & Kitchens, 2011, 2012), aligned cellulose nanofibers (Magalhaes et al., 2011), cellulose acetate (CA) (Herrera et al., 2011), silk (Huang et al., 2011; Park et al., 2012), xylan (Kohnke et al., 2012), poly(3-hydroxybutyrate-co-3-hydroxyvalerate) (PHBV) (Ten et al., 2010; Yu et al., 2012), and gelation (George & Siddaramaiah, 2012)) and synthetic polymers (polysulfone (PSf) (Noorani et al., 2006, 2007), , poly(diallyldimethylammonium chloride) (PDDA) (Sui et al., 2010), Poly(methyl vinyl ether-co-maleic acid)-Polyethylene Glycol (PMVEMA-PEG) (Goetz et al., 2010) polyacrylamide (PAM) (Zhou et al., 2011), polyvinylacetate (PVAc) (Mathew et al., 2011), poly(acrylic acid) (PAA) (Pakzad et al., 2012), stereolithographic resins (Kumar et al., 2012), healable material (Fox et al., 2012), and poly(methyl methacrylate) (PMMA) (Dong et al., 2012)).

1.2.3 Thermal properties

Thermal properties are usually determined by thermogravimetric analysis (TGA), differential scanning calorimetry (DSC), and dynamic mechanical thermal analysis (DMTA), which are able to monitoring changes of gravity (loss weight), calories (heat flow), and mechanical properties as a function of temperature to reflect the thermal properties, e.g. glass transition temperature (T_g), melting or decomposition temperature (T_m or T_d), $\tan \delta$, and so on. Generally speaking, different CNs extraction processes and the addition of CNs into other polymers have influences on the thermal properties of CNs themselves and their nanocomposites, respectively.

Firstly, we focus on different thermal properties of CNs resulting from their extraction processes. Inorganic acids are widely used for extracting CNs from different sources, such as

bio-residues obtained from a bioethanol pilot plant (Oksman et al., 2011), bacterial cellulose (BC) (Martinez-Sanz et al., 2011a), coconut husk (Rosa et al., 2010), microcrystalline cellulose (MCC) (Man et al., 2011; Wang et al., 2007), rice husk (Johar et al., 2012), kenaf bast (Kargarzadeh et al., 2012), and mengkuang leaves (*Pandanus tectorius*) (Sheltami et al., 2012). Above two extraction processes result in grafting a few of sulfate ester groups on the surface of CNs which lead to a lower thermal stability. Matinez-Sanz and Wang reported that neutralization produced a slight increase in the crystallinity index and led to a remarkable increase on the BCNs thermal stability and the degradation (decomposition) temperature (T_d) shift to the higher temperature and occurred within a narrow temperature range for spherical CNs from MCC (Martinez-Sanz et al., 2011a; Wang et al., 2007). Besides neutralization, physical extractions, including ultrasonication and homogenization, could further increase the thermal stability to 265 °C in comparison with the degradable temperature of raw material around 202 °C (Oksman et al., 2011), while the hydrolyzed CNs showed a two-stage degradation, with an initial onset of degradation around 120 °C and a second step around 255 °C which is a typical behavior of sulphuric acid-hydrolyzed CNs. Rose et al. also demonstrated that higher residual lignin content was found to increase thermal stability indicating that the thermal properties of the CNs could be tailored by controlling reaction conditions (Rosa et al., 2010). Georage et al. revealed that the thermal stability of enzyme processed BC nanocrystals (BCNs) was almost two fold higher than sulfuric acid processed ones. The activation energy required for decomposition of enzyme processed BCNs was much higher than the other (George et al., 2011).

Secondly, the thermal properties of CNs-nanocomposites produced by casting method will be reviewed.

(1) Synthesized polymers:

Poly(methyl methacrylate) (PMMA): Liu et al. reported that the glass transition of the PMMA-CN nanocomposites was shifted to lower temperatures with respect to the pure PMMA. The DMA data showed a marked increase in storage modulus (from 1.5 GPa for pure PMMA to 5 GPa) for the composite sheet containing 10 wt.% CNs at 35 °C due to the high modulus of cellulose crystals (Liu et al., 2010). Xu et al. grafted PMMAZO (Poly(6-[4-(4-methoxyphenylazo) phenoxy] hexyl methacrylate)) on the CNs surface and PMMAZO-grafted CNs showed smectic-to-nematic transition at 95 °C and nematic-to-isotropic transition at 135 °C, and exhibit analogous lyotropic liquid-crystalline phase behavior above 135 °C. It also showed a lyotropic nematic phase in chlorobenzene above a concentration of 5.1 wt% (Xu et al., 2008).

Stereolithographic Resins (SLRs): The storage modulus (E') increased steadily with increasing CNs content in the regimes below and above the glass transition (a remarkable modulus enhancement in the rubbery regime) but less pronounced in the glassy state (Kumar et al., 2012).

Polyurethane (PU): The CNs from *Eucalyptus globulus* favored the hard-segments (HSs)/soft-segments (SSs) microphase separation of the Water-borne PU (WPU), causing shifts of the SS glass transition temperature and the HS melting temperature toward higher temperatures was reported by Gao et al. (Gao et al., 2012). Auad et al. reported that CNs addition increased the PU SS melting and crystallization temperatures and the degree of crystallinity of this phase, while both neat PU and composites exhibited shape memory properties, with fixity and recovery values that depend on heating temperature, imposed deformation, deformation rate and CNs addition (Auad et al., 2012). Pei et al. however demonstrated that the decrease of T_g for the PU-CN nanocomposites was due to the fact that the CNs are strongly associated with the HS of PU, resulting in lower fraction of hydrogen bonded carbonyl groups in the HS and an increase of the degree of freedom for the SS in PU (Pei et al., 2011). The $\tan \delta$ corresponding to the glass transition of PU from DMA decreased with increasing CNs content, while the half height width of the peak increased. This could be attributed to the greatly restricted motion of PU chains resulting from the covalent bonding and cross-linking between PU molecules and nanoscale stiff rod-like CNs (Pei et al., 2011). In order to improve the compatibility of CNs with WPU, Cao et al. induced the grafting of part of the pre-synthesized WPU chains on the surface of CNs and the corresponding nanocomposites were processed by casting. Degradation temperature of nanocomposite (400 °C) was higher than WPU (337 °C), but started to decompose at the same temperature. From DSC, these grafted-WPU chains were able to form a crystalline structure on the surface of CNs, and thus induce the crystallization of the matrix which created a co-continuous phase (Cao et al., 2009).

Polyvinyl alcohol (PVOH): Georag et al. found that the thermal stability of enzyme processed BCNs was almost two fold higher than sulfuric acid processed ones. Incorporation of these BCNs in PVOH matrix resulted in a remarkable improvement in the thermal stability as well as mechanical properties of nanocomposite films, which exhibited higher melting temperature (T_m) and enthalpy of melting (ΔH_m) than those of pure PVOH, suggesting that the addition of BCNs should modify the thermal properties of PVOH (George et al., 2011).

Starch: CNs results in an increase in the glass transition temperature due to the strong interactions between CNs and plasticized starch which reduce the flexibility of starch molecular chains (Cao et al., 2008a).

Poly(styrene-co-butyl acrylate) (PSBA): A significant increase of the stiffness of the acrylic polymer beyond the glass transition temperature was shown. MFC from *Stipa tenacissima* (ST) showed higher reinforcing effect compared to ST-CN_s, probably because of higher aspect ratio and possibility of entanglement of the former (Ben Mabrouk et al., 2012).

(2) Biopolymers:

Carrageenan: Sanchez-Garcia et al. demonstrated that addition of cellulose microfibrils to unplasticized carrageenan resulted in a continuous decrease in the T_d for CN_s loadings of up to 3 wt%. The behavior of adding cellulose microfibrils to the carrageenan containing glycerol was found to be rather similar to that of CN_s (Sanchez-Garcia et al., 2010a).

Cellulose acetate butyrate (CAB): TGA and DMTA results showed a substantial improvement in the thermal stability and an increase in the storage modulus of CAB reinforced with 5 and 10 wt% CN_s for both unplasticized and plasticized cellulose acetate butyrate (CAB)-CN_s nanocomposites (Ayuk et al., 2009). Furthermore, Petersson et al. compared the storage modulus of CN_s-CAB with layered silicates (LS)-CAB and results from DMTA showed improved storage modulus for a wide temperature range for both nanocomposites compared with the pure CAB matrix. The CN_s decreased the $\tan \delta$ peak temperature of the CAB whereas LS did not affect the $\tan \delta$ peak (Petersson et al., 2009).

Methylcellulose (MC): TGA curves clearly show that addition of CN_s in MC-based films contributed to a substantial improvement in the thermal stability up to 200 °C. Melting peaks in DSC curves at 150 °C disappeared, which might be attributed to CN_s fiber covering the surface as well as the interface of the MC-based films and thus stabilized the films and the second DSC cycle indicated that the curves do not reveal either crystalline structures or other transitions due to the thermal degradation/evaporation of some components during the first heating cycle of films (Khan et al., 2010).

Natural rubber (NR): The CN_s (from *Capim Dourado*) reinforcing effect observed above T_g of the matrix was higher than the one observed for other polysaccharide nanocrystals and CN_s extracted from other sources (Siqueira et al., 2010).

Poly(3-hydroxybutyrate-co-3-hydroxyvalerate) (PHBV): Ten et al. considered the CN_s as a nucleation agent in the nanocomposite. The cold crystallization temperature (T_{cc}) progressively decreased with the addition of CN_s, but T_g was not noticeably affected (Ten et al., 2010). DMA results showed an increased $\tan \delta$ peak temperature and broadened transition peak,

indicating restrained PHBV molecular mobility in the vicinity of the CNs surface (Ten et al., 2010). Yu et al. demonstrated that decomposition temperature (T_0), temperature at 5% weight loss (T_5), maximum decomposition temperature (T_{max}) and complete decomposition temperature (T_f) increased by 51.4, 36.5, 47.1, and 52.9 °C, respectively compared to the ones of PHBV (Yu et al., 2012).

Poly lactic acid (PLA): Lin et al. found that the addition of (acetylation) A-CN_s improved the thermal property of the nanocomposites, but a marked drop in the storage modulus (E') of PLA-based nanocomposites at around 65-80 °C was attributed to the glass transition effects of the PLA component (Lin et al., 2011).

Thirdly, electrospinning is becoming one of the most important method to produce new nanocomposites. Different polymers are reinforced by CN_s via electrospinning. The DSC results showed a significant increase in T_g of the electrospun EVOH-CN_s nanocomposite during the second heating run, which may be related to the acidic character of the nanofiller (Martinez-Sanz et al., 2011b). Lalia et al. demonstrated that the electrospun poly(vinylidene fluoride-co-hexafluoropropylene) (PVDF-HP) with 2 wt% CN_s exhibited high values of tensile modulus in the 30-150 °C temperature range by DMA (Lalia et al., 2012). Dong et al. found that T_g of electrospun PMMA with 5wt% CN_s is 123 °C and T_g other percentages are around 125 °C, while their T_m slightly increased (2.7-4.6%) in comparison of neat PMMA (Dong et al., 2012). In the electrospun system of PVA reinforced by CN_s, the addition of CN_s improved the thermal stability of nanocomposite (Ago et al., 2012; Cao et al., 2011).

Above we reviewed the thermal properties of CN_s or CN_s-reinforced nanocomposites by different extraction processes, casting, and electrospinning methods. Finally, the thermal properties of CN_s-reinforced nanocomposites by other producing methods are reviewed as follows. Visakh et al. found that the addition of CN_s had a positive impact on the E' , $\tan \delta$ peak position and thermal stability of the crosslinked natural rubber (NR) by masterbatch, compounding, and curing (Visakh et al., 2012). Bondeson et al. reported that the thermal properties of PLA-CN_s nanocomposite modified by PVA was not improved compared to its unreinforced counter-part through two-feeding compounding extrusion method, probably because the majority of the CN_s were located in the PVA phase and only a negligible amount was located in the PLA phase (Bondeson & Oksman, 2007b). Goffin et al. grafted PLA with CN_s by ring-opening polymerization (PLA-g-CN_s) and produced PLA nanocomposite with PLA-g-CN_s by melting processing. The DSC and DMTA results indicated that PLA-g-CN_s enhances their compatibility with PLA, large modification of the crystalline properties such as the crystallization half-time, and thus improves the final properties of the nanocomposite

(Goffin et al., 2011a). Through solvent-exchange method, the incorporation of CNs did not significantly affect the thermal stability of the phenolic resin but clearly increased the heat of cure, suggesting that additional cure reactions took place in presence of the CNs (Liu & Laborie, 2011). The DSC and TGA results of rigid PU foam reinforced by CNs clearly indicated enhanced thermal stability (increment in T_g and T_d) (Li & Ragauskas, 2012).

Although only barrier, mechanical, and thermal properties have been reviewed, we could yet clearly realize that CNs has been applied into various polymers, mainly biopolymers, and could generally improve their properties significantly only through some simple methods. Moreover, CNs has been evaluated to be highly safe (Ni et al., 2012) and sustainable (Moon et al., 2011). Food packaging is one of the largest markets in the world, based on all CNs present advantages CNs thus will be widely used into this field and lead to more breakthroughs.

1.3 References

- Ago, M. et al., 2012, Lignin-Based Electrospun Nanofibers Reinforced with Cellulose Nanocrystals. *Biomacromolecules* 13: 918-926.
- Ahola, S. et al., 2008, Enzymatic hydrolysis of native cellulose nanofibrils and other cellulose model films: effect of surface structure. *Langmuir* 24: 11592-11599.
- Alemdar, A., Sain, M., 2008, Isolation and characterization of nanofibers from agricultural residues – Wheat straw and soy hulls. *Bioresource Technology* 99: 1664-1671.
- Anglès, M. N., Dufresne, A., 2001, Plasticized Starch/Tunicin Whiskers Nanocomposite Materials. 2. Mechanical Behavior. *Macromolecules* 34: 2921-2931.
- Araki, J. et al., 1998, Flow properties of microcrystalline cellulose suspension prepared by acid treatment of native cellulose. *Colloids and Surfaces A: Physicochemical and Engineering Aspects* 142: 75-82.
- Auad, M. L. et al., 2010, Nanocomposites Made from Cellulose Nanocrystals and Tailored Segmented Polyurethanes. *Journal of Applied Polymer Science* 115: 1215-1225.
- Auad, M. L. et al., 2012, Shape memory segmented polyurethanes: dependence of behavior on nanocellulose addition and testing conditions. *Polymer International* 61: 321-327.
- Ayuk, J. E. et al., 2009, The Effect of Plasticizer and Cellulose Nanowhisker Content on the Dispersion and Properties of Cellulose Acetate Butyrate Nanocomposites. *Journal of Applied Polymer Science* 114: 2723-2730.
- Azizi Samir, M. A. S. et al., 2005, Review of Recent Research into Cellulosic Whiskers, Their Properties and Their Application in Nanocomposite Field. *Biomacromolecules* 6: 612-626.
- Beck-Candanedo, S. et al., 2005, Effect of Reaction Conditions on the Properties and Behavior of Wood Cellulose Nanocrystal Suspensions. *Biomacromolecules* 6: 1048-1054.
- Belbekhouche, S. et al., 2011, Water sorption behavior and gas barrier properties of cellulose whiskers and microfibrils films. *Carbohydrate Polymers* 83: 1740-1748.
- Ben Mabrouk, A. et al., 2012, Cellulosic nanoparticles from alfa fibers (*Stipa tenacissima*): extraction procedures and reinforcement potential in polymer nanocomposites. *Cellulose* 19: 843-853.
- Bondeson, D. et al., 2006, Optimization of the isolation of nanocrystals from microcrystalline cellulose by acid hydrolysis. *Cellulose* 13: 171-180.
- Bondeson, D., Oksman, K., 2007a, Dispersion and characteristics of surfactant modified cellulose whiskers nanocomposites. *Composite Interfaces* 14: 617-630.
- Bondeson, D., Oksman, K., 2007b, Polylactic acid/cellulose whisker nanocomposites modified by polyvinyl alcohol. *Composites Part a-Applied Science and Manufacturing* 38: 2486-2492.
- Cao, X. et al., 2008a, Starch-based nanocomposites reinforced with flax cellulose nanocrystals. *Express Polymer Letters* 2: 502-510.
- Cao, X. D. et al., 2008b, Green composites reinforced with hemp nanocrystals in plasticized

- starch. *Journal of Applied Polymer Science* 109: 3804-3810.
- Cao, X. D. et al., 2007, New nanocomposite materials reinforced with flax cellulose nanocrystals in waterborne polyurethane. *Biomacromolecules* 8: 899-904.
- Cao, X. D. et al., 2009, One-pot polymerization, surface grafting, and processing of waterborne polyurethane-cellulose nanocrystal nanocomposites. *Journal of Materials Chemistry* 19: 7137-7145.
- Cao, X. D. et al., 2011, Cellulose nanocrystals-based nanocomposites: fruits of a novel biomass research and teaching platform. *Current Science* 100: 1172-1176.
- Chakraborty, A. et al., 2007, Dispersion of Wood Microfibers in a Matrix of Thermoplastic Starch and Starch-Polylactic Acid Blend. *Journal of Biobased Materials and Bioenergy* 1: 71-77.
- Changsarn, S. et al., 2011, Biologically Inspired Hierarchical Design of Nanocomposites Based on Poly(ethylene oxide) and Cellulose Nanofibers. *Macromolecular Rapid Communications* 32: 1367-1372.
- Choi, Y. J., Simonsen, J., 2006, Cellulose nanocrystal-filled carboxymethyl cellulose nanocomposites. *Journal of Nanoscience and Nanotechnology* 6: 633-639.
- de Souza Lima, M. M., Borsali, R., 2002, Static and Dynamic Light Scattering from Polyelectrolyte Microcrystal Cellulose. *Langmuir* 18: 992-996.
- Dong, H. et al., 2012, Cellulose nanocrystals as a reinforcing material for electrospun poly(methyl methacrylate) fibers: Formation, properties and nanomechanical characterization. *Carbohydrate Polymers* 87: 2488-2495.
- Dong, X. M. et al., 1998, Effect of microcrystallite preparation conditions on the formation of colloid crystals of cellulose. *Cellulose* 5: 19-32.
- Eichhorn, S. J. et al., 2010, Review: current international research into cellulose nanofibres and nanocomposites. *Journal of Materials Science* 45: 1-33.
- Elazzouzi-Hafraoui, S. et al., 2007, The Shape and Size Distribution of Crystalline Nanoparticles Prepared by Acid Hydrolysis of Native Cellulose. *Biomacromolecules* 9: 57-65.
- Favier, V. et al., 1995, Polymer Nanocomposites Reinforced by Cellulose Whiskers. *Macromolecules* 28: 6365-6367.
- Filson, P. B. et al., 2009, Enzymatic-mediated production of cellulose nanocrystals from recycled pulp. *Green Chemistry* 11: 1808-1814.
- Fortunati, E. et al., 2012, Effects of modified cellulose nanocrystals on the barrier and migration properties of PLA nano-biocomposites. *Carbohydrate Polymers* 90: 948-956.
- Fox, J. et al., 2012, High-Strength, Healable, Supramolecular Polymer Nanocomposites. *Journal of the American Chemical Society* 134: 5362-5368.
- Fujisawa, S. et al., 2011, Preparation and characterization of TEMPO-oxidized cellulose nanofibers with different counter ions. *Abstracts of Papers of the American Chemical Society*

241.

Fukuzumi, H. et al., 2009, Properties of TEMPO-oxidized cellulose nanofiber film. Abstracts of Papers of the American Chemical Society 237.

Fukuzumi, H. et al., 2011, Pore Size Determination of TEMPO-Oxidized Cellulose Nanofibril Films by Positron Annihilation Lifetime Spectroscopy. *Biomacromolecules* 12: 4057-4062.

Gao, Z. Z. et al., 2012, Biocompatible elastomer of waterborne polyurethane based on castor oil and polyethylene glycol with cellulose nanocrystals. *Carbohydrate Polymers* 87: 2068-2075.

George, J. et al., 2011, Bacterial cellulose nanocrystals exhibiting high thermal stability and their polymer nanocomposites. *International Journal of Biological Macromolecules* 48: 50-57.

George, J., Siddaramaiah, 2012, High performance edible nanocomposite films containing bacterial cellulose nanocrystals. *Carbohydrate Polymers* 87: 2031-2037.

Goetz, L. et al., 2010, Poly(methyl vinyl ether-co-maleic acid)-Polyethylene Glycol Nanocomposites Cross-Linked In Situ with Cellulose Nanowhiskers. *Biomacromolecules* 11: 2660-2666.

Goffin, A. L. et al., 2011a, From Interfacial Ring-Opening Polymerization to Melt Processing of Cellulose Nanowhisker-Filled Polylactide-Based Nanocomposites. *Biomacromolecules* 12: 2456-2465.

Goffin, A. L. et al., 2011b, Poly(epsilon-caprolactone) based nanocomposites reinforced by surface-grafted cellulose nanowhiskers via extrusion processing: Morphology, rheology, and thermo-mechanical properties. *Polymer* 52: 1532-1538.

Grunert, M., Winter, W. T., 2002, Nanocomposites of Cellulose Acetate Butyrate Reinforced with Cellulose Nanocrystals. *Journal of Polymers and the Environment* 10: 27-30.

Håkansson, H., Ahlgren, P., 2005, Acid hydrolysis of some industrial pulps: effect of hydrolysis conditions and raw material. *Cellulose* 12: 177-183.

Habibi, Y. et al., 2008, Bionanocomposites based on poly(epsilon-caprolactone)-grafted cellulose nanocrystals by ring-opening polymerization. *Journal of Materials Chemistry* 18: 5002-5010.

Habibi, Y. et al., 2010, Cellulose Nanocrystals: Chemistry, Self-Assembly, and Applications. *Chemical Reviews* 110: 3479-3500.

Herrera, N. V. et al., 2011, Randomly oriented and aligned cellulose fibres reinforced with cellulose nanowhiskers, prepared by electrospinning. *Plastics Rubber and Composites* 40: 57-64.

Huang, J. et al., 2011, Electrospinning of Bombyx mori Silk Fibroin Nanofiber Mats Reinforced by Cellulose Nanowhiskers. *Fibers and Polymers* 12: 1002-1006.

Imai, T. et al., 1998, Unidirectional processive action of cellobiohydrolase Cel7A on Valonia cellulose microcrystals. *FEBS Letters* 432: 113-116.

Isogai, A. et al., 2011, TEMPO-oxidized cellulose nanofibers. *Nanoscale* 3: 71-85.

- Iwamoto, S. et al., 2007, Nano-fibrillation of pulp fibers for the processing of transparent nanocomposites. *Applied Physics A: Materials Science & Processing* 89: 461-466.
- Iwamoto, S. et al., 2005, Optically transparent composites reinforced with plant fiber-based nanofibers. *Applied Physics A: Materials Science & Processing* 81: 1109-1112.
- Johansson, C. et al., 2012, Renewable Fibers and Bio-Based Materials for Packaging Applications - a Review of Recent Developments. *Bioresources* 7: 2506-2552.
- Johar, N. et al., 2012, Extraction, preparation and characterization of cellulose fibres and nanocrystals from rice husk. *Industrial Crops and Products* 37: 93-99.
- Kargarzadeh, H. et al., 2012, Effects of hydrolysis conditions on the morphology, crystallinity, and thermal stability of cellulose nanocrystals extracted from kenaf bast fibers. *Cellulose* 19: 855-866.
- Khan, R. A. et al., 2010, Production and Properties of Nanocellulose-Reinforced Methylcellulose-Based Biodegradable Films. *Journal of Agricultural and Food Chemistry* 58: 7878-7885.
- Kohnke, T. et al., 2012, Nanoreinforced xylan-cellulose composite foams by freeze-casting. *Green Chemistry* 14: 1864-1869.
- Kovacs, T. et al., 2010, An ecotoxicological characterization of nanocrystalline cellulose (NCC). *Nanotoxicology* 4: 255-270.
- Kumar, S. et al., 2012, Reinforcement of Stereolithographic Resins for Rapid Prototyping with Cellulose Nanocrystals. *ACS Appl Mater Interfaces*.
- López-Rubio, A. et al., 2007, Enhanced film forming and film properties of amylopectin using micro-fibrillated cellulose. *Carbohydrate Polymers* 68: 718-727.
- Lalia, B. S. et al., 2012, Nanocrystalline-cellulose-reinforced poly(vinylidene fluoride-co-hexafluoropropylene) nanocomposite films as a separator for lithium ion batteries. *Journal of Applied Polymer Science* 126: E441-E447.
- Lee, J., Deng, Y. L., 2012, Increased mechanical properties of aligned and isotropic electrospun PVA nanofiber webs by cellulose nanowhisker reinforcement. *Macromolecular Research* 20: 76-83.
- Li, F. et al., 2013, Tunable green oxygen barrier through layer-by-layer self-assembly of chitosan and cellulose nanocrystals. *Carbohydrate Polymers* 92: 2128-2134.
- Li, Y., Ragauskas, A. J., 2012, Ethanol organosolv lignin-based rigid polyurethane foam reinforced with cellulose nanowhiskers. *Rsc Advances* 2: 3347-3351.
- Lin, N. et al., 2011, Surface acetylation of cellulose nanocrystal and its reinforcing function in poly(lactic acid). *Carbohydrate Polymers* 83: 1834-1842.
- Liu, H. Y. et al., 2010, Fabrication and properties of transparent polymethylmethacrylate/cellulose nanocrystals composites. *Bioresource Technology* 101: 5685-5692.

- Liu, H. Z., Laborie, M. P. G., 2011, Bio-based nanocomposites by in situ cure of phenolic prepolymers with cellulose whiskers. *Cellulose* 18: 619-630.
- Magalhaes, W. L. E. et al., 2011, Novel all-cellulose composite displaying aligned cellulose nanofibers reinforced with cellulose nanocrystals. *Tappi Journal* 10: 19-25.
- Man, Z. et al., 2011, Preparation of Cellulose Nanocrystals Using an Ionic Liquid. *Journal of Polymers and the Environment* 19: 726-731.
- Marchessault, R. H. et al., 1961, Some hydrodynamic properties of neutral suspensions of cellulose crystallites as related to size and shape. *Journal of Colloid Science* 16: 327-344.
- Martinez-Sanz, M. et al., 2011a, Optimization of the nanofabrication by acid hydrolysis of bacterial cellulose nanowhiskers. *Carbohydrate Polymers* 85: 228-236.
- Martinez-Sanz, M. et al., 2012, On the Optimization of the Dispersion of Unmodified Bacterial Cellulose Nanowhiskers into Polylactide Via Melt Compounding to Significantly Enhance Barrier and Mechanical Properties. *Biomacromolecules*.
- Martinez-Sanz, M. et al., 2011b, Development of electrospun EVOH fibres reinforced with bacterial cellulose nanowhiskers. Part I: Characterization and method optimization. *Cellulose* 18: 335-347.
- Mathew, A. P. et al., 2011, Moisture Absorption Behavior and Its Impact on the Mechanical Properties of Cellulose Whiskers-Based Polyvinylacetate Nanocomposites. *Polymer Engineering and Science* 51: 2136-2142.
- Mathew, A. P. et al., 2008, Mechanical properties of nanocomposites from sorbitol plasticized starch and tunicin whiskers. *Journal of Applied Polymer Science* 109: 4065-4074.
- Mendez, J. et al., 2011, Bioinspired Mechanically Adaptive Polymer Nanocomposites with Water-Activated Shape-Memory Effect. *Macromolecules* 44: 6827-6835.
- Meyabadi, T. F., Dadashian, F., 2012, Optimization of Enzymatic Hydrolysis of Waste Cotton Fibers for Nanoparticles Production Using Response Surface Methodology. *Fibers and Polymers* 13: 313-321.
- Moon, R. J. et al., 2011, Cellulose nanomaterials review: structure, properties and nanocomposites. *Chem Soc Rev* 40: 3941-3994.
- Nakagaito, A. N. et al., 2005, Bacterial cellulose: the ultimate nano-scalar cellulose morphology for the production of high-strength composites. *Applied Physics A: Materials Science & Processing* 80: 93-97.
- Ni, H. et al., 2012, Cellulose nanowhiskers: Preparation, characterization and cytotoxicity evaluation. *Bio-Medical Materials and Engineering* 22: 121-127.
- Nickerson, R. F., Habrle, J. A., 1947, Cellulose Intercrystalline Structure. *Industrial & Engineering Chemistry* 39: 1507-1512.
- Nishiyama, Y., 2009, Structure and properties of the cellulose microfibril. *Journal of Wood Science* 55: 241-249.

- Noorani, S. et al., 2006, Polysulfone-cellulose nanocomposites. *Cellulose Nanocomposites: Processing, Characterization, and Properties* 938: 209-220.
- Noorani, S. et al., 2007, Nano-enabled microtechnology: polysulfone nanocomposites incorporating cellulose nanocrystals. *Cellulose* 14: 577-584.
- Okita, Y. et al., 2011, TEMPO-Oxidized Cellulose Nanofibrils Dispersed in Organic Solvents. *Biomacromolecules* 12: 518-522.
- Oksman, K. et al., 2011, Cellulose nanowhiskers separated from a bio-residue from wood bioethanol production. *Biomass & Bioenergy* 35: 146-152.
- Paakko, M. et al., 2007, Enzymatic hydrolysis combined with mechanical shearing and high-pressure homogenization for nanoscale cellulose fibrils and strong gels. *Biomacromolecules* 8: 1934-1941.
- Pakzad, A. et al., 2012, Elastic properties of thin poly(vinyl alcohol)-cellulose nanocrystal membranes. *Nanotechnology* 23.
- Paralikara, S. A. et al., 2008, Poly(vinyl alcohol)/cellulose nanocrystal barrier membranes. *Journal of Membrane Science* 320: 248-258.
- Park, D. J. et al., 2012, Bacterial cellulose nanocrystals-embedded silk nanofibers. *J Nanosci Nanotechnol* 12: 6139-6144.
- Pei, A. H. et al., 2011, Strong Nanocomposite Reinforcement Effects in Polyurethane Elastomer with Low Volume Fraction of Cellulose Nanocrystals. *Macromolecules* 44: 4422-4427.
- Pei, A. H. et al., 2010, Functionalized cellulose nanocrystals as biobased nucleation agents in poly(L-lactide) (PLLA) - Crystallization and mechanical property effects. *Composites Science and Technology* 70: 815-821.
- Peresin, M. S. et al., 2010, Effect of Moisture on Electrospun Nanofiber Composites of Poly(vinyl alcohol) and Cellulose Nanocrystals. *Biomacromolecules* 11: 2471-2477.
- Petersson, L. et al., 2009, Dispersion and Properties of Cellulose Nanowhiskers and Layered Silicates in Cellulose Acetate Butyrate Nanocomposites. *Journal of Applied Polymer Science* 112: 2001-2009.
- Postek, M. T. et al., 2011, Development of the metrology and imaging of cellulose nanocrystals. *Measurement Science and Technology* 22: 024005.
- Roman, M., Winter, W. T., 2004, Effect of Sulfate Groups from Sulfuric Acid Hydrolysis on the Thermal Degradation Behavior of Bacterial Cellulose. *Biomacromolecules* 5: 1671-1677.
- Rosa, M. F. et al., 2010, Cellulose nanowhiskers from coconut husk fibers: Effect of preparation conditions on their thermal and morphological behavior. *Carbohydrate Polymers* 81: 83-92.
- Rueda, L. et al., 2011, Isocyanate-rich cellulose nanocrystals and their selective insertion in elastomeric polyurethane. *Composites Science and Technology* 71: 1953-1960.
- Saito, T. et al., 2007, Cellulose nanofibers prepared by TEMPO-mediated oxidation of native cellulose. *Biomacromolecules* 8: 2485-2491.

- Saito, T. et al., 2006, Homogeneous Suspensions of Individualized Microfibrils from TEMPO-Catalyzed Oxidation of Native Cellulose. *Biomacromolecules* 7: 1687-1691.
- Saito, T. et al., 2005, Distribution of carboxylate groups introduced into cotton linters by the TEMPO-mediated oxidation. *Carbohydrate Polymers* 61: 414-419.
- Sanchez-Garcia, M. D. et al., 2010, Morphology and Water Barrier Properties of Nanobiocomposites of k/i-Hybrid Carrageenan and Cellulose Nanowhiskers. *Journal of Agricultural and Food Chemistry* 58: 12847-12857.
- Sheltami, R. M. et al., 2012, Extraction of cellulose nanocrystals from mengkuang leaves (*Pandanus tectorius*). *Carbohydrate Polymers* 88: 772-779.
- Shinoda, R. et al., 2012, Relationship between Length and Degree of Polymerization of TEMPO-Oxidized Cellulose Nanofibrils. *Biomacromolecules* 13: 842-849.
- Siqueira, G. et al., 2010, High reinforcing capability cellulose nanocrystals extracted from *Syngonanthus nitens* (Capim Dourado). *Cellulose* 17: 289-298.
- Siqueira, G. et al., 2011, Processing of cellulose nanowhiskers/cellulose acetate butyrate nanocomposites using sol-gel process to facilitate dispersion. *Composites Science and Technology* 71: 1886-1892.
- Siro, I., Plackett, D., 2010, Microfibrillated cellulose and new nanocomposite materials: a review. *Cellulose* 17: 459-494.
- Stenstad, P. et al., 2008, Chemical surface modifications of microfibrillated cellulose. *Cellulose* 15: 35-45.
- Sui, L. et al., 2010, Brillouin Light Scattering Investigation of the Mechanical Properties of Layer-by-Layer Assembled Cellulose Nanocrystal Films. *Macromolecules* 43: 9541-9548.
- Ten, E. et al., 2010, Thermal and mechanical properties of poly(3-hydroxybutyrate-co-3-hydroxyvalerate) / cellulose nanowhiskers composites. *Polymer* 51: 2652-2660.
- Urena-Benavides, E. E. et al., 2010, Effect of Jet Stretch and Particle Load on Cellulose Nanocrystal-Alginate Nanocomposite Fibers. *Langmuir* 26: 14263-14270.
- Urena-Benavides, E. E., Kitchens, C. L., 2011, Wide-Angle X-ray Diffraction of Cellulose Nanocrystal-Alginate Nanocomposite Fibers. *Macromolecules* 44: 3478-3484.
- Urena-Benavides, E. E., Kitchens, C. L., 2012, Cellulose Nanocrystal Reinforced Alginate Fibers-Biomimicry Meets Polymer Processing. *Molecular Crystals and Liquid Crystals* 556: 275-287.
- Visakh, P. M. et al., 2012, Crosslinked natural rubber nanocomposites reinforced with cellulose whiskers isolated from bamboo waste: Processing and mechanical/thermal properties. *Composites Part a-Applied Science and Manufacturing* 43: 735-741.
- Wang, B., Sain, M., 2007a, Dispersion of soybean stock-based nanofiber in a plastic matrix. *Polymer International* 56: 538-546.

- Wang, B., Sain, M., 2007b, Isolation of nanofibers from soybean source and their reinforcing capability on synthetic polymers. *Composites Science and Technology* 67: 2521-2527.
- Wang, N. et al., 2007, Thermal degradation behaviors of spherical cellulose nanocrystals with sulfate groups. *Polymer* 48: 3486-3493.
- Wik, V. M. et al., 2011, Castor Oil-based Polyurethanes Containing Cellulose Nanocrystals. *Polymer Engineering and Science* 51: 1389-1396.
- Xu, Q. X. et al., 2008, A novel amphotropic polymer based on cellulose nanocrystals grafted with azo polymers. *European Polymer Journal* 44: 2830-2837.
- Yu, H. Y. et al., 2012, Simultaneous improvement of mechanical properties and thermal stability of bacterial polyester by cellulose nanocrystals. *Carbohydrate Polymers* 89: 971-978.
- Zhou, C. J. et al., 2011, Electrospun Polyethylene Oxide/Cellulose Nanocrystal Composite Nanofibrous Mats with Homogeneous and Heterogeneous Microstructures. *Biomacromolecules* 12: 2617-2625.
- Zhou, C. J. et al., 2012, UV-initiated crosslinking of electrospun poly(ethylene oxide) nanofibers with pentaerythritol triacrylate: Effect of irradiation time and incorporated cellulose nanocrystals. *Carbohydrate Polymers* 87: 1779-1786.
- Zimmermann, T. et al., 2004, Cellulose Fibrils for Polymer Reinforcement. *Advanced Engineering Materials* 6: 754-761.
- Zoppe, J. O. et al., 2009, Reinforcing Poly(epsilon-caprolactone) Nanofibers with Cellulose Nanocrystals. *Acs Applied Materials & Interfaces* 1: 1996-2004.

2 AIM OF STUDY

Cellulose as the most abundant natural polymer in biosphere has received more and more attention on its sustainability, renewability, and new possible functionalities. Furthermore, nowadays conventional packaging materials cannot meet the increasing demands for full sustainability and performance; new materials therefore are discovered, synthesized, and developed for varieties of applications in different fields globally by a number of funded research groups and companies.

Food packaging materials is one of the largest products we are using in daily life, but most of conventional materials are still based on fossil and un-renewable resources. In this PhD project, we propose to use cellulose nanocrystals (CNs) in combination with current food packaging materials in order to improve performance, especially barrier, mechanical, and anti-fog properties. The aim of this study is to use green material, CNs, as coatings of conventional plastic films, to promote the sustainability of food packaging materials, while keeping or improving different properties.

3 RESULTS AND DISCUSSION

3.1 Topic/theme 1: The process, structure, morphology of different-form cellulose nanocrystals (CNs)

Introduction

The acidic hydrolysis methods (Araki et al., 1998; Beck-Candanedo et al., 2005; Bondeson et al., 2006; de Souza Lima & Borsali, 2002; Dong et al., 1998; Elazzouzi-Hafraoui et al., 2007; Favier et al., 1995; Håkansson & Ahlgren, 2005; Marchessault et al., 1961; Nickerson & Habrle, 1947; Roman & Winter, 2004) were commonly used for extracting varieties of CNs from sources whose morphologies are characterized mainly by electronic microscopy. The concentrated acid firstly attacks and hydrolyzes the hemi- and amorphous (defects) parts of native cellulose. After the hydrolysis, the high crystallinity regions remain intact (Anglès & Dufresne, 2001) and the final products show rod-like nanocrystals with different morphologies and aspect ratio due to the source of native cellulose, including cotton (Dong et al., 1998), wood pulp (Elazzouzi-Hafraoui et al., 2007), ramie (Habibi et al., 2008), tunicate (Elazzouzi-Hafraoui et al., 2007), Valonia (Imai et al., 1998), bacterial cellulose (Grunert & Winter, 2002) and so on. In fact, acidic hydrolysis of native cellulose induces a rapid reduction of the degree of polymerization, which is correlated with crystals sized of the original cellulose chains (Håkansson & Ahlgren, 2005).

The basic chemical structures of CNs are generally determined by Fourier transform infrared spectroscopy (FTIR) (de Mesquita et al., 2010). From the peaks of FTIR spectra, the typical functional groups could be confirmed efficiently and easily. Moreover, the crystallinity and crystal structures could be detected by X-ray diffraction (XRD) (Eichhorn et al., 2004), nuclear magnetic resonance NMR (Bergenstrahle et al., 2008; Koch et al., 2000; Witter et al., 2006), Raman spectroscopy (Štuncová et al., 2005), and neutron crystallography (Nishiyama et al., 2008). These data combined with experimental measurements could be helpful to establish or validate crystal structure models or molecular simulation. At a minimum, these models are made for the axial length of the crystalline cellulose unit cell, often referred to in the literature as the c-spacing. Besides the cellulose crystal structure, the grafted groups from acidic hydrolysis or chemical modifications which always occur on the surface due to intact highly ordered CNs, are determined by FTIR (Habibi et al., 2008) or X-ray photoelectron spectroscopy (XPS) (Yang et al., 2011). The resolution of XPS is much higher than FTIR and is able to scan only a few nano meters on the surface of samples, which is quite suitable for ultrathin

deposition.

The geometrical dimensions (length, L , and diameter, d) of CNs vary due to the different sources of the raw material and the hydrolytic conditions. Such variations are partially ascribed to the diffusion-controlled nature of the acid hydrolysis. Their morphologies are usually investigated by microscopy (TEM, AFM, E-SEM, (Miller & Donald, 2003) etc.) or light scattering techniques, including small angle neutron scattering (SANS) (Šturcová et al., 2005), polarized and depolarized dynamic light scattering (DLS, DDLS) (De Souza Lima et al., 2002). TEM images of CNs typically show aggregation of the particles, mainly due to the drying step for the preparation of the specimens after negative staining. Besides aggregation, additional instrumental artifacts usually lead to an overestimation of CNs dimensions (Elazzouzi-Hafraoui et al., 2007) therefore, it is suggested the use of TEM in cryogenic mode (cryo-TEM) to prevent aggregation. Atomic force microscopy (AFM) has been widely used to provide surface topography of CNs (Hanley et al., 1997; Hanley et al., 1992; Kvien et al., 2005; Miller & Donald, 2003). But sometimes AFM topography may show different profiles compared with TEM images, which are attributed to substrate shape perturbations induced by AFM tip and tip-broadening effects.

3.2 Materials and methods 1

3.2.1 CNs extraction process

Whatman No. 1 filter paper (98% cotton, pore size 11 μm) or cotton linter was milled by lab mill into small pieces. The milled cotton was added to a preheated solution of 64% w/w sulfuric acid (ratio of fiber and acid 1 : 17.5 <g/mL>) and hydrolysis proceeded under vigorous stirring at 45 $^{\circ}\text{C}$ for 45 min. To quench the reaction, the reaction mixture was diluted with 10 times-volume deionized water (18 M Ω cm, Millipore Milli-Q Purification System) and allowed to settle for 2 h. In order to concentrate the cellulose and remove excess acid and water, the suspension was centrifuged at 5000 rpm for 20 min. The pellet that precipitated was repeatedly rinsed and centrifuged with deionized water until the supernatant became turbid (after the 3rd time centrifugation). The next step was to further remove the excess sulfuric acid by dialysis. Before used, the dialysis tubes should be boiled in deionized water for 3 h. Further purification was then done by dialysis against deionized water until the effluent remained at neutral pH (Molecular weight cut-off, MWCO 12 000 and higher). The suspension was sonicated (UP400S 400 W, Hielscher Co., Germany) repeatedly (0.7 cycles of 15 min at 70% output) to create cellulose crystals of colloidal dimensions. During the ultrasonic treatment, the suspension was cooled with an ice water bath to avoid overheating, and the sonication process was performed in a plastic beaker to avoid possible ion release from glass containers. Mixed-bed research grade ion-exchange resin (Dowex Marathon MR-3, Sigma-Aldrich) was added to the cellulose suspension for 24 h to complex any stray ions and was then removed by filtering through ashless filter paper (Munktell grade GF/C, 1.2 μm). Finally, the suspension was filtered under vacuum with a Whatman glass microfiber filter (grade GF/F, 0.7 μm) to remove sonicator tip contamination and largest cellulose-fiber agglomerates. The cellulose content of the resulting aqueous suspension was determined by drying several samples (1 mL) at 105 $^{\circ}\text{C}$ for 15 min intervals (to avoid decomposition or burning) until weight constancy, giving a cellulose concentration of 1 % w/w and a yield of ~50%.

3.2.2 Freeze-dried powder

Firstly, according to US patent (US 005629055A), the pH value of 1% CNs dispersion was adjusted to ~7 by 1M NaOH(aq) in order to gain fully charged CNs. Secondly, the dispersion was frozen at the -18 $^{\circ}\text{C}$ for overnight and then moved it to freeze dryer (LIO-10P). Finally, the freeze-dried powder could be obtained and stored in tightly close bottle for conservation under dry conditions.

3.2.3 CNs gel

The CNs dispersion was prepared from freeze-dried powder by ultrasonication (0.7 cycle of 5 min at 70% output). When the CNs dispersion concentration is above than 3.5% (w/w), the

dispersion converted into gel status.

Characterization

3.2.4 Fourier transform infrared spectroscopy (FTIR)

FTIR spectra were recorded using a Perkin Elmer instrument (Spectrum 100) equipped with an ATR. Spectra were recorded using a spectral width ranging from 650 to 4000 cm^{-1} , with 4 cm^{-1} resolution and an accumulation of 16 scans.

3.2.5 Solid-state nuclear magnetic resonance (NMR) spectroscopy

All NMR spectra were acquired at room temperature on a Bruker AVANCE-600 spectrometer (Bruker Spectrospin GmbH, Rheinstetten, Germany), equipped with a 4 mm broad-band CP-MAS probe for solid state measurements. About 100 mg of cellulose sample were directly pressed into a 4 mm ZrO_2 rotor without further treatment. ^{13}C spectra were acquired at 150.9 MHz using Cross Polarization (CP) and Magic Angle Spinning (MAS) at 6-10 KHz (Pines et al., 1973). Proton decoupling was achieved with GARP-based composite pulse. Standard acquisition parameters were as follows: Spectral width: 75.7 KHz; acquisition time: 3.4 ms; relaxation delay: 2s (fast acquisition conditions); contact time for Cross Polarization: 1 ms; number of scans: 7000-24000. The contact time was optimised by systematic variation of the corresponding pulse within the 0.3-3 ms range. Adamantane was used as external chemical shift reference.

3.2.6 XPS (X-ray photoelectron spectroscopy)

XPS scans were acquired with a Phoibos 150 hemispherical analyzer at normal emission. X-ray excitation was provided by a twin anode X-ray source operated at 200 W. Mg $K\alpha$ radiation (photon energy: 1253.6 eV) was used. The wide scans were acquired with a pass energy of 50 eV, while detailed scans were acquired with a pass energy of 25 eV.

3.2.7 Transmission electronic microscopy (TEM)

Drops of aqueous dispersions of CNs (0.05% w/v) were deposited on carbon-coated electron microscope grids, negatively stained with uranyl acetate and allowed to dry. The samples were analyzed with a Hitachi Jeol-10084 transmission electron microscope (TEM) operated at an accelerating voltage of 80 kV.

3.2.8 Scanning electronic microscopy (SEM)

(1) Field emission SEM (FE-SEM) observation of the film cross-sections was carried out with a Zeiss Sigma field-emission microscope at 5 kV. The samples subjected to the SEM observation were pre-coated with gold using a Polaron E5100 Coater at 18 mA for 20 s.

(2) Environmental SEM (E-SEM) analysis was performed on freeze-dried CNs samples at 10 kV with Evo 50 EP Instrumentation (Zeiss, Jena, Germany).

3.2.9 Atomic force microscopy (AFM)

An atomic force microscope (AFM, AlphaSNOM, WITec GmbH, Germany) was employed both to systematically study the thickness of the deposited multilayers and to analyze their morphology. For thickness measurements, the LbL coating on glass slides was gently scratched in order to expose part of the glass substrate and thus measure the thickness of the coating. Topography images were acquired with soft tapping mode at low oscillation amplitudes, stabilized by an amplitude-modulation feedback system based on the optical lever deflection method. Standard AFM Si probes have been used.

3.2.10 Size distribution

1% CNs dispersion was scanned by laser diffraction particle size analyzer (Mastersizer 2000, Malvern Instruments) wavelength from 0.020 to 2000 μm .

3.3 Results and discussion 1

3.3.1 Modified process and different forms of CNs

As mentioned in the introduction, the process of producing CNs leads to a slightly chemical modification of cellulose by acidic hydrolysis (Dong et al., 1998), and the detailed steps of process are as follows: milling, hydrolysis, centrifugation, dialysis, ultrasonication, ion exchange, and filtering, and freeze drying for producing CNs powder. The yield of the process is ca. 55%, in our case, using cotton linter as raw material. The dialysis step is the most time-consuming, we therefore skip this step and directly neutralize CNs suspension by 5M NaOH (aq) till pH \sim 7. The neutralization process is relatively long, since the suspension is a dispersion of high molecular weight of cellulose. If compared with dialysis process (3-5 days), neutralization is a much easier to handle and less time-consuming way. Then eliminating the excess ions from dispersion is through ion exchange step. Through this slightly modified preparation CNs process, the finally obtained product was similar with before from eye inspection. The \sim 1% dispersion is obtained directly after filtration step, which is colloid and its color ivory white. To improve the storability, the powder-form CNs was prepared by lyophilization. The specific concentrations of CNs dispersion could be prepared from re-dispersing CNs powder into distilled water through ultrasonication till no aggregations appeared and the light could pass the dispersion (colloid). If the dispersion concentration is higher than \sim 5%, CNs become to gel state after settling down due to the strong hydrogen bonds between cellulose molecular chains and inter molecular (Beck et al., 2012). The 1% dispersion, freeze-dried powder, and gel of CNs are presented in Figure 5.



Figure 5 1% dispersion (a), freeze-dried powder (b), and 3.5% CNs gel (c), from left to right. The yellow parts caused by the light of the lamps.

The final CNs products are grafted with a few sulfate ester groups ($-\text{O}-\text{SO}_3^-$) from sulfuric acid. The sulfate ester groups bring negative charges on the surface of CNs, which result in the repulsion between charged chains thereby CNs can be dispersed into water or other polar solvents (Viet et al., 2007). As known, the charge density of polymer chains could be adjusted by changing the pH values of solutions or dispersions. For CNs dispersion, when $\text{pH} > 7$, the repulsions between chains are stronger and the molecular chains might be rigid. On the other hand, when $\text{pH} < 7$, repulsions are weaker and the molecular chains might be loose. It is noticed

that CNs precipitate under $\text{pH} < 1$ due to the associations between sulfate ester groups ($-\text{O}-\text{SO}_3^-$) and hydrogen ion (H^+) from acidic condition which lead to be non-charged CNs. Based on above principles, flexible CNs films of $\text{pH} 2$ and $\text{pH} 7$ were casted from 1% dispersion in polyethylene petri disk under room temperature and presented different transparency, which are shown in Figure 6. Thickness of the films is 20-30 μm and the transparency of $\text{pH} 2$ and $\text{pH} 7$ films are 88% and 63% at 550 nm, respectively.

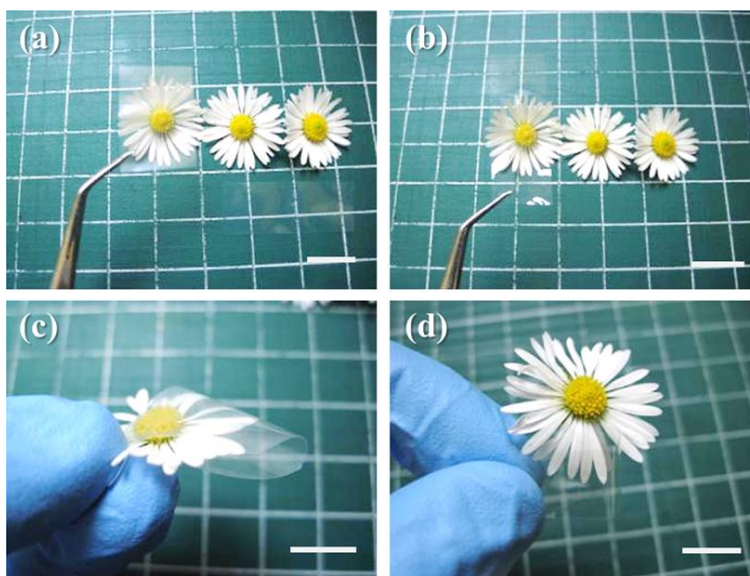


Figure 6 $\text{pH} 7$ CNs cast films (a) and (c), $\text{pH} 2$ CNs cast films (b) and (d). Scale 1.5 cm.

3.3.2 Structure of CNs

3.3.2.1 Fourier transform infrared spectroscopy (FTIR)

The structures of raw material (cotton linter) and final product (freeze-dried CNs) were determined by FT-IR, shown in Figure 7. In raw material, pure CNs film with and without dialysis, the band at 3338 cm^{-1} is attributed to the O-H stretching vibration. The bands at 2899 and 1428 cm^{-1} are characteristic of C-H stretching and bending of $-\text{CH}_2$ groups, respectively, while the peaks at 1162 and 1057 cm^{-1} are ascribed to the saccharide structure (Li et al., 2009). The band at 1135 cm^{-1} is assigned to the SO_4^{2-} which origins from sulfuric acid. This intensive band might be due to the skipping dialysis step, which could remove most of the substances ($M_w > 20,000$ Dalton, Sigma) including huge amount of SO_4^{2-} . Even though the ion exchange step was carried out in the modified process, it is yet not sufficient to thoroughly remove all of SO_4^{2-} . The possible solution could be increasing the amount of ion exchange resin and the adequate quantity should be optimized in the future work. The sulfate salt could not have dramatic influence to CNs nano filler usage but could change the optical properties (Nogi et al.,

2009; Yano et al., 2005), the ion exchange step could therefore be dependent on the CNs applications. The sulfate ester groups in dialyzed samples were not detected because the number of these groups was very small. The freeze-dried powders from two processes have the highly similar re-dispersed properties into water. The 1% dispersions were prepared from two varieties of CNs under the same condition of ultrasonic treatment (70% cycle, 70% amplify, and 3 min), and presented in Figure 8.

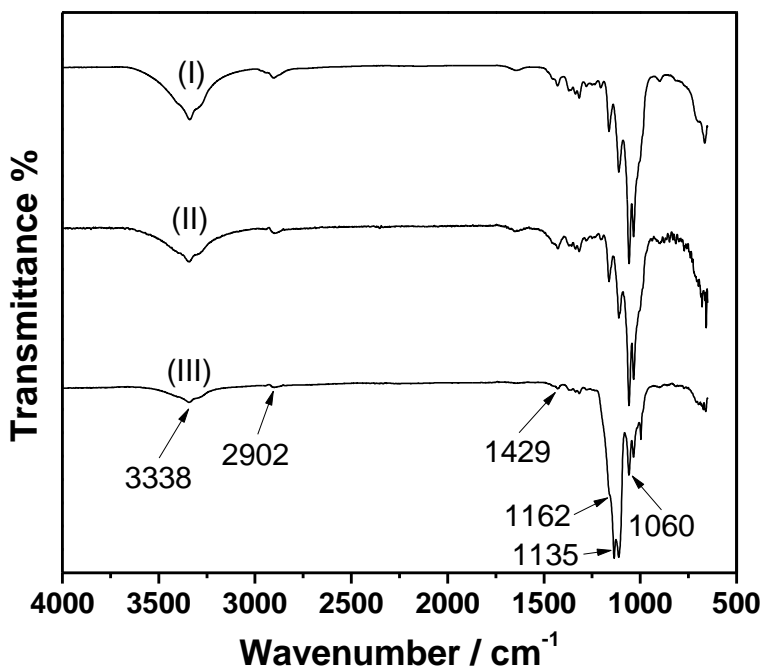


Figure 7 FTIR of the raw material cotton linters (I), freeze-dried CNs (II), and freeze-dried CNs (III) without dialysis

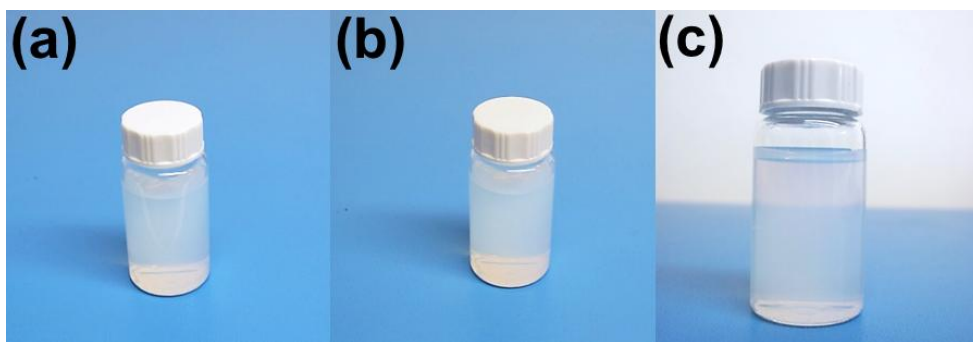


Figure 8 1% dispersion of CNs from original (a) and modified process (b) (c).

From Figure 7, we could conclude that there are no significant differences before and after the CNs producing process, which indicates that no strongly chemical modifications occurred. Producing CNs by acidic hydrolysis is therefore only an extraction process from raw material without strongly chemical modifications. Also, some literature reported that nano cellulose are relatively safe for human beings (Kovacs et al., 2010), which might be widely considered and used as safe food contact material in future.

3.3.2.2 Nuclear magnetic resonance (NMR)

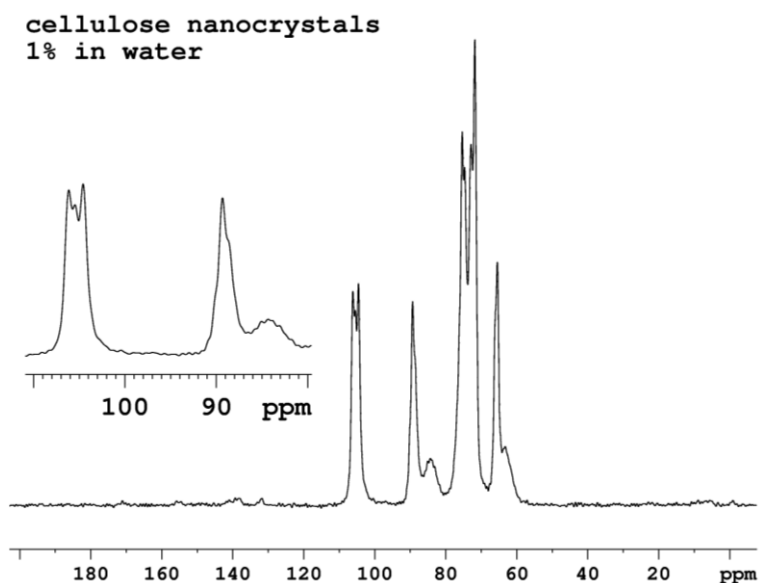


Figure 9 NMR spectra of CNs

^{13}C -NMR spectrum of CNs freeze-dried powder is shown in Figure 9. The spectrum presented the characteristic signals of native cellulose (Atalla & VanderHart, 1999). The anomeric carbon, C-1, appears furthest downfield, at around 105 ppm. Characteristic signals of C-2, C-3 and C-5 carbons are shown between 70 and 78 ppm. The signal between 87 and 90 ppm corresponds to C-4 of the highly ordered cellulose crystallite, whereas the broader upfield signals, between 79 and 86 ppm, were assigned to the C-4 of disordered cellulose, as well as to the less ordered cellulose chains of the crystallite surfaces (Larsson, 2003). Also, the signal centered at 64.5 ppm is attributed to C-6 of ordered cellulose chains and the slight shoulder, between 60 and 63 ppm, is attributed to C-6 of cellulose in the amorphous and disordered component of CNs. In particular, the C-4 region was used for this analysis, the signals from ordered and less ordered regions being well separated. Larsson et al. used spectral fitting for the C-4 region of cotton cellulose and assigned three Lorentzian's lineshapes for the signals from celluloses I_{α} , $I_{(\alpha+\beta)}$, and

I_{β} and four Gaussian's lineshapes for the signals from para-crystalline cellulose, inaccessible fibril surfaces, and two accessible fibril surfaces (Larsson, 2003). The degree of cellulose crystallinity, in the case of CNs from cotton linter, was determined using the areas of the crystalline and amorphous C-4 signals according to Larsson's fitting (Habibi et al., 2009; Larsson, 2003). The results indicated that the degree of crystallinity of CNs from cotton is around 85%.

3.3.2.3 XPS (X-ray photoelectron spectroscopy)

WIDE SCANS

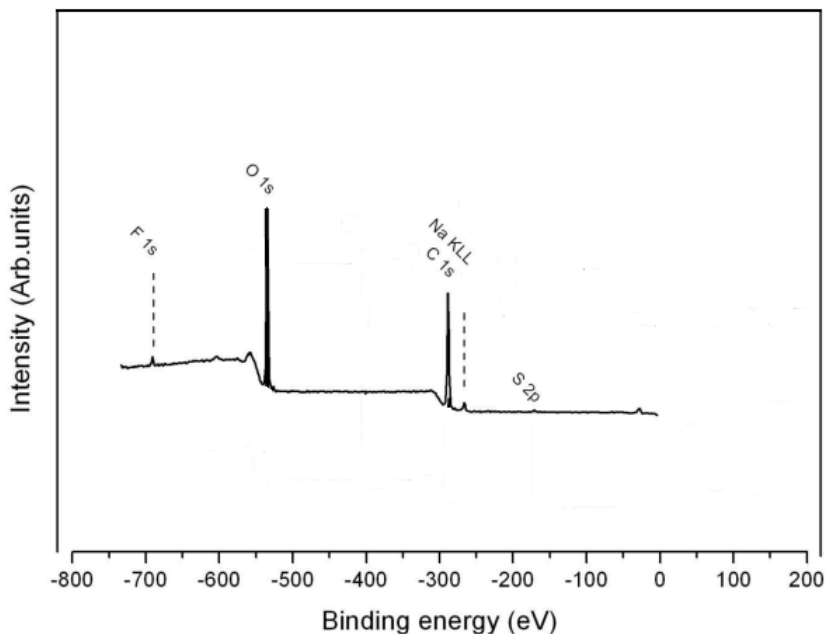


Figure 10 XPS wide scan for CNs deposition on PET

The XPS spectrum is presented in Figure 10 and CNs did show additional peaks related to fluorine and Na Auger signals, and did not show a nitrogen peak. Table 1 lists all the elements present in the analyzed samples and their atomic concentration (x_i), assuming homogeneous samples. Raw intensities (A_i) have been corrected according to the following formula:

$$x_i = \frac{A_i/s_i}{\sum_n A_n/s_n}$$

By making use of tabulated relative sensitivity factors (s_i)^a.

^a Photoelectron cross sections from report (Reilman et al., 1976) (with $\theta = 60^\circ$), transmission function from literature (Hemminger et al., 1990) (with $n = 0.5$), attenuation length from related literature (Powell, 1988) (with $p = 0.7414$).

Table 1 Concentration of atomic species (in terms of number of atoms) for the CNs samples

O [%]	C [%]	N [%]	S [%]	F [%]
39.1±0.2	59.4±0.4	-	0.6±0.1	0.8±0.1

From Table 1, it is shown additional peaks related to fluorine without a nitrogen peak. Fluorine did not come from improper handling of the samples during XPS analysis, probably from the impurity of raw material or sulfuric acid. The oxygen signal shows that about 90% of the oxygen is related to C–O bonds, while only a smaller amount (<10%) is related to O–H and C=O bonds, likely due to the presence of acidic groups, and thus to the presence of oxidized cellulose species.

(1) Carbon peaks

Carbon peaks.

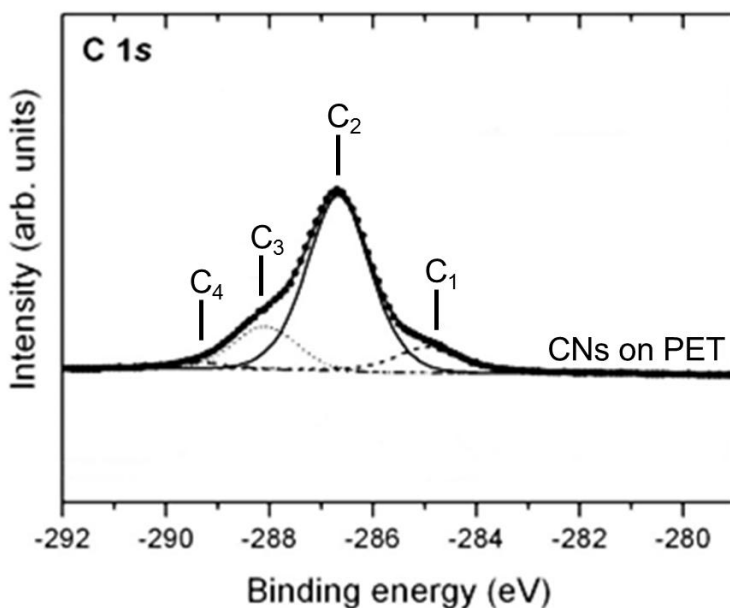


Figure 11 Carbon peaks of XPS

The carbon peaks were presented in Figure 11 and decomposed into a sum of Gaussian/Lorentzian lineshapes with the same FWHM. The lineshape used to model the carbon peaks was a weighted product of a Gaussian (~30 %) and a Lorentzian (~70%) lineshape. Peak C₁ is associated to photoemission from C 1s orbitals in carbon atoms with C–C bonds and its position was set to -285.0 eV (Beamson & Briggs, 1992). Peak C₂ is associated to C–O bonds,

peak C_3 is associated to O-C-O or C=O bonds and peak C_4 to O=C-O bonds. The chemical shift between peak C_1 and C_2 is 1.7 ± 0.1 eV (ΔE_{12}) in good agreement with the literature (Fras et al., 2005), while ΔE_{13} and ΔE_{14} were fixed to 3.1 and 4.4 eV, according to reference (Fras et al., 2005). Table 2 lists the results of the C 1s peak decomposition:

Table 2 Carbon signal features related to different bonds

C-C [$C_1\%$]	C-O [$C_2\%$]	O-C-O/C=O [$C_3\%$]	O=C-O [$C_4\%$]
10.9 ± 0.2	69.9 ± 0.4	16.7 ± 0.3	2.5 ± 0.2

(2) Oxygen peaks

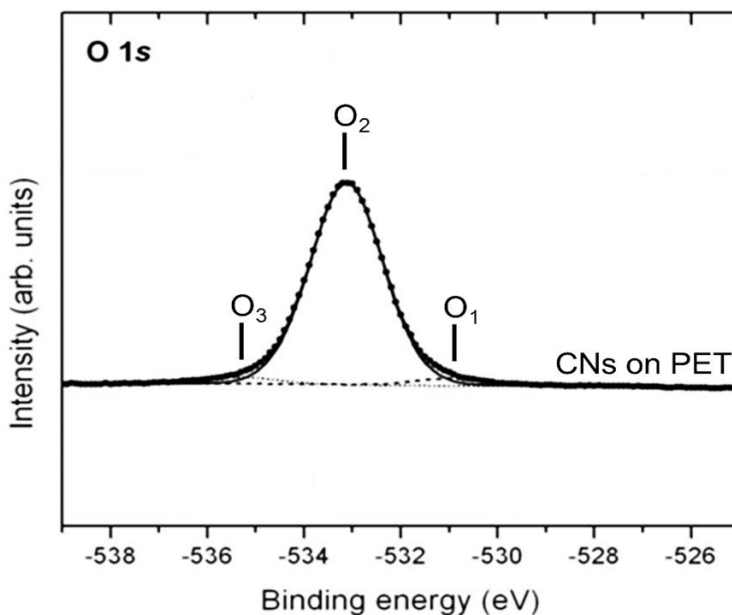
Oxygen peaks

Figure 12 Oxygen peaks of XPS

The oxygen peaks were presented in Figure 12 decomposed into a sum of Gaussian/Lorentzian lineshapes with the same FWHM. The lineshape used to model the oxygen peaks was a weighted product of a Gaussian (70 %) and a Lorentzian (30 %) lineshape. The most intense peak, peak O_2 , is associated to photoemission from O 1s orbitals in oxygen atoms bonded to one carbon atom (C-O bonds). The binding energy of O_2 electrons is -532.9 eV, in good agreement with the value reported in the literature (Shen et al., 2004). Peak O_1 is associated to oxygen atoms in carbonyl groups (C=O bonds) (Beamson & Briggs, 1992), while peak O_3 is associated to free O-H groups (Beamson & Briggs, 1992; Marchessault et al., 1961; Shen et al., 2004). The

chemical shifts between peak O₂ and the side peaks O₁ and O₃ were not fixed, and the optimized values are $\Delta E_{12}=1.9 \pm 0.2$ eV and $\Delta E_{23}=2.2 \pm 0.1$ eV. These values are somewhat higher than those found in the literature ($\Delta E_{12}=1.6$ eV and $\Delta E_{23}=1.5$ eV) (Da Róz et al., 2010). Table 3 lists the results of the O 1s peak decomposition:

Table 3 Oxygen signal features related to different bonds

C=O [O ₁ %]	C-O [O ₂ %]	O-H [O ₃ %]
3.2±0.2	93.7±0.5	3.1±0.3

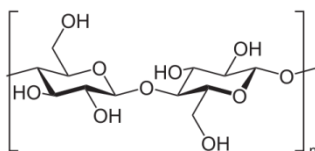


Figure 13 Cellulose monomer

The Figure 13 represents the cellulose monomer, made by two units with molecular formula $(C_6H_{10}O_5)_n$. Carbons atoms are present in two different configurations, corresponding to one (peak C₂) and two bonds (peak C₃) with oxygen with an intensity ratio of 5 to 1. The oxygen to carbon ratio should be 0.83 (Fras et al., 2005). According to Table 1, the O/C ratio in the CNs sample is 0.65 (0.63 from the detailed scans analysis, see Table 4 below), smaller than expected. Furthermore, a considerable amount of C₁ carbons (i.e. carbons without oxygen neighbors) is observed, which should not be present in pure cellulose. If we neglect the signal from C₁ peak, the oxygen to carbon ratio equals 0.73, while the C₃/C₂ ratio 0.24, in good agreement with the results obtained from the XPS analysis of spin coated cellulose fibers (see reference (Da Róz et al., 2010) for further details).

Table 4 the ratios between the peak intensities, determined from the detailed scans and corrected by the tabulated relative sensitivity factors.

O/C _{Total}	O/(C ₂ +C ₃) ^a	C ₃ /C ₂ ^a
0.63 (0.83)	0.73	0.24 (0.2)

^a Number within brackets are the expected values from bond counting arguments.

According to references (Fras et al., 2005; Johansson et al., 1999), the total amount of surface contamination on cellulose fibers due to exposure to ambient atmosphere is 2-4% of the total amount of carbon. The signal from C₁ peak thus cannot be attributed to atmospheric contamination. XPS analysis of cotton cellulose fibers (Fras et al., 2005) attribute the observed C1 peak to laminar layer of waxes, proteins and pectin, which conceal the cellulose backbone.

Reference (Fras et al., 2005) reports on the formation of acidic groups (O-C=O) upon cellulose fibers oxidation; these groups can, in principle, explain the existence of peak C₄. The determination of the exact concentration of acidic groups from the C₄ peak intensity is however not very accurate, since slight peak asymmetries in peak C₃ could, in principles, almost completely mask the presence of this side peak.

The oxygen peak of pure cellulose is expected to be composed only of O₂ species. The shoulder at lower (absolute) binding energy can be linked to the presence of acidic groups, and thus to the presence of oxidized cellulose species. The quantitative estimation of O₁ and O₃ signal is affected by some uncertainty because of the vicinity of the two peaks to peak O₂ and their low intensity.

The treatment with sulfuric acid causes the grafting of the CNs with sulfate groups (i.e. the replacement of an O-H with an O-SO₃H group) (de Mesquita et al., 2010). This explains the origin of the sulfur signal which has been detected in the wide scans. According to Table 1, the oxygen to sulfur ratio is 65:1, which means approximately 8 sulfate groups every 100 cellulose monomers.

3.3.2.4 Morphology and dimensions of CNs by TEM, SEM, AFM and mastersizer

(1) TEM

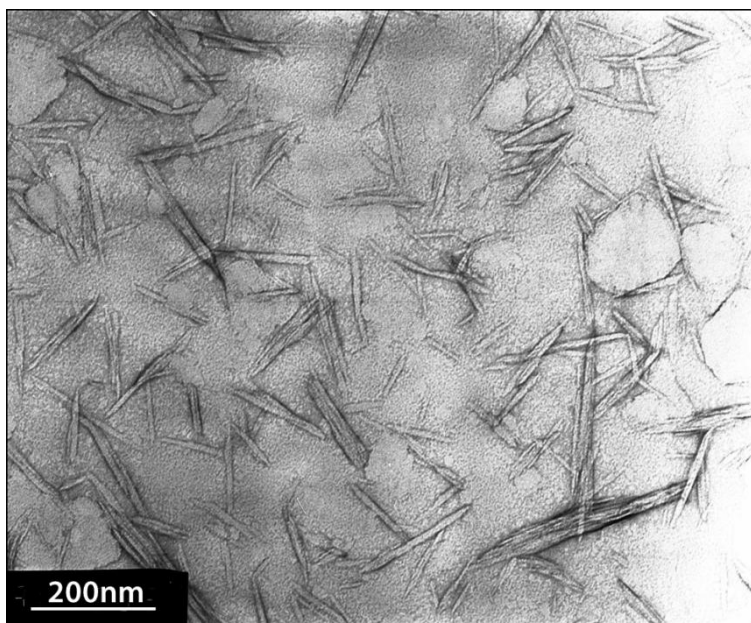


Figure 14 TEM of CNs

The rod-like CNs produced from sulfuric acid hydrolysis of cotton linters were characterized by TEM as shown in Figure 14. Observations of the CNs obtained from diluted suspensions (approximate 0.05% w/w) show individual nanocrystals and some aggregates. The appearance of aggregated elementary crystallites in TEM images is expected due to the high specific area and strong hydrogen bonds established between the CNs. From several TEM images, the mean values of the length (L) and diameter (D) of the isolated CNs were determined to be 145 ± 25 nm and 6 ± 1.5 nm, respectively, giving an aspect ratio (L/D) of around 24. These dimensions agreed well with the literature values reported for CNs (Dufresne, 2008). However, a wide distribution of CNs size, especially the length, is inevitable owing to the acid diffusion-controlled nature of the hydrolysis (Podsiadlo et al., 2005).

(2) SEM

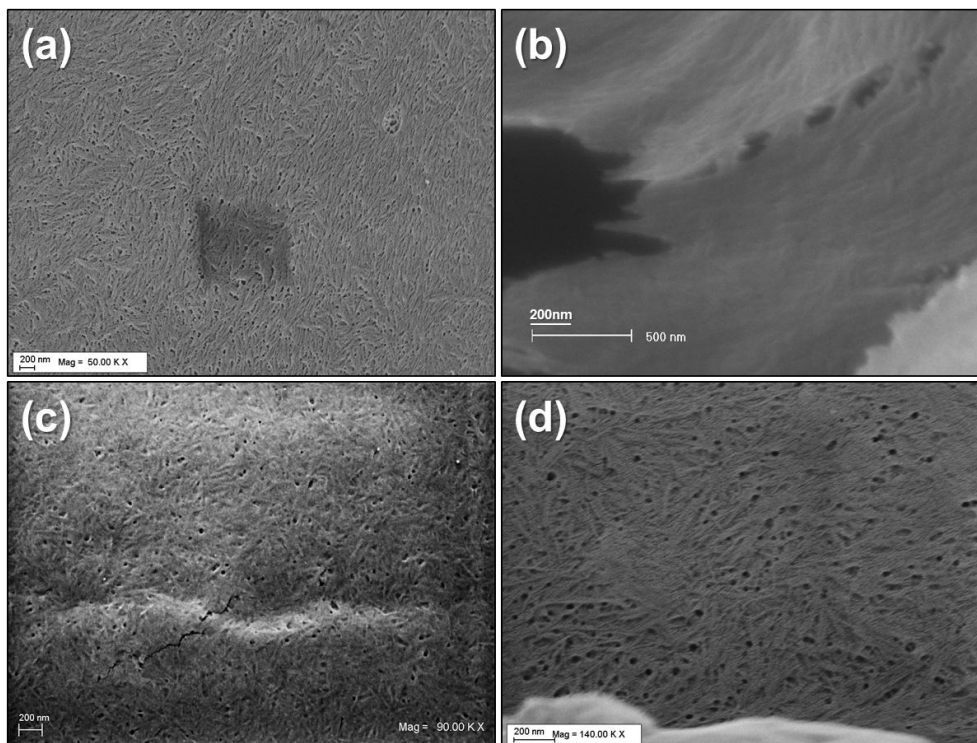


Figure 15 Freeze-dried CNs powder observed by FE-SEM (a) and E-SEM (b), CNs casting film (c), and CNs deposition on PET observed by FE-SEM (d).

The high-resolution FE-SEM or E-SEM figures of CNs freeze-dried powder, casting film, and deposition are presented in Figure 15. The image clearly shows highly dense packing and uniform nanofibers likely due to the hydrogen bonds formed during the drying process. The dense packing of the CNs has been previously described in other reports (Podsiadlo et al., 2005).

Meanwhile, the morphologies of CNs network present the porous surfaces, which probably will have some influences on the final properties, such as gas barrier. It was reported that different porosities, caused by diverse original cellulose sources, led to significantly distinct gas barrier properties (Fukuzumi et al., 2011). The SEM figures could be only used to estimate the profile and dimension of CNs, since the CNs real morphology is covered by gold particles which is used to make the CNs more conductive for better resolution observations.

(3) AFM

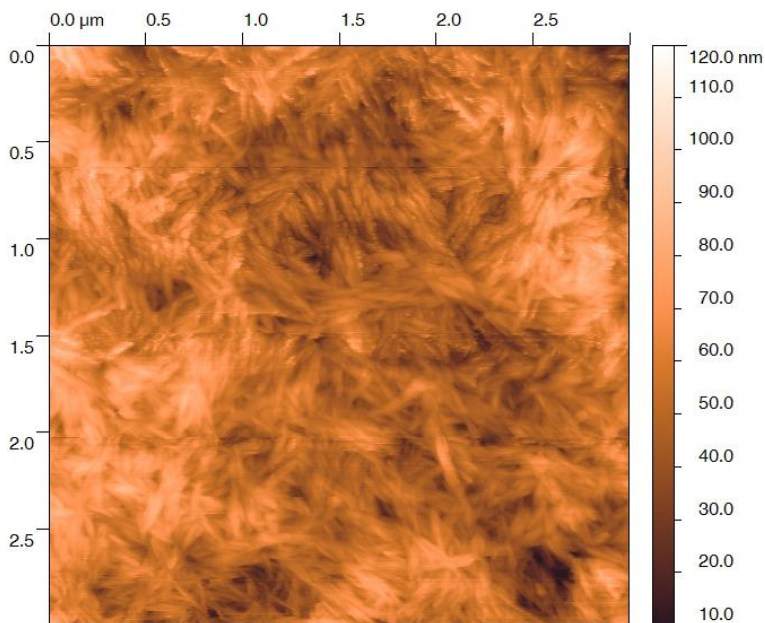


Figure 16 High-resolution AFM of CNs deposition on OPA substrate

The bundles of CNs are shown in Figure 16. The CNs are clearly presented but majority of them are swelling and aggregating each other, since the deposition originates from 3.5% (w/w) CNs dispersion and then was dried by air dryer. The air drying step results in the aggregating via strong hydrogen bonds and swelling phenomena was caused by the small water content in CNs deposition. This AFM figure might not therefore indicate the exact dimension of CNs, but it could reveal the profile (shape) of CNs. In this case, the shape of CNs is clearly rod like, highly agreement with other reports (Edgar & Gray, 2003; Lefebvre & Gray, 2005).

(4) CNs size distribution

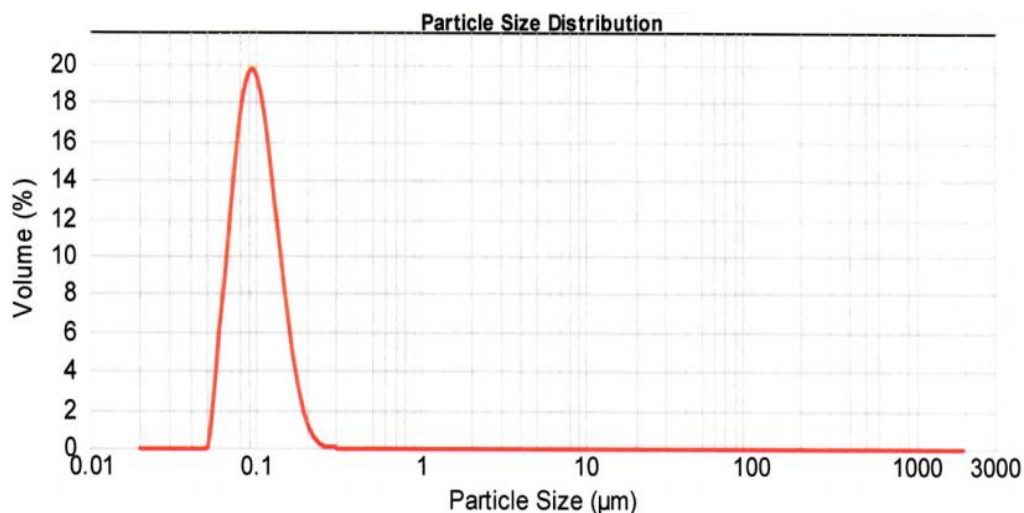


Figure 17 Particle size distribution of 1% CNs dispersion

The particle size distribution of 1% CNs dispersion is shown in Figure 17. It indicates that the range of the CNs length is from 90 to 160 nm, which is similar with the most precise results obtained from TEM and other literatures (Habibi et al., 2010). Compared with TEM-CN's dimension, the one from particle size distribution has larger range. It is reasonable that larger ranges are due to different forms of CNs. Since the working range of this instrument (Mastersizer 2000) is from 0.020 to 2000.00 µm, the average of CNs diameter (~6 nm), which is beyond, the work range could not be obtained from Figure 17. The results disclose that the acidic hydrolysis process is highly compatible and effective to extract relatively uniform CNs from cotton linter, because this measurement was carried out for size distribution of dispersion not only limited to local dimensions.

The dimension of CNs was determined by different advanced techniques, including TEM, FE-/E-SEM, AFM, and particle size distributor, respectively. In our case, the most efficient and illustrative method is TEM, since the dimension (diameter and length) are easily obtained from high resolution figures. But for TEM, the limitations are related with small observation area (highly locally dependent) and vacuum working condition which sometimes leads to agglomeration and change the original morphology of samples. For example, the CNs are strongly aggregated with each other under the vacuum due to the hydrogen bonds (Habibi et al., 2010). As for the SEM, all of observations could be carried out under vacuum and it is more suitable for the surface morphology of samples at relatively larger scale. FE-SEM could provide high-resolution images even at small scale but the conductive samples and vacuum condition

are required, while E-SEM could observe samples under ambient condition and no requirements for samples. For AFM, it is a very powerful tool for observations and no special requirements for samples and testing conditions. Through AFM, the dimension and morphology could be gained easily and efficiently even at larger scale. The dimension for AFM from figure is not as accurate as the one from TEM and particle size distributor, since the CNs were aggregated with each other in the deposition and influenced by surroundings, such as temperature, humidity and so on. To obtain precise dimension of CNs, it is suggested that relatively lower concentration of CNs dispersion should be prepared for TEM and particle size distributor.

3.4 Conclusions 1

To better understand the structure and status of CNs itself or in other polymers, we used different powerful tools for qualification and quantification. Firstly, we have obtained the relatively precise dimensions of CNs and observe its re-dispersability in different solvents, in our case in water. In the following, we could gain the information of the CNs status in other polymers in order to interpret the final performance efficiently. Finally, if we observe individual crystals, TEM is the most suitable tool; if we estimate the roughness, AFM is the most efficient tool; if we generally learn the morphology in different scale, the SEM is the best choice. As for the size distribution, functional groups, and interactions between the atoms of CNs, the particle size distributor, FTIR, XPS, and NMR are used for determinations, respectively.

3.5 References

- Anglès, M. N., Dufresne, A., 2001, Plasticized Starch/Tunicin Whiskers Nanocomposite Materials. 2. Mechanical Behavior. *Macromolecules* 34: 2921-2931.
- Araki, J. et al., 1998, Flow properties of microcrystalline cellulose suspension prepared by acid treatment of native cellulose. *Colloids and Surfaces A: Physicochemical and Engineering Aspects* 142: 75-82.
- Atalla, R. H., VanderHart, D. L., 1999, The role of solid state ^{13}C NMR spectroscopy in studies of the nature of native celluloses. *Solid State Nuclear Magnetic Resonance* 15: 1-19.
- Beamson, G., Briggs, D. High resolution XPS of organic polymers: the Scienta ESCA300 database. Chichester [England]; New York: Wiley, 1992, pp. 120-130.
- Beck-Candanedo, S. et al., 2005, Effect of Reaction Conditions on the Properties and Behavior of Wood Cellulose Nanocrystal Suspensions. *Biomacromolecules* 6: 1048-1054.
- Beck, S. et al., 2012, Dispersibility in water of dried nanocrystalline cellulose. *Biomacromolecules* 13: 1486-1494.
- Bergenstrahle, M. et al., 2008, Dynamics of Cellulose–Water Interfaces: NMR Spin–Lattice Relaxation Times Calculated from Atomistic Computer Simulations. *The Journal of Physical Chemistry B* 112: 2590-2595.
- Bondeson, D. et al., 2006, Optimization of the isolation of nanocrystals from microcrystalline cellulose by acid hydrolysis. *Cellulose* 13: 171-180.
- Da Róz, A. L. et al., 2010, Adsorption of chitosan on spin-coated cellulose films. *Carbohydrate Polymers* 80: 65-70.
- de Mesquita, J. P. et al., 2010, Biobased Nanocomposites from Layer-by-Layer Assembly of Cellulose Nanowhiskers with Chitosan. *Biomacromolecules* 11: 473-480.
- de Souza Lima, M. M., Borsali, R., 2002, Static and Dynamic Light Scattering from Polyelectrolyte Microcrystal Cellulose. *Langmuir* 18: 992-996.
- de Souza Lima, M. M. et al., 2002, Translational and Rotational Dynamics of Rodlike Cellulose Whiskers. *Langmuir* 19: 24-29.
- Dong, X. M. et al., 1998, Effect of microcrystallite preparation conditions on the formation of colloid crystals of cellulose. *Cellulose* 5: 19-32.
- Dufresne, A., 2008, Polysaccharide nano crystal reinforced nanocomposites. *Canadian Journal of Chemistry* 86: 484-494.
- Edgar, C. D., Gray, D. G., 2003, Smooth model cellulose I surfaces from nanocrystal suspensions. *Cellulose* 10: 299-306.
- Eichhorn, S. J. et al., 2004, Modeling Crystal and Molecular Deformation in Regenerated Cellulose Fibers. *Biomacromolecules* 6: 507-513.
- Elazzouzi-Hafraoui, S. et al., 2007, The Shape and Size Distribution of Crystalline Nanoparticles Prepared by Acid Hydrolysis of Native Cellulose. *Biomacromolecules* 9: 57-65.

- Favier, V. et al., 1995, Polymer Nanocomposites Reinforced by Cellulose Whiskers. *Macromolecules* 28: 6365-6367.
- Fras, L. et al., 2005, Analysis of the oxidation of cellulose fibres by titration and XPS. *Colloids and Surfaces A: Physicochemical and Engineering Aspects* 260: 101-108.
- Fukuzumi, H. et al., 2011, Pore Size Determination of TEMPO-Oxidized Cellulose Nanofibril Films by Positron Annihilation Lifetime Spectroscopy. *Biomacromolecules* 12: 4057-4062.
- Grunert, M., Winter, W. T., 2002, Nanocomposites of Cellulose Acetate Butyrate Reinforced with Cellulose Nanocrystals. *Journal of Polymers and the Environment* 10: 27-30.
- Håkansson, H., Ahlgren, P., 2005, Acid hydrolysis of some industrial pulps: effect of hydrolysis conditions and raw material. *Cellulose* 12: 177-183.
- Habibi, Y. et al., 2010, Cellulose Nanocrystals: Chemistry, Self-Assembly, and Applications. *Chemical Reviews* 110: 3479-3500.
- Habibi, Y. et al., 2008, Bionanocomposites based on poly(ϵ -caprolactone)-grafted cellulose nanocrystals by ring-opening polymerization. *Journal of Materials Chemistry* 18: 5002-5010.
- Habibi, Y. et al., 2009, Microfibrillated cellulose from the peel of prickly pear fruits. *Food Chemistry* 115: 423-429.
- Hanley, S. et al., 1997, Atomic force microscopy and transmission electron microscopy of cellulose from *Micrasterias denticulata*; evidence for a chiral helical microfibril twist. *Cellulose* 4: 209-220.
- Hanley, S. J. et al., 1992, Atomic force microscopy of cellulose microfibrils: comparison with transmission electron microscopy. *Polymer* 33: 4639-4642.
- Hemminger, C. S. et al., 1990, An empirical electron spectrometer transmission function for applications in quantitative XPS. *Surface and Interface Analysis* 15: 323-327.
- Imai, T. et al., 1998, Unidirectional processive action of cellobiohydrolase Cel7A on *Valonia* cellulose microcrystals. *FEBS Letters* 432: 113-116.
- Johansson, L.-S. et al., 1999, Evaluation of surface lignin on cellulose fibers with XPS. *Applied Surface Science* 144-145: 92-95.
- Koch, F.-T. et al., 2000, Calculation of solid-state ^{13}C NMR spectra of cellulose I α , I β and II using a semi-empirical approach and molecular dynamics. *Macromolecular Chemistry and Physics* 201: 1930-1939.
- Kovacs, T. et al., 2010, An ecotoxicological characterization of nanocrystalline cellulose (NCC). *Nanotoxicology* 4: 255-270.
- Kvien, I. et al., 2005, Characterization of Cellulose Whiskers and Their Nanocomposites by Atomic Force and Electron Microscopy. *Biomacromolecules* 6: 3160-3165.
- Larsson, P. T. (2003). Interaction between Cellulose I and Hemicelluloses Studied by Spectral Fitting of CP/MAS ^{13}C -NMR Spectra. *Hemicelluloses: Science and Technology* (Vol. 864, pp.

254-268): American Chemical Society.

Lefebvre, J., Gray, D. G., 2005, AFM of adsorbed polyelectrolytes on cellulose I surfaces spin-coated on silicon wafers. *Cellulose* 12: 127-134.

Li, Q. et al., 2009, Structure and properties of the nanocomposite films of chitosan reinforced with cellulose whiskers. *Journal of Polymer Science Part B: Polymer Physics* 47: 1069-1077.

Marchessault, R. H. et al., 1961, Some hydrodynamic properties of neutral suspensions of cellulose crystallites as related to size and shape. *Journal of Colloid Science* 16: 327-344.

Miller, A. F., Donald, A. M., 2003, Imaging of Anisotropic Cellulose Suspensions Using Environmental Scanning Electron Microscopy. *Biomacromolecules* 4: 510-517.

Nickerson, R. F., Habrle, J. A., 1947, Cellulose Intercrystalline Structure. *Industrial & Engineering Chemistry* 39: 1507-1512.

Nishiyama, Y. et al., 2008, Neutron Crystallography, Molecular Dynamics, and Quantum Mechanics Studies of the Nature of Hydrogen Bonding in Cellulose I β . *Biomacromolecules* 9: 3133-3140.

Nogi, M. et al., 2009, Optically Transparent Nanofiber Paper. *Advanced Materials* 21: 1595-1598.

Pines, A. et al., 1973, Proton-enhanced NMR of dilute spins in solids. *The Journal of Chemical Physics* 59: 569-590.

Podsiadlo, P. et al., 2005, Molecularly Engineered Nanocomposites: Layer-by-Layer Assembly of Cellulose Nanocrystals. *Biomacromolecules* 6: 2914-2918.

Powell, C. J., 1988, The quest for universal curves to describe the surface sensitivity of electron spectroscopies. *Journal of Electron Spectroscopy and Related Phenomena* 47: 197-214.

Reilman, R. F. et al., 1976, Relative intensities in photoelectron spectroscopy of atoms and molecules. *Journal of Electron Spectroscopy and Related Phenomena* 8: 389-394.

Roman, M., Winter, W. T., 2004, Effect of Sulfate Groups from Sulfuric Acid Hydrolysis on the Thermal Degradation Behavior of Bacterial Cellulose. *Biomacromolecules* 5: 1671-1677.

Shen, G. et al., 2004, X-ray photoelectron spectroscopy and infrared spectroscopy study of maleimide-activated supports for immobilization of oligodeoxyribonucleotides. *Nucleic Acids Research* 32: 5973-5980.

Šturcová A. et al., 2005, Elastic Modulus and Stress-Transfer Properties of Tunicate Cellulose Whiskers. *Biomacromolecules* 6: 1055-1061.

Viet, D. et al., 2007, Dispersion of cellulose nanocrystals in polar organic solvents. *Cellulose* 14: 109-113.

Witter, R. et al., 2006, ^{13}C Chemical Shift Constrained Crystal Structure Refinement of Cellulose I α and Its Verification by NMR Anisotropy Experiments. *Macromolecules* 39: 6125-6132.

Yang, J. Z. et al., 2011, Biotemplated preparation of CdS nanoparticles/bacterial cellulose

hybrid nanofibers for photocatalysis application. *Journal of Hazardous Materials* 189: 377-383.
Yano, H. et al., 2005, Optically Transparent Composites Reinforced with Networks of Bacterial Nanofibers. *Advanced Materials* 17: 153-155.

3.6 Topic/theme 2: Multi-functional green coating of cellulose nanocrystals (CNs) on conventional films for food packaging applications

Introduction

Nowadays, the vast majority of flexible food packaging materials is constituted of oil-based plastics whose resources are non-renewable, resulting in low sustainability. Considering the issues, the interest in bio-based materials have been rising, such as poly lactic acid (PLA) (Auras et al., 2004; Drumright et al., 2000; Lim et al., 2008; Vert et al., 1995), starch, (Avella et al., 2005; Tharanathan, 2003) and so on. However, such materials are not yet widely applied because of their inferior properties (Krikorian & Pochan, 2003; Ray et al., 2002, 2003) and high cost, compared with conventional ones. Therefore, it is likely that there will be a long journey for substituting bio-based materials for conventional plastics.

The use of plastic materials also poses a challenge in finding appropriate strategies to improve their barrier properties. In current research, inorganic fillers, such as SiO₂ (Creatore et al., 2002; Erlat et al., 1999; Haas et al., 1999) or nano-clays (Ghasemi et al., 2012; Priolo et al., 2010; Sánchez-Valdes et al., 2006; Svagan et al., 2012) are used for coatings or composites as oxygen or water vapor barriers with inevitable disadvantages that include a tendency to crack, (Priolo et al., 2010) and potential health risks (Lordan et al., 2011). Therefore, there is an increasing tendency to at least partially replace conventional plastics with bio-based materials, for instance, utilizing bio-coatings with the two-fold aim of improving the original plastic properties and reducing the plastic use, thereby, increasing the sustainability. Bio-coatings can, therefore, be considered as one of the suitable solutions for food packaging applications. Nevertheless, the number of directly related bio-coating publications is still limited. Gelation (Farris et al., 2009), or pullulan (Farris et al., 2012) have been recently reported as oxygen barriers on PET or OPP plastic films. Isoga *et al.* (Kato et al., 2005) compared the oxygen barrier properties of 12 µm-thick PET films coated by TEMPO-oxidized microcrystalline cellulose, chitosan and starch, whilst TEMPO-oxidized nano-fiber coatings have been demonstrated as an oxygen barrier on PLA film (Fukuzumi et al., 2008). Besides cast coating, some research groups successfully improved barrier properties of food packaging materials through layer-by-layer (LbL) assembly (de Mesquita et al., 2010; Jang et al., 2008; Priolo et al., 2010; Svagan et al., 2012; Yang et al., 2011b; Zhang & Sun, 2010). However, TEMPO-oxidized and LbL coating process might be difficult to be applied at the industrial scale due to their safety, cost and process complexity.

In this part of the PhD thesis, we thoroughly investigate the physical, mechanical, and optical properties of bio-coating made of cellulose nanocrystals (CNs), which can be obtained from the

most abundant natural polymer on earth. Besides the promising results that are discussed throughout the paper, such material brings advantages also in terms of low weight, low cost, and biodegradability. Over the last few years, CNs have been extracted from different original sources by chemical, physical, enzymatic or a combination of them (Siro & Plackett, 2010). However, physical and enzymatic processes imply high cost and high energy consumption, respectively, hence we choose a chemical-hydrolysis method for their production from cotton linter, whose thorough characterization has been the focus of the first part of this project, and we deposit them on different conventional flexible food packaging materials to produce a multi-functional coating. In particular, we use a water dispersion of CNs, with relatively low concentration, deposited on polyethylene terephthalate (PET), oriented polypropylene (OPP), oriented polyamide (OPA) and cellophane films. The morphology, coefficient of friction, anti-fog, and oxygen and water vapor barrier properties of coated films were measured and interpreted systematically.

3.7 Materials and methods 2

3.7.1 Materials.

Cotton linter was provided by S.S.C.C.P. (Milan, Italy), as the raw material to produce CNs.

Four different plastic substrates were coated and used for experiments: (1) poly(ethylene terephthalate) (PET, 12.0 ± 0.5 μm thickness, Radici Film, San Giorgio di Nogaro, Italy), (2) oriented polypropylene (OPP, 20 ± 0.5 μm thickness, San Giorgio di Nogaro, Italy), (3) oriented polyamide (OPA, 12 ± 0.5 μm thickness, San Giorgio di Nogaro, Italy), and cellophane (12 ± 0.5 μm thickness, San Giorgio di Nogaro, Italy).

3.7.2 CNs producing process.

As described in 3.1, the brief process of producing CNs is as follow. 1% Cellulose nanocrystals (CNs) dispersion was produced from cotton linter using a procedure already established for cotton from powdered filter paper (Dong et al., 1998). Briefly, milled cotton linter was hydrolyzed by 64% (w/w) sulfuric acid with vigorous stirring at 45 °C for 45 minutes. The reaction mixture was diluted with 10 times-volume deionized water (resistivity, 18.2 M Ω cm, Millipore Milli-Q Purification System), settled for 2 hours, and then rinsed and centrifuged at 5000 rpm repeatedly until the supernatant became turbid. Further purification was then done by dialysis against deionized water until the effluent remained at neutral pH (MWCO 12 000 and higher). Sequentially, the suspension was sonicated (UP400S 400 W, Hielscher Co., Germany) repeatedly (0.7 cycles of 5 min at 70% output) to create cellulose crystals of colloidal dimensions. Finally, the suspension was filtered under vacuum with MukteLL (grade GF/C, 1.2 μm pore diameter) and Whatman glass microfiber filter (grade GF/F, 0.7 μm pore diameter) to remove contamination and big aggregations. The CNs content of the resulting aqueous suspension was determined by drying several samples (1 ml) at 105 °C for 15 min intervals (to avoid decomposition or burning) until weight constancy, giving a cellulose concentration of ~1 % w/w and a yield of ~50%. To prepare a given concentration of CNs solution, the resulting CNs dispersion was adjusted pH to ~7 by 1M NaOH(aq), freeze-dried and stored in tightly sealed container under dry conditions for later analysis and experiments.

3.7.3 Preparation of Coating Dispersion.

A 3.5 wt% CNs water dispersion was obtained by dissolving the CNs into distilled water assisted with ultrasonic treatments until the dispersion became visually homogenous. During the process, the sonication should be carried out every ten minute under water bath to avoid overheating. After recovering to room temperature, the CNs dispersion was coated on different plastic substrates.

3.7.4 Coated Film Preparation.

According to ASTM D823-07, practice C, the corona-treated sides of rectangular ($25 \times 20 \text{ cm}^2$) four different plastic films were coated by an automatic film applicator (ref 1137, Sheen Instruments, Kingston, U.K., shown in Figure 18) at a constant speed of 2.5 mm s^{-1} . In this work, the 24 μm bar was used for coatings on different substrates, whose final thickness is ca. 0.6 μm . It is noticed that the horizontal flat is one of the most important factors to obtain homogenous CNs coating. Water was evaporated using a constant mild flowing air ($25 \pm 0.3 \text{ }^\circ\text{C}$ for 5 min) at a perpendicular distance of 40 cm from the automatic applicator. The coated films were stored under controlled conditions ($20 \pm 2 \text{ }^\circ\text{C}$, $45 \pm 2.0\% \text{ RH}$) for 24 h, and then stored in sealed anhydrous desiccators for 24 h before analysis.



Figure 18 Automatic applicator

3.7.5 Thickness measurement

For the coating thickness measurement, a $10 \times 10 \text{ cm}^2$ sample (plastic substrate with coating) was cut and weighed (m_1 , g). The coating was removed by running hot water ($\sim 70 \text{ }^\circ\text{C}$), and then the resulting bare film was weighed (m_2 , g). The coating thickness (L , μm) was obtained according to the following equation:

$$L = \frac{m_1 - m_2}{\rho} \times 100 \quad (1)$$

where ρ (g cm^{-3}) is the density of CNs ($\sim 1.58 \text{ g cm}^{-3}$) (Mazeau & Heux, 2003). Three replications were determined.

3.7.6 Transmission Electron Microscopy.

Drops of aqueous dispersions of CNs (0.05% w/v) were deposited on carbon-coated electron microscope grids, negatively stained with uranyl acetate and allowed to dry. The samples were analyzed with a Hitachi Jeol-10084 transmission electron microscope (TEM) operated at an accelerating voltage of 80 kV.

3.7.7 Atomic force microscopy

Atomic-force microscopy (AFM) topography images have been acquired in tapping mode with a Veeco Innova instrument. Super-sharp silicon probes (typical radius of curvature 2 nm) have been used for high-resolution imaging of nanocrystals, while standard silicon probes have been employed for large-area scans in order to evaluate the sample roughness.

The root mean square roughness S is calculated as the standard deviation of the topography ($M \times N$ pixels):

$$S = \sqrt{\frac{1}{MN} \sum_{i=1}^M \sum_{j=1}^N |z(x_i, y_j) - \bar{z}|^2}, \quad (2)$$

where \bar{z} is the mean value of the topography $z(x, y)$.

3.7.8 Transparency measurements

The transmittance of the sample was measured at a wavelength of 550 nm, according to the ASTM D 1746-70, by means of a Perkin-Elmer L650 spectro-photometer.

3.7.9 Haze

Haze was measured in accordance with ASTM D 1003-61 with spectrophotometer (Perkin Elmer L650). The haze values of uncoated and coated films were obtained as (Lee et al., 2008):

$$\text{haze} = 100 \times \frac{I_s}{I_T}, \quad (3)$$

where I_s and I_T are the scattered and total transmitted light, respectively.

3.7.10 Oxygen Transmission Rate (OTR), oxygen permeability (P_{O_2}) and Water Vapor Transmission Rate (WVTR) measurements.

The OTR and WVTR of CNs coated plastic films were tested by permeation instrument

(MOCON, OX-TRAN[®] Model 702 and PERMATRAN-W[®] Model 700) under the 23 °C and 0% relative humidity(RH) for OTR and 38 °C and 90% RH for WVTR, complying with ASTM D-3985, F-1927, F-1307 (OTR) and ASTM F-1249 (WVTR), respectively.

The P_{O₂} of the CNs coating in the coated film [i.e., P_{O₂} (Coating)] was calculated using the following equation (Lee et al., 2008):

$$\frac{1}{P_{O_2}(\text{coated A - PET})} = \frac{1}{P_{O_2}(\text{coating})} + \frac{1}{P_{O_2}(\text{A - PET})}$$

3.7.11 Contact angle measurements

Contact angles were measured to estimate the surface energies of the tested substrates by OCA 15 Plus angle goniometer (Data Physics Instruments GmbH, Filderstadt, Germany). The softwares (SCA20 and SCA21) delivered by the instrument manufacturer calculates the contact angles on the basis of a numerical solution of the full Young-Laplace equation and surface energy. Measurements of static and advancing contact angle were performed at room temperature with three liquids: two polar: Milli-Q water and formamide (FOM, ≥99.5%, Carlo Erba, Milan); one apolar diiodomethane (DIM, 99%, Sigma Aldrich) at minimal five different positions on each sample. The surface energies were calculated from the contact angle data at equilibrium by the Van Oss method (Van Oss, 2006), which divides the total surface free energy into two components, the dispersive and the polar components, where the polar interactions originate from the Lewis acid-base interactions

$$\gamma_s^{total} = \gamma_s^D + \gamma_s^P \quad (4)$$

where

$$\gamma_s^P = 2\sqrt{\gamma_s^+ \gamma_s^-} \quad (5)$$

The subscripts indicate the solid, s, or liquid, l, phase, and γ_s^{LW} and γ_s^{AB} refer to the dispersive and polar components of the total surface energy, respectively. γ^+ is the acceptor and γ^- the donor part of the Lewis acid-base interactions.

When combined with Young's equation, the equations developed by Chaudhury, Good, and Van Oss yield the equation

$$\gamma_l(1 + \cos\theta) = 2(\sqrt{\gamma_l^D \gamma_s^D} + \sqrt{\gamma_s^+ \gamma_l^-} + \sqrt{\gamma_s^- \gamma_l^+}) \quad (6)$$

Where, θ is contact angle (°), γ_l is the liquid surface tension (mJ/m²), and γ_s^+ , γ_l^- and γ_s^- , γ_l^+ are the acid and base contributions to the surface energies of the solid and liquid, respectively (mJ/m²). The values of the surface tension and its components for the liquids that were used in calculations were determined by Van Oss (van Oss, 2003). Water, formamide, and

diiodomethane, with known γ_l^D , γ_l^+ , and γ_l^- values (Table 5), and measured contact angle (θ) were used to determine the γ_s^D , γ_s^+ , and γ_s^- combined with Equation (6). Finally, γ_s^{total} and γ_s^P were calculated from Equation (4) and (5).

Table 5 Surface tension components and parameters of liquids used in direct contact angle determination in mJ/m², at 20 °C (Van Oss, 2006)

Liquid	γ_l	γ_l^D	γ_l^P	γ_l^+	γ_l^-
APOLAR					
Diiodomethane	50.8	50.8	0	≈0	0
POLAR					
Water	72.8	21.8	51.0	25.5	25.5
Formamide	58.0	39.0	19.0	2.28	39.6

3.7.12 Coefficient of friction.

The static (μ_s) and kinetic (μ_d) friction coefficients were measured by a dynamometer (model Z005, Zwick Roell, Ulm, Germany), in accordance with the standard method ASTM D 1894-87. The software TestXpert V10.11 (Zwick Roell, Ulm, Germany) Master was used for data analysis. 5 replications for each sample.

3.8 Results and discussion 2

3.8.1 Morphology of CNs and CNs on different substrates

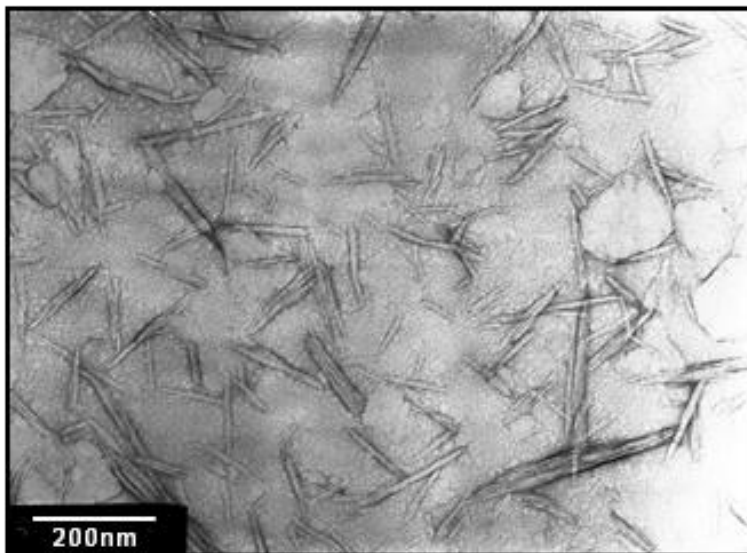


Figure 19 TEM image of individual CNs

The rod-like CNs produced from sulfuric acid hydrolysis of cotton linters were characterized by TEM as shown in Figure 19. CNs observations obtained from diluted dispersion (approximate 0.05% w/w) show individual nanocrystals and some aggregates. The appearance of aggregated elementary crystallites in TEM images is expected due to the high specific area and strong hydrogen bonds established between the CNs. From several TEM images, the mean values of the length (L) and diameter (d) of the isolated CNs were determined to be 150 ± 30 nm and 6 ± 3 nm, respectively, giving an aspect ratio (L/d) ~ 25 . Similar dimensions have been reported in the literatures (Angles & Dufresne, 2000; Elazzouzi-Hafraoui et al., 2007). However, a wide distribution of CNs size, especially of their length, is inevitable owing to the acid diffusion-controlled nature of the hydrolysis (de Mesquita et al., 2010). It means that from the molecular level point of view, the diffusion of sulfuric acid is relatively inhomogeneous which results in the different hydrolysis degree of cotton linter, thereby leads to a relatively wide distribution of CNs size. The size distribution was presented in 3.3.2.4 (4).

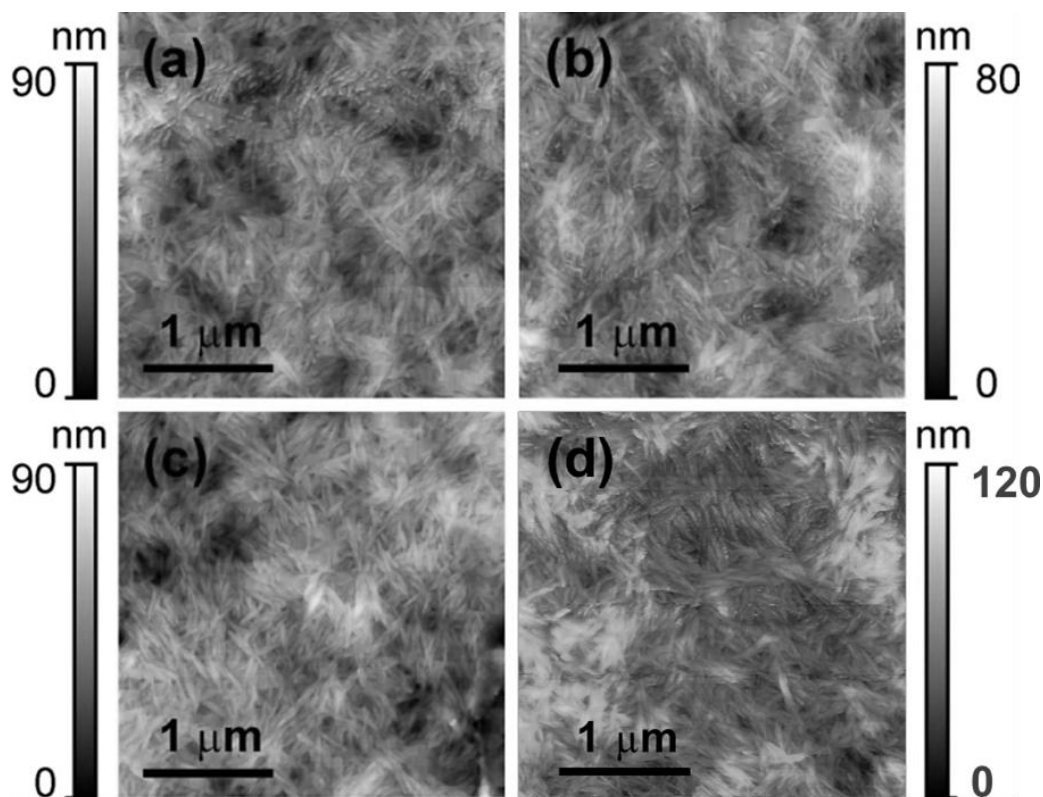


Figure 20 High-resolution AFM images of CNs-coated films, coated PET (a), OPP (b), cellophane (c), and OPA (d).

Figure 20 shows high-resolution AFM images of CNs-coated films. The image clearly shows a dense packing and uniform coverage of nanofibers. A dense packing of CNs has been previously described in other reports (Fujisawa et al., 2011). The continuous layer of overlapping CNs fibers (Siró & Plackett, 2010) points towards possible improvements in the oxygen barrier properties of the different substrates, which we will demonstrate and discuss later on.

3.8.2 Coefficient of friction of bare and coated substrates

The values for the coefficient of friction (COF) of CNs-coated films against films are presented in Table 6. By means of the statistical analysis, we conclude that the casting deposition created a completely new CNs-coating layer on different substrates with one exception. In fact, it can be clearly noted that three of the investigated systems (coated-PET, OPA, and cellophane) present similar values in dynamic (μ_d) COFs, while only CNs-coated OPP is significantly different from the other coated films probably due to weak adhesion between CNs coating and OPP surface

which leads to the removal of CNs from substrate during dynamic measurements. The COF results and oxygen permeability shown later indicate that for 600 nm CNs coating, a homogenous independent CNs layer was established by cast coating.

Table 6 Plastic films (Ex) against plastic film (In)

Substrate	Bare (Ex)		Coated (600 nm ^a)	
	μ_s	μ_d	μ_s	μ_d
PET	0.57±0.02 ^D	0.52±0.03 ^H	0.38±0.01 ^C	0.33±0.01 ^G
OPP	0.18±0.01 ^A	0.17±0.00 ^F	0.30±0.02 ^B	0.18±0.01 ^F
OPA	0.79±0.02 ^E	0.74±0.03 ^J	0.32±0.01 ^{BC}	0.32±0.02 ^G
Cellophane	0.62±0.03 ^D	0.57±0.01 ^I	0.38±0.02 ^C	0.34±0.01 ^G

^a Thickness of CNs coating

^A to ^E, different letters mean that static COFs are significantly different ($p < 0.01$);

^F to ^J, different letters mean that dynamic COFs are significantly different ($p < 0.01$).

Table 7 Roughness of bare and coated substrates

Substrates	PET			OPP			Cellophane			OPA		
	Bare		Coate	Bare		Coate	Bare		Coate	Bare		Coate
	Ex	In		Ex	In		Ex	In		Ex	In	
10×10 μm^2	a	b	d	a	b	d	a	b	d	a	b	d
Roughness (nm)	10	3	6	2	7	6	4	2	13	21	8	11

^a External side of substrates, which generally were treated by corona;

^b Internal side of substrates, which usually were not treated.

In order to complement the COF data with those for the sample roughness, we acquired large-area AFM images, as shown in Figure 21, where cobble stone pathway like aggregations of CNs where cobble-stone pathway-like aggregations of CNs due to the strong hydrogen bonds are visible in all images, which are qualitatively very similar with each other. Roughness values calculated from such AFM investigations all lay in the 6-13 nm range (see Table 7), which is definitely lower than the one of bare films from 2-21 nm (external side). We therefore could conclude that a new CNs layer was homogeneously established on different substrates.

Generally speaking, CNs coating could result in improvements of practical applications, reduction of friction between the films, which probably lead to a premium feature for industrial applications.

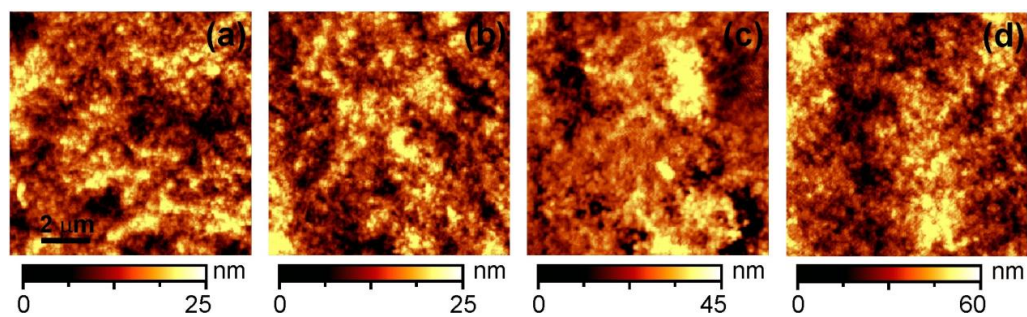


Figure 21 AFM for roughness of coated substrates, coated PET (a), OPP (b), OPA (c), and cellophane (d).

3.8.3 Optical properties

Table 8 Transparency at 550 nm and haze of bare and CNs-coated films

Substrates	Transparency (%)		Haze (%)	
	Bare	CNs-coated	Bare	CNs-coated
PET	88.0±0.2	89.4±0.2	2.7±0.1	5.1±0.2
OPP	91.9±0.0	91.3±0.2	2.9±0.1	5.2±0.2
OPA	89.7±0.3	90.3±0.1	4.1±0.1	6.2±1.0
Cellophane	87.6±0.2	88.5±0.4	4.3±0.1	5.8±0.1

Regarding the optical properties of CNs-coated films, results from transparency and haze measurements in Table 8 show that the CNs-coated films still maintain high transparency, as requested to ensure easy evaluation of the product quality by eye inspection. The excellent optical properties are attributed to the thin CNs coating (around 600 nm, as determined by weighting the samples). Nevertheless, small reduction and increase of the transparency and haze values, respectively, are due to the nano-scale dimensions of CNs. Moreover, it is noticed that the transmittance values at 300 nm reduced by 10% with CNs-OPP film, which indicates that CNs coating slightly decrease the UV light.

3.8.4 Anti-fog property

Boiling water and breathe (Huff) tests both showed that the CNs-coated films have excellent anti-fog property, which are presented in Figure 22(b). Particularly, we deposited 3.5% CNs directly on different substrates without any primers or any chemicals to guarantee the safety of food contact. In Figure 22 we show the results for the coated OPP film, since OPP it is the most hydrophobic material among the substrates under investigation, but very similar results were obtained for all the substrates. We observed the border (the blue dashed line) between bare and

coated films through the fog from our eye inspection. In order to observe the anti-fog property better, we set a black sponge in the water containers, as shown in Figure 22. As known, fog is formed by small discontinuous water droplets which could reflect the incident light, thereby decrease the transparency and increase the haze (Introzzi et al., 2012; Nuraje et al., 2010). Figure 22(a) and (c) obtained from optical microscopy, presents two parts, uncoated part with water droplets which forms fog and coated part homogeneous water layer without any droplets, which remained transparent. In the following part, we will further interpret the excellent anti-fog of CNs-coated films from the comparison of surface energies obtained from contact angle goniometry.

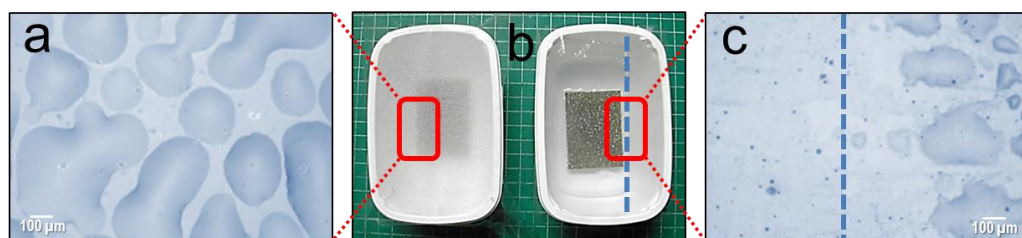


Figure 22 Boiling water test; the foggy bare OPP photo from optical microscope, (a); comparison of bare and CNs-coated OPP during the test, (b); the border between CNs-coated and bare parts taken from optical microscope, (c).

Table 9a Static contact angles of bare and CNs-coated films

Films	Static CA ^a		
	$\theta_{\text{Water}}(^{\circ})$	$\theta_{\text{DIM}}(^{\circ})^{\text{b}}$	$\theta_{\text{FOM}}(^{\circ})^{\text{b}}$
Bare PET	57.44±5.84	22.41±2.73	39.55±1.77
Bare OPP	63.03±1.00	52.22±1.61	41.39±1.70
CNs-PET	12.32±1.33	37.15±3.02	7.41±1.33
CNs-OPP	12.08±0.95	36.37±1.70	8.78±0.73

Table 9b Advancing contact angles of bare and CNs-coated films

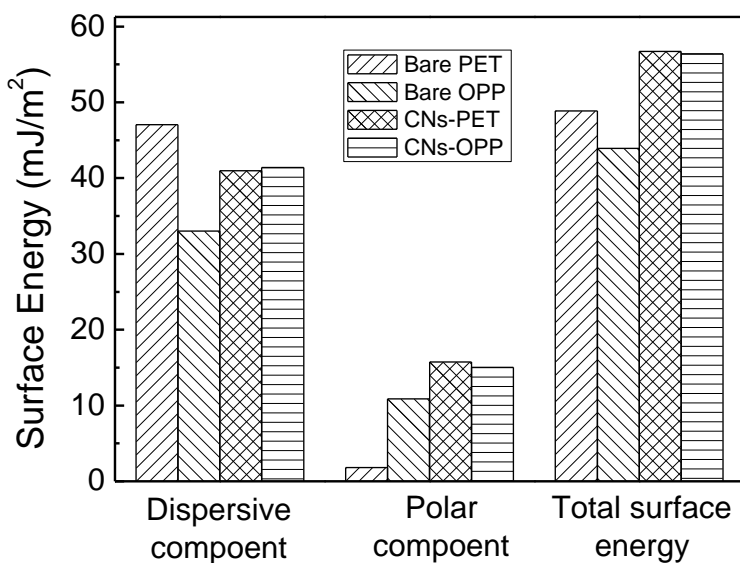
Films	Advancing CA ^a		
	$\theta_{\text{Water}}(^{\circ})$	$\theta_{\text{Water}}(^{\circ})^{\text{b}}$	$\theta_{\text{Water}}(^{\circ})^{\text{b}}$
Bare PET	72.57±2.96	72.57±2.96	72.57±2.96
Bare OPP	90.06±1.84	90.06±1.84	90.06±1.84
CNs-PET	26.29±3.27	26.29±3.27	26.29±3.27
CNs-OPP	27.33±3.07	27.33±3.07	27.33±3.07

^a static contact angle values recorded at 60th second

^b Diiodomethane, DIM and formamide, FOM

We did static and dynamic (advancing) contact angle measurements specifically on PET and OPP which have different wettability and are the most widely used in food packaging field. From Table 9a, we could notice that the CNs-coating showed highly similar static contact angles, which indicates that the completely new CNs layer was established through cast coating process. Moreover, the static contact angles of CNs coated substrates presented much lower than the ones of bare substrates, since cellulose chains are full of hydroxyl (-OH) groups leading to very hydrophilic.

We will use advancing contact angles (shown in Table 9b) of CNs coating to interpret the principles behind the anti-fog performance. It was reported that one possible measure of the level of interaction of water with a material is the advancing contact angle and it has been suggested that hydrophilic surfaces with values less than 40° should exhibit anti-fog behavior (Briscoe & Galvin, 1991; Howarter & Youngblood, 2008). The advancing contact angle value (θ_{Water}) of CNs-coated films is around 26.5° , which is much lower the 40° thereby leads to excellent anti-fog performance.



(a)

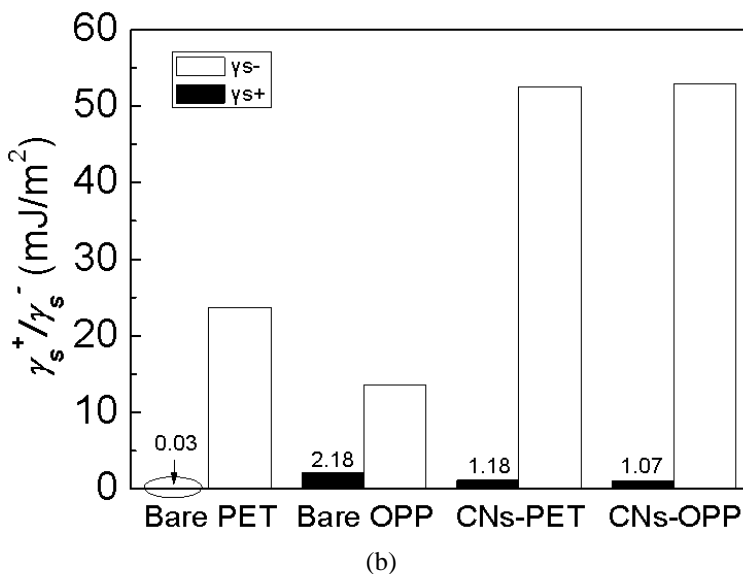


Figure 23 Surface energies and their respective polar and dispersive components of bare and CNs-coated PET and OPP, (a); the electron-acceptor and donor of polar component, (b)

To further interpret the anti-fog behavior, we calculated the surface energies values from static contact angles, which were presented in the Figure 23. Contact angles were measured by using water, FOM, and DIM to provide information regarding the contributions of dispersive (D) and polar (P) components to the total surface energy of the substrates. The calculated values in Figure 23 show that the dispersive part of the cellulose surface energy is larger than the polar contribution, since the surface energy of cellulose determined by contact angle measurements is known to be ~ 55 mJ/m² (Aulin et al., 2009). Also, a surface energy of CNs films on different substrates was reported as high as 65 mJ/m² with $\pm 15\%$ experimental error (Kontturi et al., 2007). These values are consistent with the values obtained in our results of CNs-coated PET and OPP. From Figure 23a, CNs-coated PET and OPP, have the similar surface energies. As the Van Oss method (Van Oss et al., 1989) frequently used to determine surface energies often results in surfaces with basic characteristics or electron-donor properties (Aulin et al., 2009), yet in our case this method discloses that the thin CNs coating could provide an independent and homogeneous basic layer on PET and OPP substrates which did not have significant influences to surface energies of CNs coating. From γ_s^+ and γ_s^- values shown in Figure 23b, we could well interpret different anti-fog performances between bare and coated films. The electron-donor component (γ_s^-) values of coated PET and OPP are at least 2 and 3.8 times of bare ones, while the electron-acceptor component (γ_s^+) have some differences but since the absolute values are small, thus we could consider them similar and also Van Oss (Van Oss, 2006) mentioned that electron-acceptor/electron-donor interactions are essentially asymmetrical in the sense that of a

given polar substrate and the electron-acceptor and donor components are quite different, which suggested normally only one of two parameters has the significant influence to the final performance. Moreover, cellulose always presents polar and hydrophilic surface (Moon et al., 2011) and CNs are grafted with a few sulfate ester groups (-O-SO₃H) due to the sulfuric acid hydrolysis process. These results, therefore, suggest that the anti-fog property induced on the PET and OPP substrates should be attributed to the electron-donor parameter of the polar component. For hydrophilic biopolymers, similar results were also reported (Introzzi et al., 2012; Nuraje et al., 2010).

3.8.5 Barrier properties.

Table 10 OTR and WVTR

Substrates (Thickness)	Status	OTR ^a	WVTR ^b
PET (12 μm)	Bare	97.0±4.2	52.0±0.3
	Coated	7.6±3.0	38.5±0.7
OPP (20 μm)	Bare	2500.0±12.5	8.7±0.0
	Coated	157.0±52.3	5.8±0.2
OPA (12 μm)	Bare	90.0±0.5	1136.0±5.7
	Coated	12.1±5.5	865.0±4.3
Cellophane (12 μm)	Bare	152±0.8	41.0
	Coated	4.4±0.0	41.0

^a cm³ m⁻² day⁻¹, test condition 23 °C 0% RH

^b g day⁻¹ atm⁻¹, test condition 38 °C 90% RH

The Table 10 shows that the barrier properties of coated films improve significantly thanks to the thin (~600 nm) CNs coating. The oxygen transmission rates (OTR) of all samples have been measured and analyzed under the dry condition. PET and OPA are both relatively hydrophilic materials with already good oxygen barrier properties. After coating, their oxygen barrier is significantly improved, with a further reduction of about 90% in OTR value. The cellophane is regenerated from cellulose and could have similar hydrophilic properties. After CNs coating, oxygen resistance increases almost 40-fold and OTR of coated cellophane is reduced to 0.044 cm³ m⁻² 24h⁻¹ kPa⁻¹. Coefficient oxygen permeability (KP_{O₂}) of CNs coating on cellophane is 0.027 cm³ μm m⁻² 24h⁻¹ kPa⁻¹, which is similar with that of EVOH under dry conditions and smaller than that of PVDC (Lee et al., 2008). Such excellent oxygen barrier property of cellophane with CNs coating can be tentatively attributed to the strong hydrogen bonds among CNs and between CNs and cellophane. On the other hand, OPP is a definitely hydrophobic material with low oxygen barrier. CNs deposition on OPP dramatically reduces the oxygen permeability, which isolates ~94% oxygen compared to the bare OPP.

The water vapor transmission rate (WVTR) of CNs is limited by their hydrophilicity (Moon et al., 2011). Nevertheless, the WVTR of CNs-coated PET, OPP and OPA films is reduced by 26%, 33%, and 24% respectively under 38 °C and 90% RH conditions, compared to bare films. It is obvious that CNs obtained from cotton linters are hydrophilic and could absorb certain amount of water vapor during the measurements, leading to reduction of WVTR, which were also reported in other literatures (Fukuzumi et al., 2012; Hult et al., 2010; Sanchez-Garcia et al., 2010). On the other hand, bare and coated cellophane films have the same WVTR values because of both originate from cellulose.

Thus, thin CNs coating improves the oxygen and water vapor barrier properties of conventional flexible food packaging. In another words, substitution of conventional plastics is difficult because of the cost, flexibility, availability and etc. But at least, CNs coated thin plastic films might be partially instead of the thicker ones, thereby, save the plastic and make our food packaging more friendly-environmental and sustainable. In this work, the OTR values were measured only under the dry condition and obtained relatively good performance. Since CNs is hydrophilic biopolymer, we suppose that the oxygen barrier will be reduced under high RH as other reports by the form of coating or filler on to in other polymers (Fukuzumi et al., 2011; Kato et al., 2005). The CNs, however, has the highest crystallinity (~85-87%) compared with MFC, MFC/PEI LbL coatings (Aulin et al., 2009) and TEMPO-oxidized cellulose nanofibers (~74%) (Isogai et al., 2011), which might result in relatively better oxygen barrier under the high RH than other form nano-cellulose. This point should be still under the investigation and be proved by more evidence.

3.9 Conclusions 2

In conclusion, we have systematically investigated the properties of conventional films coated with CNs. In particular, we have analyzed their optical properties (transparency and haze), mechanical properties (static and dynamic coefficient of friction), anti-fog (contact angle and surface energy) and barrier properties (oxygen and water vapor transmission rates). In doing this, we have demonstrated that CNs coatings mainly lead to a reduction of friction, a premium feature for industrial applications, and that their influence on the optical properties of the packaging is not significant. Excellent anti-fog property guarantees customers more convenient to evaluate the product easily. At last but not the least, CNs coatings dramatically not only improve the oxygen barrier properties of conventional flexible food packaging, but also leading to a certain reduction in the water vapor transmission rate. While substitution of conventional plastics might still be far ahead because of the low cost, large flexibility and availability, the perspective use of CNs as multi-functional coatings to favor a reduction of the required thickness for plastic films, towards a more environmentally-friendly and sustainable approach to packaging.

3.10 References

- Angles, M. N., Dufresne, A., 2000, Plasticized starch/tunicin whiskers nanocomposites. 1. Structural analysis. *Macromolecules* 33: 8344-8353.
- Aulin, C. et al., 2009, Nanoscale Cellulose Films with Different Crystallinities and Mesostructures—Their Surface Properties and Interaction with Water. *Langmuir* 25: 7675-7685.
- Auras, R. et al., 2004, An overview of polylactides as packaging materials. *Macromolecular Bioscience* 4: 835-864.
- Avella, M. et al., 2005, Biodegradable starch/clay nanocomposite films for food packaging applications. *Food Chemistry* 93: 467-474.
- Briscoe, B. J., Galvin, K. P., 1991, The effect of surface fog on the transmittance of light. *Solar Energy* 46: 191-197.
- Creatore, M. et al., 2002, Deposition of SiO_x films from hexamethyldisiloxane/oxygen radiofrequency glow discharges: Process optimization by plasma diagnostics. *Plasmas and Polymers* 7: 291-310.
- de Mesquita, J. o. P. et al., 2010, Biobased Nanocomposites from Layer-by-Layer Assembly of Cellulose Nanowhiskers with Chitosan. *Biomacromolecules* 11: 473-480.
- Dong, X. M. et al., 1998, Effect of microcrystallite preparation conditions on the formation of colloid crystals of cellulose. *Cellulose* 5: 19-32.
- Drumright, R. E. et al., 2000, Polylactic acid technology. *Advanced Materials* 12: 1841-1846.
- Elazzouzi-Hafraoui, S. et al., 2007, The Shape and Size Distribution of Crystalline Nanoparticles Prepared by Acid Hydrolysis of Native Cellulose. *Biomacromolecules* 9: 57-65.
- Erlat, A. G. et al., 1999, SiO_x gas barrier coatings on polymer substrates: Morphology and gas transport considerations. *Journal of Physical Chemistry B* 103: 6047-6055.
- Farris, S. et al., 2012, Self-Assembled Pullulan-Silica Oxygen Barrier Hybrid Coatings for Food Packaging Applications. *Journal of Agricultural and Food Chemistry* 60: 782-790.
- Farris, S. et al., 2009, Evaluation of a bio-coating as a solution to improve barrier, friction and optical properties of plastic films. *Packaging Technology and Science* 22: 69-83.
- Fujisawa, S. et al., 2011, Preparation and characterization of TEMPO-oxidized cellulose nanofibril films with free carboxyl groups. *Carbohydrate Polymers* 84: 579-583.
- Fukuzumi, H. et al., 2012, Influence of TEMPO-oxidized cellulose nanofibril length on film properties. <http://dx.doi.org/10.1016/j.carbpol.2012.04.069>.
- Fukuzumi, H. et al., 2011, Pore Size Determination of TEMPO-Oxidized Cellulose Nanofibril Films by Positron Annihilation Lifetime Spectroscopy. *Biomacromolecules* 12: 4057-4062.
- Fukuzumi, H. et al., 2008, Transparent and High Gas Barrier Films of Cellulose Nanofibers Prepared by TEMPO-Mediated Oxidation. *Biomacromolecules* 10: 162-165.
- Ghasemi, H. et al., 2012, Properties of PET/clay nanocomposite films. *Polymer Engineering and Science* 52: 420-430.

- Haas, K. H. et al., 1999, Functionalized coatings based on inorganic-organic polymers (ORMOCER (R) s) and their combination with vapor deposited inorganic thin films. *Surface & Coatings Technology* 111: 72-79.
- Howarter, J. A., Youngblood, J. P., 2008, Self-Cleaning and Next Generation Anti-Fog Surfaces and Coatings. *Macromolecular Rapid Communications* 29: 455-466.
- Hult, E. L. et al., 2010, Efficient approach to high barrier packaging using microfibrillar cellulose and shellac. *Cellulose* 17: 575-586.
- Introzzi, L. et al., 2012, "Wetting Enhancer" Pullulan Coating for Antifog Packaging Applications. *ACS Applied Materials & Interfaces* 4: 3692-3700.
- Isogai, A. et al., 2011, TEMPO-oxidized cellulose nanofibers. *Nanoscale* 3: 71-85.
- Jang, W.-S. et al., 2008, Layer-by-layer assembly of thin film oxygen barrier. *Thin Solid Films* 516: 4819-4825.
- Kato, Y. et al., 2005, Oxygen Permeability and Biodegradability of Polyuronic Acids Prepared from Polysaccharides by TEMPO-Mediated Oxidation. *Journal of Polymers and the Environment* 13: 261-266.
- Kontturi, E. et al., 2007, Cellulose Nanocrystal Submonolayers by Spin Coating. *Langmuir* 23: 9674-9680.
- Krikorian, V., Pochan, D. J., 2003, Poly (L-lactic acid)/layered silicate nanocomposite: Fabrication, characterization, and properties. *Chemistry of Materials* 15: 4317-4324.
- Lee, D. S. et al. *Food Packaging Science and Technology*. CRC Press, 2008, 58-59, 86-93.
- Lim, L. T. et al., 2008, Processing technologies for poly(lactic acid). *Progress in Polymer Science* 33: 820-852.
- Lordan, S. et al., 2011, Cytotoxic effects induced by unmodified and organically modified nanoclays in the human hepatic HepG2 cell line. *Journal of Applied Toxicology* 31: 27-35.
- Mazeau, K., Heux, L., 2003, Molecular Dynamics Simulations of Bulk Native Crystalline and Amorphous Structures of Cellulose. *The Journal of Physical Chemistry B* 107: 2394-2403.
- Moon, R. J. et al., 2011, Cellulose nanomaterials review: structure, properties and nanocomposites. *Chemical Society Reviews* 40: 3941-3994.
- Nuraje, N. et al., 2010, Durable Antifog Films from Layer-by-Layer Molecularly Blended Hydrophilic Polysaccharides. *Langmuir* 27: 782-791.
- Priolo, M. A. et al., 2010, Super Gas Barrier of Transparent Polymer-Clay Multilayer Ultrathin Films. *Nano Letters* 10: 4970-4974.
- Ray, S. S. et al., 2002, Polylactide-layered silicate nanocomposite: A novel biodegradable material. *Nano Letters* 2: 1093-1096.
- Ray, S. S. et al., 2003, New polylactide-layered silicate nanocomposites. 2. Concurrent improvements of material properties, biodegradability and melt rheology. *Polymer* 44: 857-866.
- Sánchez-Valdes, S. et al., 2006, Effect of Ionomeric Compatibilizer on Clay Dispersion in

- Polyethylene/Clay Nanocomposites. *Macromolecular Materials and Engineering* 291: 128-136.
- Sanchez-Garcia, M. D. et al., 2010, Morphology and Water Barrier Properties of Nanobiocomposites of k/i-Hybrid Carrageenan and Cellulose Nanowhiskers. *Journal of Agricultural and Food Chemistry* 58: 12847-12857.
- Siró, I., Plackett, D., 2010, Microfibrillated cellulose and new nanocomposite materials: a review. *Cellulose* 17: 459-494.
- Siro, I., Plackett, D., 2010, Microfibrillated cellulose and new nanocomposite materials: a review. *Cellulose* 17: 459-494.
- Svagan, A. J. et al., 2012, Transparent Films Based on PLA and Montmorillonite with Tunable Oxygen Barrier Properties. *Biomacromolecules* 13: 397-405.
- Tharanathan, R. N., 2003, Biodegradable films and composite coatings: past, present and future. *Trends in Food Science & Technology* 14: 71-78.
- van Oss, C. J., 2003, Long-range and short-range mechanisms of hydrophobic attraction and hydrophilic repulsion in specific and aspecific interactions. *Journal of Molecular Recognition* 16: 177-190.
- Van Oss, C. J. *Interfacial Forces in Aqueous Media*. New York: CRC Press, 2006, pp 18-21 and 89-107.
- Van Oss, C. J. et al., 1989, Estimation of the polar parameters of the surface tension of liquids by contact angle measurements on gels. *Journal of Colloid and Interface Science* 128: 313-319.
- Vert, M. et al., 1995, Present and Future of PLA Polymers. *Journal of Macromolecular Science-Pure and Applied Chemistry* A32: 787-796.
- Yang, Y.-H. et al., 2011, Super Gas Barrier of All-Polymer Multilayer Thin Films. *Macromolecules* 44: 1450-1459.
- Zhang, L., Sun, J., 2010, Layer-by-Layer Codeposition of Polyelectrolyte Complexes and Free Polyelectrolytes for the Fabrication of Polymeric Coatings. *Macromolecules* 43: 2413-2420.

3.11 Topic/theme 3 Tunable Green Oxygen Barrier through Layer by Layer Self-assembly of Chitosan (CS) and Cellulose Nanocrystals (CNs)

Introduction

High gas-barrier materials are urgent and important need for food, drug packaging applications (Cooper et al., 2011; Priolo et al., 2010; Svagan et al., 2012). Particularly, the oxygen permeability of conventional plastic films is not able to meet assurance of the long shelf lives required for a wide variety of foods and expected by the market (Cooper et al., 2011). Facing a tough situation, we simultaneously cannot neglect environmental factors: the food should be effectively protected from oxygen by the films, whilst it is recommended that the barrier materials or coatings should be sustainable and environmentally friendly (Svagan et al., 2012). In other words, the conventional materials could not be completely and immediately substituted by bio-based ones. Thus, the high-barrier coatings are considered as a current key solution to significantly reduce the thickness of conventional materials, thereby, lead to make our present films more environmentally friendly.

Up to now, the main strategies to increase the barrier properties of flexible and transparent materials for food packaging applications have been limited to vacuum metallization, silicon oxide (SiO_x) coatings (Jang et al., 2008; Leterrier, 2003), manufacturing of multi-layers (by co-extrusion and/or laminating) (Affinito et al., 1996), or development of clay-nanocomposites (Chang et al., 2003; Donadi et al., 2011; Ghasemi et al., 2012). However, these solutions do not completely fulfill the sustainability expectations and the needs of transparency, while some technological drawbacks still exist. For instance, SiO_x vapor-deposited thin films are prone to cracking when flexed and show poor adhesion to plastic substrates (Leterrier, 2003); multilayer materials can also present adhesion problems denoting delaminating occurrences; nanoclay-reinforced polymer composites and metallized films suffer from low transparency and relatively high values of the oxygen transmission rate (Osman et al., 2005; Sánchez-Valdes et al., 2006). Also, although the most claimed option to increase gas barrier properties of flexible packaging materials is currently represented by nanoclays inclusions (Jang et al., 2008; Priolo et al., 2010; Svagan et al., 2012), yet it was demonstrated that various nanoclays are highly cytotoxic, posing a possible risk to human health (Lordan et al., 2011). Ideally, a barrier coating made of natural bio-polymers could achieve all the goals of high transparency, low gas permeability, bio-compatibility, sustainability and good adhesion. Layer-by-layer (LbL) assembly is a basic technique for the fabrication of multicomponent films on solid supports by controlled adsorption from solutions or dispersions (Decher, 1997) and is also considered as a good candidate for versatile surface applications including gas barrier coatings (Jang et al., 2008; Priolo et al., 2010; Svagan et al., 2012; Yang et al., 2011), anti-fog and super-hydrophobic

coatings (Nuraje et al., 2010; Zhai et al., 2004; Zhang & Sun, 2010), antimicrobial surfaces (Dvoracek et al., 2009; Etienne et al., 2005), drug delivery (Chung & Rubner, 2002; Kim et al., 2008), and electrically conductive films (Daiko et al., 2008; Park et al., 2010). When a nanofiller needs to be integrated within a polymer matrix in order to provide it with specific novel functionalities, LbL techniques represent a means to avoid aggregation and thus achieve a high level of dispersion and a large filler load.

Since cellulose nanocrystals and chitosan come from the first and second most abundant natural polymers on the earth (de Mesquita et al., 2010), their sustainability seems beyond doubt. Due to its nontoxicity, biodegradability, and anti-microbial properties, chitosan has been widely applied to food packaging and medical fields as a polycationic material (Ravi Kumar, 2000), whilst cellulose nanocrystals recently gained a great attention as optically-transparent reinforcement and barrier coatings (Eichhorn et al., 2010; Kontturi et al., 2007; Sanchez-Garcia et al., 2010) and were found to have neither genotoxicity nor effects on survival and growth of nine aquatic species in the ecotoxicological tests conducted so far (Kovacs et al., 2010). Furthermore, cellulose nanofibers were reported as effective gas barriers, also thanks to their high degree of crystallinity and strong hydrogen bonds: casted coatings based on TEMPO-oxidized cellulose nanofibers (TOCNs) reduced the oxygen permeability (P_{O_2}) of bare poly lactic acid (PLA) and PET films (Fukuzumi et al., 2008; Kato et al., 2005). Recently, well-controlled LbL assembly of CNs/CS multilayers has been proposed as a novel solution to improve the performance of CS coatings by exploiting the large electrostatic interaction and hydrogen bonds with CNs nanofillers (de Mesquita et al., 2010; Qi et al., 2012). At present, however, the barrier properties of such nanocomposites, as well as the influence of pH values on the assembly process, have not yet been fully investigated.

The aim of our work refers to the development of a bio-nanocomposite coating, able to enhance the gas barrier properties of one of the currently most used synthetic plastics, maintaining its intrinsic transparency and reducing the environmental impact of the coated materials, lowering their final thickness. Our goal was also the full comprehension of the mechanism involved in the nanocomposite growth, in order to be able to modulate the final thickness and porosity, leading to a possible design of the barrier properties.

3.12 Materials and methods 3

3.12.1 Materials

Shellfish chitosan (CS, GiustoFaravelli SpA, Milan, Italy) had a degree of deacetylation of 85% and a molecular weight ranging from 50 000 to 60 000 (data provided by the supplier). Cotton linter board, provided by SSCCP (Italian pulp and paper research institute, Milan, Italy), was used for producing cellulose nanocrystals. Amorphous poly(ethylene terephthalate) (A-PET, ~180 μm thick) was used as the plastic substrate for layer-by-layer coating, provided from ILPA srl (Bazzano, Italy). Other reagents were purchased from Sigma-Aldrich, Italy.

3.12.2 Preparation of biopolymer dispersions for layer-by-layer coating

1 wt % chitosan water dispersion was prepared by dissolving the polysaccharide in 0.1 M HCl(aq) at 25 $^{\circ}\text{C}$ for 3 h under stirring. After adjusting pH and filtration, the chitosan dispersion was used for the layer-by-layer coating.

1wt % cellulose nanocrystals (CNs) water dispersion was prepared from cotton linter using a procedure already established for cotton from powdered filter paper (Dong et al., 1996). Briefly, milled cotton linter was hydrolyzed by 64% (wt/wt) sulfuric acid with vigorous stirring at 45 $^{\circ}\text{C}$ for 45 min. The reaction mixture was diluted with 10 times-volume deionized water (18.2 M Ω cm, Millipore Milli-Q Purification System) and settled for 2 h, and then was rinsed and centrifuged at 5000 rpm repeatedly until the supernatant became turbid. Further purification was then done by dialysis against deionized water until the effluent remained at neutral pH (Molecular Weight Cut Off 12 000 and higher). Sequentially, the suspension was sonicated (UP400S 400 W, Hielscher Co., Germany) repeatedly (5 cycles of 10 min at 70% output) to create cellulose crystals of colloidal dimensions. Finally, the suspension was filtered under vacuum with MukteLL (grade GF/C, 1.2 μm) and Whatman glass microfiber filter (grade GF/F, 0.7 μm) to remove contamination and big aggregations. The CNs content of the resulting aqueous suspension was determined by drying several samples (1 ml) at 105 $^{\circ}\text{C}$ for 15 min intervals (to avoid decomposition or burning) until weight constancy, giving a cellulose concentration of ~1 % wt/wt and a yield of ~50%.

3.12.3 Surface charge density measurements

Surface charge densities were measured by means of conductometric titration. For the CNs dispersion, a commercial particle charge detector was used (PCD-04, Müteck, Germany), while for the CS dispersion, the same procedure described by Farris *et al.* (Farris et al., 2012) was employed.

3.12.4 Layer-by-Layer assembly

Glass slides and silicon wafers were used as the substrates for AFM and ellipsometry thickness evaluation, respectively. Firstly, the glass slides or silicon wafer were rinsed and pre-treated into the Piranha solution (96% H_2SO_4 : 30% H_2O_2 = 3:1 (v:v)) to remove the contaminations and generate the negative charge on the surface of glass slides [*Caution! Cleaning solution reacts violently with organic materials and should be handled with extreme caution*]. The coating procedure is as follows: (1) The glass slide or silicon wafer was dipped into the chitosan dispersion for 5 min (for the first bilayer) and 3 min (for other bilayers); (2) The substrates were rinsed in distilled water for 3 min for removing the excess chitosan; (3) The CS coated surfaces were dried by filtered compressed air and dipped into the CNs dispersion for certain time (5 min for the first bilayer and 3 min for other bilayers); (4) The rinsing and drying steps were the same as the one for chitosan. Finally, the different numbers of bilayers were achieved by the recycle of (1)-(4) steps. For the coating on flexible plastic, A-PET films were rinsed with distilled water, methanol, and again distilled water for removing the lipids and other contaminants, dried by filtered air, and submitted to corona treatment (BD-20 high frequency generator, Electro-technic products, Inc., Chicago, IL, USA) to increase the surface energy and generate a negative-charge surface. Sequentially, the coating procedure is the same as the one on glass slides and silicon wafer. All of the samples were stored into desiccators at 0% RH ready for following measurements. The pH of CS or CNs dispersions is presented next to their name in the figures and text. For example, one bilayer of CS (pH = 4)/CNs (pH = 2) is abbreviated as $(\text{CS}_{\text{pH}4}/\text{CN}_{\text{pH}2})_1$.

3.12.5 Transparency measurements

The transmittance of the sample was measured at a wavelength of 550 nm, according to the ASTM D 1746-70, by means of a Perkin-Elmer L650 spectro-photometer.

3.12.6 Fourier transform infrared spectroscopy (FTIR)

FTIR spectra were recorded using a Perkin Elmer instrument (Spectrum 100) equipped with an ATR. Spectra were recorded using a spectral width ranging from 650 to 4000 cm^{-1} , with 4 cm^{-1} resolution and an accumulation of 16 scans.

3.12.7 XPS (X-ray photoelectron spectroscopy)

XPS scans were acquired with a Phoibos 150 hemispherical analyzer at normal emission. X-ray excitation was provided by a twin anode X-ray source operated at 200 W. Mg $K\alpha$ radiation (photon energy: 1253.6 eV) was used. The wide scans were acquired with a pass energy of 50 eV, while detailed scans were acquired with a pass energy of 25 eV.

3.12.8 Atomic Force Microscopy

An atomic force microscope (AFM, AlphaSNOM, WITec GmbH, Germany) was employed both to systematically study the thickness of the deposited multilayers and to analyze their morphology. For thickness measurements, the LbL coating on glass slides was gently scratched in order to expose part of the glass substrate and thus measure the thickness of the coating. Topography images were acquired with soft tapping mode at low oscillation amplitudes, stabilized by an amplitude-modulation feedback system based on the optical lever deflection method. Standard AFM Si probes have been used.

3.12.9 Ellipsometry

The thickness of each layer from 0 to 8 bilayers was also determined by a variable angle spectroscopic ellipsometer (VASE[®] J.A. Woollam Co. Inc., USA) with a wide spectral range capability of 200-1700 nm. In order to provide the system with a standard reference substrate, CS/CNs multilayers were here deposited on a Si wafer. Data were collected at different angles of incidence (60°, 65° and 70°), between 400 and 800 nm. The ellipsometric amplitude ratio, Ψ , and the phase difference, Δ , data were fitted using a Cauchy model for the refractive index of the deposited material, with its given uncertainty based on data reported in the literature (Angles & Dufresne, 2000; Frank et al., 1996; Kasarova et al., 2007; Ligler et al., 2001; Sei-ichi et al., 2001).

In order to increase the fitting accuracy, the Bruggeman model of the effective medium approximation (EMA) layer was employed (Hoeger et al., 2011). This approximation allowed for film thickness analysis by incorporating air as an integral part of the ultrathin film. The positive free parameters of the fitting were the thickness of the deposited layers and their percentage P of air-filled voids. The fitting of the experimental data was performed by minimizing the mean-squared-error defined as

$$MSE = \sqrt{\frac{\sum_{i=1}^N \left[\left(\frac{\Psi_i^{\text{mod}} - \Psi_i^{\text{exp}}}{\sigma_{\Psi,i}^{\text{exp}}} \right)^2 + \left(\frac{\Delta_i^{\text{mod}} - \Delta_i^{\text{exp}}}{\sigma_{\Delta,i}^{\text{exp}}} \right)^2 \right]}{2N - M}}$$

where N is the number of measured Ψ and Δ pairs and M is the total number of model fit parameters.

Since the layer thickness and the material refractive index are expected to be correlated in the fitting procedure, the reported thickness values were found within some uncertainty, which reflects the uncertainty in the material refractive index. However, this uncertainty was found to be lower than 1%, with the exception of thicknesses below about 20 nm (with uncertainty of the

order of few %).

3.12.10 Field-Emission Scanning Electron Microscopy

SEM observation of the film cross-sections was carried out with a Zeiss Sigma field-emission microscope at 5 kV. The samples subjected to the SEM observation were pre-coated with gold using a Polaron E5100 Coater at 18 mA for 20 s.

3.12.11 Oxygen barrier properties

Oxygen permeability measurements of coated A-PET films were performed by OX-TRAN[®] Model 702 (MOCON, USA), complying with ASTM-3985, under the condition of 23 °C and 0% relative humidity (RH). The samples, with a surface of 50 cm², were measured at atmospheric pressure. Each sample was conditioned in the chamber for 24 h, and the oxygen transmission rate (OTR) was measured over 1-2 days until it reached a stable value. The P_{O_2} of the CS/CNs nanocomposite coating in the coated film [i.e., P_{O_2} (Coating)] was calculated using the following equation (Lee et al., 2008):

$$\frac{1}{P_{O_2}(\text{coated A} - \text{PET})} = \frac{1}{P_{O_2}(\text{coating})} + \frac{1}{P_{O_2}(\text{A} - \text{PET})}$$

3.13 Results and discussion 3

3.13.1 Layer-by-layer assembly

We first investigated the layer-by-layer self-assembled growth of the CS/CNs nanocomposite. The growth process and the resulting multilayer structure created by polycationic 1 wt % CS and polyanionic 1 wt % CNs are sketched in Figure 24(a) and 1(b). Scheme Figure 24(a) presents one cycle of layer-by-layer assembly and the numbers of cycles are directly related with the thickness of coating and indirectly correlated to the properties of coated substrates. Figure 24(b) clearly exhibits the CS and CNs layers deposited on substrate. The different layers, however, are not exactly independent and they overlap and attract each other tightly due to the low thickness of each layer and hydrogen bonds and electrostatic interactions between CS and CNs. Also, the thickness of CS is lower than CNs by reason of the big differences of charge density of two polymers. The proportion of CS and CNs-layer thickness in Figure 24(b) does not show the actual situation, just for illustration. In the next section (3.2), we will discuss the interaction between the two polymers at length.

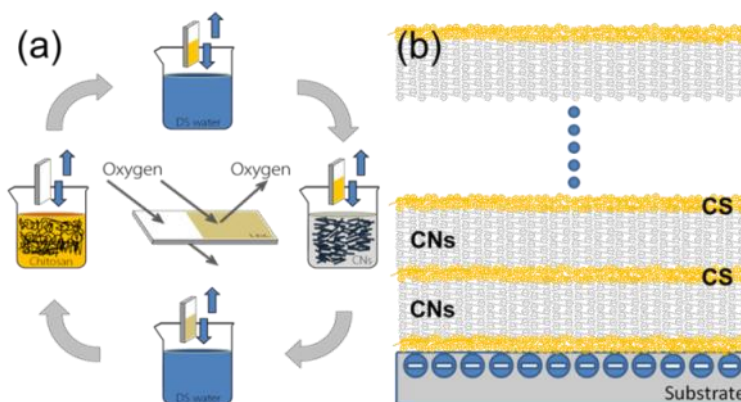


Figure 24 (a) Illustrations of the LbL self-assembly process and (b) the nanostructure constructed by the alternate adsorption of CS (orange) and CNs (gray) onto a substrate.

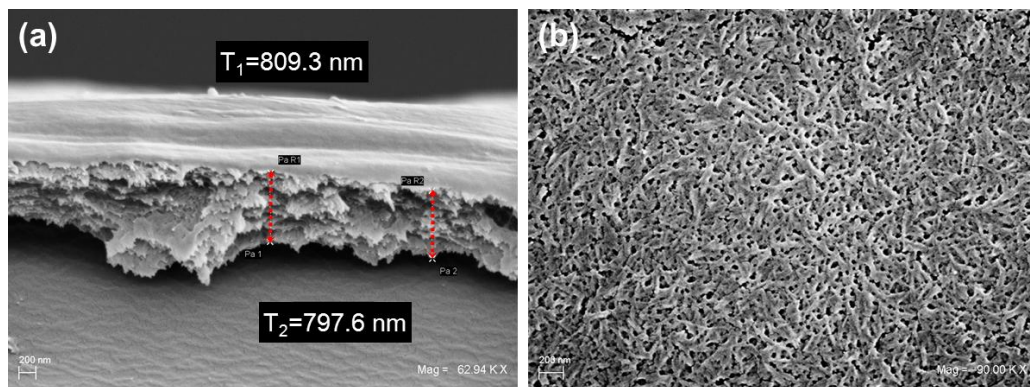


Figure 25 Scanning electron microscopy images of the multilayer cross section and morphology, after cutting it with blade and coating it with a few nm Au layer. The average thickness of the multilayer is about 800 nm.

Hereafter, we will refer to a single CS/CNs assembly as one bilayer. A cross section of the multilayer film, obtained after 30 deposition cycles on an amorphous-polyethylene terephthalate (A-PET) substrate, is presented in Figure 25(a). Multiple-layer structures are clearly observed, confirming that nano-scale layers were established by the LbL assembly. The total thickness of the 30 bilayers CS/CNs coating can be estimated to be ~ 800 nm on average from FE-SEM figure (T_1 and T_2). Owing to the warming phenomena of SEM, the cross section was blend and occasionally not only the cross section of LbL coating but also the planes of inside layers are vividly shown, which ascertain again the overlapped multiple layers. Morphology of 30-bilayer sample is presented in Figure 25(b). Although the Au particles partially cover the real morphology, we still could see CNs network with each other. There are pores on the surface, whereas most of them are closed or blocked by the nether layer, which was also reported in other papers (Siró & Plackett, 2010).

We also measured the optical transparency of the same film at 550 nm, obtaining a transmittance of about 70% (representing a reduction of approximately 13% compared to the bare A-PET substrate). Figure 26 presents high transparency of CS/CNs nanocomposite coating. The boarder of coated and uncoated part is marked by red in Figure 26, from which we could not significantly distinguish the transparency differences by eye inspection.

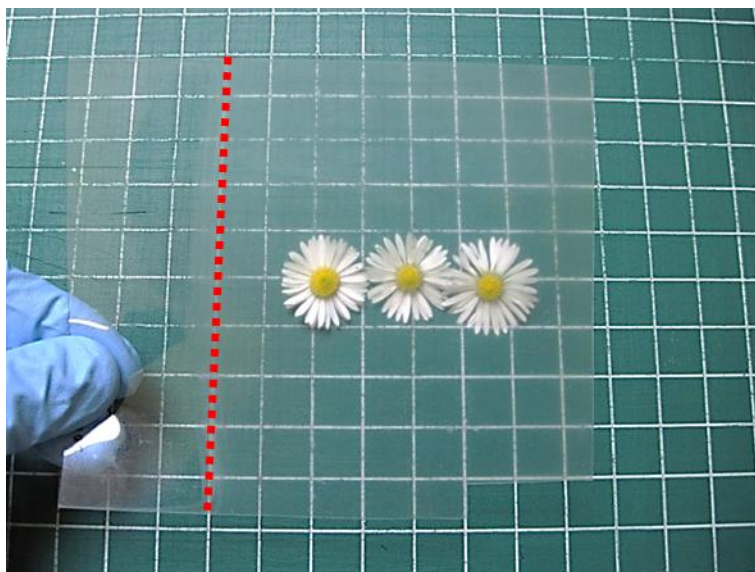
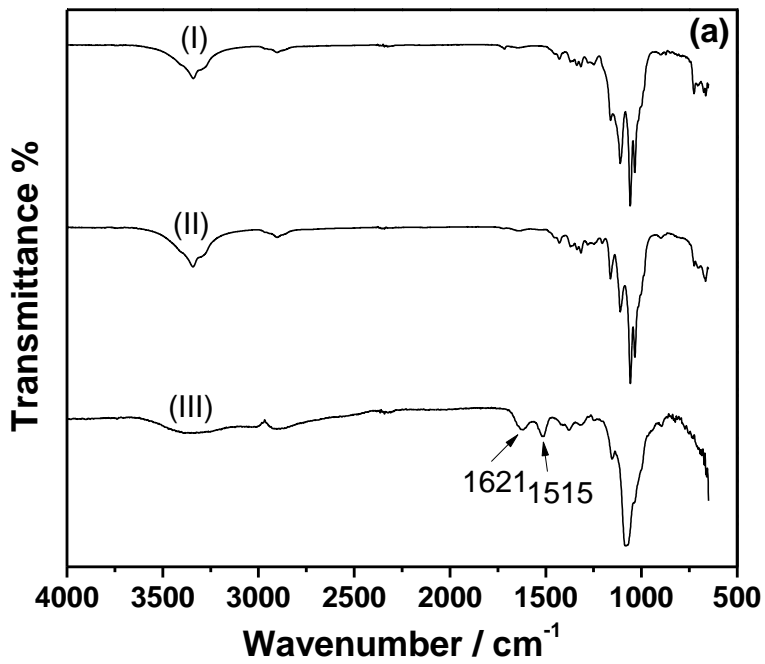


Figure 26 Optical property of coated A-PET.

3.13.2 Structure of CS/CNs nanocomposite

(1) FTIR



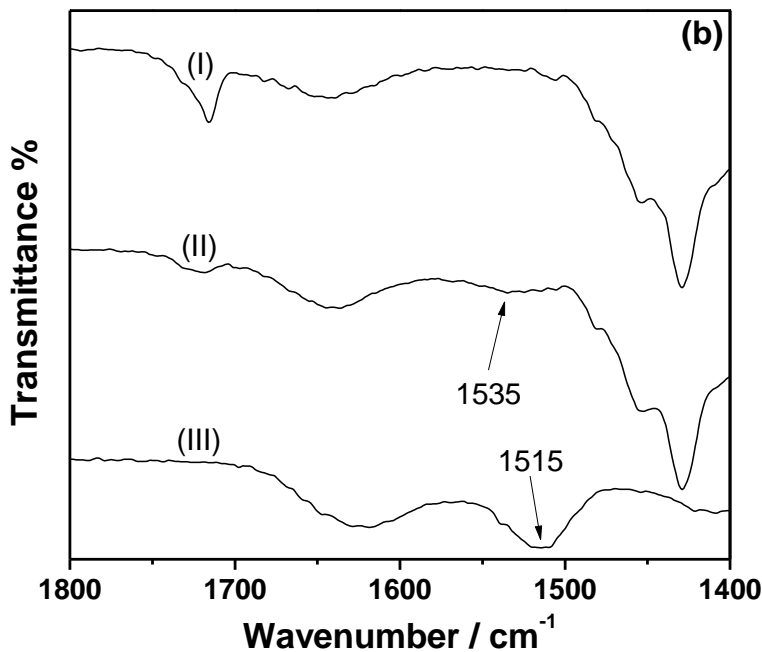


Figure 27 FTIR of pure CNs (I), 30-bilayer CS/CNs nanocomposite (II), and pure chitosan (III). (a) FTIR spectrum from 650 to 4000 cm^{-1} . (b) Close-up of the spectrum showing the displacement of the N-H bending in the nanocomposite from 1515 to 1535 cm^{-1} .

Figure 27 shows the FTIR spectra of cellulose nanocrystals, chitosan, and 30-bilayer CS/CNs nanocomposite. The main bands that appear in the spectrum of chitosan are located around 1621 and 1515 cm^{-1} which is shifted to 1535 cm^{-1} in CS/CNs nanocomposite due to the proportion of amide and amine groups by pH conditions. The first one corresponds to the C=O stretching of acetyl groups and the second one arises from N-H bending vibrations (amide and amine groups). The bands at 1070 and 1030 cm^{-1} are attributed to the C-O stretching vibrations, whereas the broadband at 3200-3450 is assigned to the O-H and N-H stretching. The peaks at 1375 and 1450 cm^{-1} are due to the $-\text{CH}_3$ groups of N-acetylglucosamine residue and $-\text{CH}_2$ groups, respectively (de Mesquita et al., 2010; Li et al., 2009). In pure CNs, the band at 3338 cm^{-1} is attributed to the O-H stretching vibration. The bands at 2902 and 1429 cm^{-1} are characteristic of C-H stretching and bending of $-\text{CH}_2$ groups, respectively, whereas the peaks at 1162 and 1060 cm^{-1} are attributed to the saccharide structure (Li et al., 2009). The sulfate groups were not detected in that the amount of these groups was very small, whereas it was determined by XPS in Table 11. The spectrum of the CS/CNs nanocomposite shows characteristic bands of both materials. The saccharide and the C-H stretching bands could be observed in the spectrum of the nanocomposite film as well as the bands related to C=O stretching and N-H bending. The broadband around 3200-3450 cm^{-1} in the nanocomposite moved slightly and became broader

compared to the spectrum obtained for pure CNs. Zhang et al. (Li et al., 2009) stated that these effects result from the interaction between the negatively charged sulfate ester groups on the CNs surface and the positive charged ammonium groups of chitosan. Besides these interactions, the formation of hydrogen bonds between CNs and chitosan is highly expected given the chemical structure of these polysaccharides.

(2) XPS

Table 11 Concentration of atomic species (in terms of number of atoms) for the CS/CNs nanocomposite, CNs, and CS samples

	O [%]	C [%]	N [%]	S [%]	Cl [%]	Na [%]	F [%]
CS/CNs	28.7±0.2	68.7±0.6	2.2±0.2	0.3±0.1			
CNs	39.1±0.2	59.4±0.4	-	0.6±0.1	~0	~0	0.8±0.1
CS	20.3±0.3	43.6±0.8	5.2±0.3		15.5±0.2	14.8±0.5	0.6±0.1

Table 11 did show peaks related to oxygen, carbon, nitrogen and a faint signal from sulfur for CS/CNs nanocomposite sample, additional peaks related to fluorine and not a nitrogen peak for CNs sample, and peaks related to oxygen, carbon, nitrogen, chlorine, fluorine and sodium for CS sample.

Fluorine, sodium and chlorine did not come from improper handling of the samples during XPS analysis but were already present in the films, which were likely originated from the impurity of reagents.

The nitrogen signal allows us to distinguish between two different situations:

(N₁) nitrogen atoms bonded to one carbon atom (N–C bonds) or in non-protonated amine groups; (N₂) oxidized or protonated nitrogen atoms. The amount of N₁ and N₂ contributions in the two samples containing CS is in the following Table 12:

Table 12 Nitrogen signal features related to different bonds for the CS/CNs nanocomposite and CS samples

	N ₁ [%]	N ₂ [%]
CS/CNs ^a	68±5	32±4
CS	47±5	53±6

^a CS/CNs, CS/CNs nanocomposite

However, these numbers should be considered only as qualitative information, since we have evidence that after long exposure to X-ray, part of the protonated nitrogen (N₂) is converted into

non-protonated (N_1) in Appendix 1 (Chitosan XPS plots comparison between the 30 and 60 min). Interestingly, this change upon irradiation was seen only in CS sample and not in CS/CNs sample (multilayer).

The relative amount of protonated amine groups in the CS/CNs sample is much lower than in the CS reference sample. A possible explanation should be as follows: due to the reduced thickness of the chitosan layer, the process of de-protonation by X-ray is much faster in CS/CNs than in CS sample. On the other side, the percentage of protonated nitrogen groups is much more stable in CS/CNs sample, maybe because linked to the underlying cellulose layer. Considering the CS sample, the oxygen to nitrogen ratio is 4, in perfect agreement with the expectations from the chitosan molecular structure.

Nitrogen peaks.

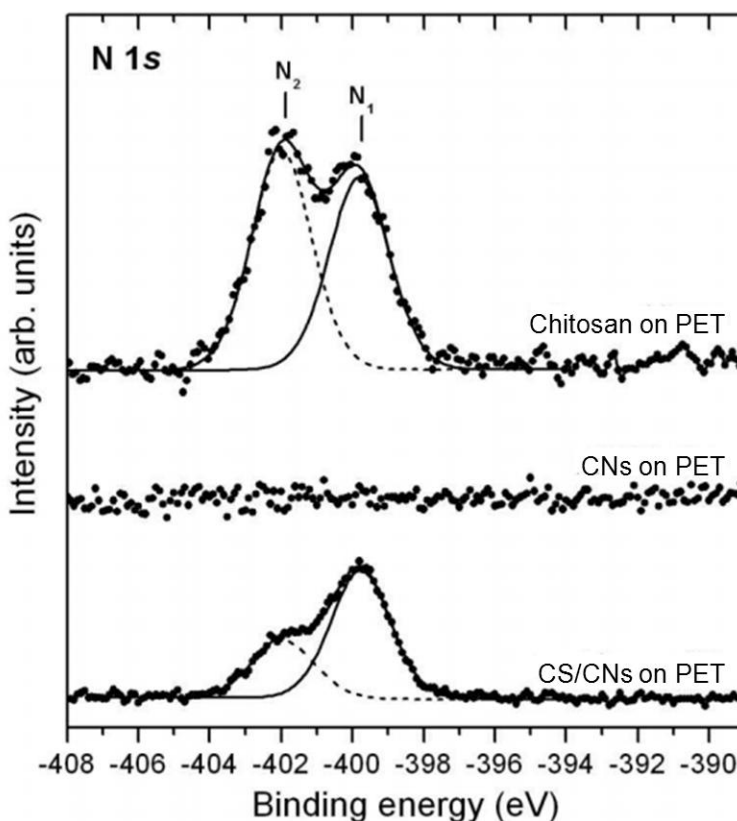


Figure 28 Nitrogen peaks of XPS

The peaks in Figure 28 were decomposed into a sum of Gaussian/Lorentzian lineshapes with the same FWHM. The lineshape used to model the nitrogen peaks is a weighted product of a

Gaussian (70 %) and a Lorentzian (30 %) lineshape. The peak at the lowest (absolute) binding energy, peak N_1 , is associated to photoemission from N 1s orbitals in nitrogen atoms bonded to one carbon atom (N-C bonds) or in non-protonated amine groups (Matienzo & Winnacker, 2002), while peak N_2 is associated to oxidized or protonated nitrogen atoms (Dambies et al., 2000; Matienzo & Winnacker, 2002). The binding energy of N1 electrons is -399.8 ± 0.1 eV, in good agreement with the value reported in the literature (-400.0 eV) (Matienzo & Winnacker, 2002). The chemical shift between peak N_2 and peak N_1 is $\Delta E_{12} = 2.2 \pm 0.2$ eV, in good agreement with the literature ($\Delta E_{12} = 2.1 \pm 0.3$ eV) (Da Róz et al., 2010).

3.13.3 Thickness of CS/CNs nanocomposite coating

Figure 29(a) and (b) show the thickness, obtained by atomic force microscopy (AFM) and ellipsometry, respectively, for films constituted of an increasing number of bilayers and deposited under two different pH conditions (CS_{pH2}/CNS_{pH6}) and (CS_{pH4}/CNS_{pH2}). CS_{pH4}/CNS_{pH2} combination is one of best compromises between the transparency and oxygen barrier, while the pH 4 CS and pH 2 CNs are close to the original pH of two polymers which dissolve in 1 M HCl and water. We chose these two combinations in order to better interpret another method for changing the coating thickness, thereby, manipulating the oxygen barrier properties. The two individual thickness measurements provide accordant results on each measured sample. Notice that the thickness increase is proportional to the nominal number of deposited bilayers, clearly indicating a stable and replicable growth process. Under the (CS_{pH2}/CNS_{pH6}) deposition conditions, an average thickness of ~ 7 nm per bilayer was gained and as shown in Figure 29(a) and 2(b) (empty circles), consistent with previous values reported in the literature for a similar pH combination (de Mesquita et al., 2010). Remarkably, the pH conditions of the employed solutions can be suitably controlled as a means to tune the thickness of the individual layers. Indeed, under the (CS_{pH4}/CNS_{pH2}) conditions, we observe a huge change in the thickness of the individual bilayers, which increases more than 3 times, from ~ 7 up to ~ 26 nm (solid squares). The principle behind the significant thickness differences will be interpreted in the following paragraph.

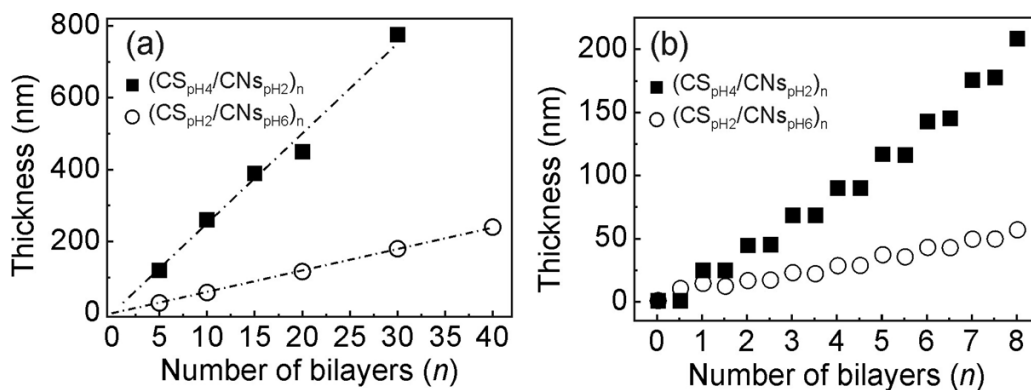


Figure 29 (a) Thickness, obtained from AFM, as a function of the number of CS/CNs bilayers (n) deposited on a glass substrate at two different combinations of pH values: (CS_{pH4}/CNs_{pH2})_n (■) (dashed line: linear fitting with adjusted $R^2=0.996$) and (CS_{pH2}/CNs_{pH6})_n (○) ($R^2=0.999$). (b) Thickness, obtained by ellipsometry, as a function of the number of bilayers (n) deposited on silicon wafer for the same conditions as in panel (a). Non integer values of n represent deposition of CS layers, while integer values are related to CNs deposition.

In order to further investigate the role of charges on the growth process, we measured surface charge density of two polymers by means of conductometric titration at neutral conditions. From such measurements, the amounts of cationic and anionic groups are determined to be about 4600 mmol kg⁻¹ of CS and 220 mmol kg⁻¹ for CNs, respectively, in a good agreement with other report (de Mesquita et al., 2010). In other words, the ratio of $-\text{NH}_3^+$ (from CS) to $-\text{O}-\text{SO}_3^-$ (from CNs hydrolyzed by H₂SO₄) is about 21. A highly different surface charge density leads to large differences in the CS and CNs-layer thickness, as confirmed by Figure 29(b). Combining the evidence of surface charge density with the thickness values obtained for each individual layer by ellipsometry, we conclude that electrostatic interactions are the main driving force in the LbL assembling of CS and CNs and in establishing their thickness. On the other hand, the overcompensation has also to be taken into account as a crucial factor in determining the thickness (Yang et al., 2011), especially under the CS_{pH4}/CNs_{pH2} conditions. In this case, surface charges on the CNs layer (pH 2) are particularly sensitive to local pH (CS pH 4), thus when top CNs layer was dipped into CS solution, the pH of the CS solution makes cellulose segments more charged, which are able to attract more CS molecules than usual. A similar process occurs for the complementary situation as well, when the CS layer (pH 4) is dipped into the CNs solution (pH 2), the pH of CNs makes the CS chains become more charged and attract more CNs. Regarding the original charge density of CS is much higher one of CNs, thus under the local pH effect, a larger number of charged groups induces overcompensation, thereby significantly changing the thickness of deposition.

In CS_{pH2}/CNs_{pH6} system, when the pH value of chitosan is 2, the amino groups on the chitosan chains are more protonated than pH 6. The more protonated amino groups (at pH 2) mean that the chitosan chains are more charged and the repulsions between the chains are stronger, thereby the chains become more rigid, than the ones at pH 6. For CNs, when the pH value is approaching 7 (pH 6), the CNs chains are more charged and rigid than the ones at pH 2. The rigid chains of both chitosan and CNs result in the higher porosity of the films. Meanwhile, if the samples whose top layer is chitosan is dipped into CNs pH 6 solution, the local pH 6 could significantly decrease the charge density of chitosan, which brings on attracting much less CNs, thereby the lower film thickness, vice versa (dipping CNs pH 6 into pH 2 chitosan solution).

Hence, adjusting the pH of two polyelectrolytes solutions or dispersions can tune both the individual thicknesses and the relative proportion of the two biopolymers, thereby influencing the oxygen permeability of LbL coating (Lee et al., 2008; Svagan et al., 2012; Yang et al., 2011). In CS_{pH4}/CNs_{pH2} system, the local pH has more influence on the thickness of CNs due to its much lower charge density. Control over the pH conditions seems, therefore, an easy way to achieve ideal properties (ex. lower permeability) while keeping the number of deposition steps reasonably low.

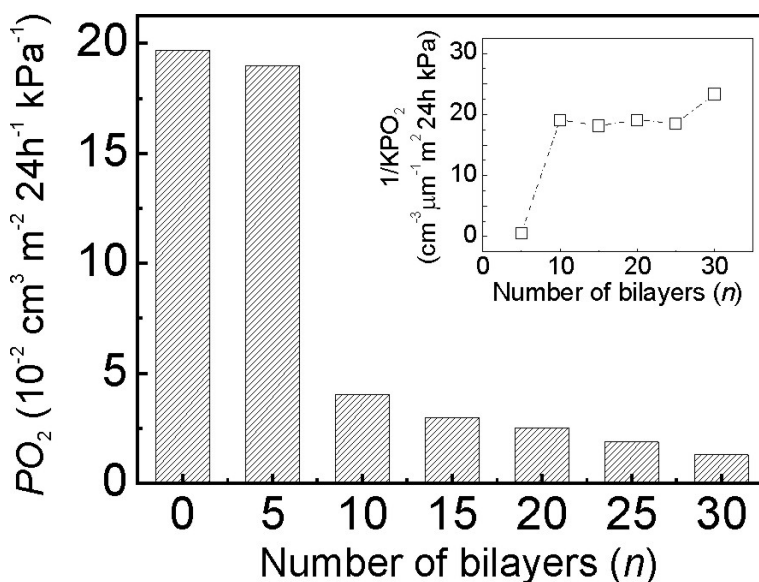


Figure 30 Oxygen permeability (P_{O_2} , $\text{cm}^3 \text{ m}^{-2} \text{ 24h}^{-1} \text{ kPa}^{-1}$) for a $180 \mu\text{m}$ A-PET substrate coated with increasing numbers of $(CS_{pH4}/CNs_{pH2})_n$ bilayers ($n = 0, 5, 10, 15, 20, 25,$ and 30). Inset, reciprocal value of the oxygen permeability coefficient (KP_{O_2}) ($\text{cm}^{-3} \mu\text{m}^{-1} \text{ m}^2 \text{ 24h kPa}$) of the bio-nanocomposite coating only. All of the measurements were performed under ‘dry condition’ (namely, $23 \text{ }^\circ\text{C}$ and 0% RH). For each number of bilayers, two independent samples were prepared and tested, with typical deviation between the two measurements around 20%.

3.13.4 Oxygen permeability of CS/CNs nanocomposite coating

The oxygen permeability of the CS/CNs coating only and those of the coated A-PET are presented in Figure 30 for the (CS_{pH4}/CN_{s_pH2}) condition, according to the number of bilayers (n) which vary from 0 to 30. Following the thickness increase of LbL coating, the oxygen permeability (P_{O_2}) value of coated A-PET is decreasing dramatically. At 30 bilayers, the P_{O_2} value of coated A-PET reduces by ~94%, compared to uncoated A-PET, from about 0.2 down to about $0.013 \text{ cm}^3 \text{ m}^{-2} \text{ 24h}^{-1} \text{ kPa}^{-1}$, as a result of the strong electrostatic interaction and hydrogen bonding between CS and CNs. In order to have the same oxygen permeability, a bare PET should be about 2.7 mm thick. In the inset of Figure 30, the reciprocal value of the oxygen permeability coefficient KP_{O_2} is also reported to highlight the oxygen resistance of the LbL coating only (after subtraction of the PET contribution). It is a remarkable evidence that from 10 to 30 bilayers, i.e. from 260 to 780 nm (thickness of one-side coatings on A-PET), this index remains quite stable, hence KP_{O_2} is approximately constant. We can thus assume that at the testing temperature neither the oxygen diffusion coefficient, nor the oxygen solubility changes in the CS/CNs nanocomposite, which therefore acts as a homogeneous material, independently of the thickness and the number n of bilayers (for $n \geq 10$). (Lee et al., 2008) This is a relevant assessment in order to design LbL self-assembly nanoscale coatings with a specific oxygen permeability and optimized thickness. The most significant decrease of P_{O_2} value is observed from 5 to 10 bilayers, denoting a likely inhomogeneous structure of the LbL coating for the first 5 bilayers: some pores or extremely thin parts might exist, resulting in easier oxygen penetration. In order to test this hypothesis, we studied the sample topography over $(100 \times 100) \mu\text{m}^2$ areas by AFM. Figure 31 shows the topography for the bare A-PET substrate (a) and for the coated substrate with 5 (b), 10 (c), 20 (d), and 30 (e) bilayers. Scratches on the bare A-PET surface are likely caused by the friction between films during the handling, but most parts of the PET are smooth. Noticeably, the overall height excursion of the 5 bilayers topography is comparable with the average thickness of the film, denoting a non-uniform coverage of the substrate by the coating, as can also be clearly seen by simple eye inspection of Figure 31b). For the 10-bilayer coating, on the contrary, a fully covered surface, with many small CS/CNs aggregates, is apparent from the AFM image, in qualitative agreement with the results of the oxygen permeability measurements. For the 20- and 30-bilayer samples deposited under the same conditions, the surface topography is qualitatively similar to the one observed for the 10-bilayer film.

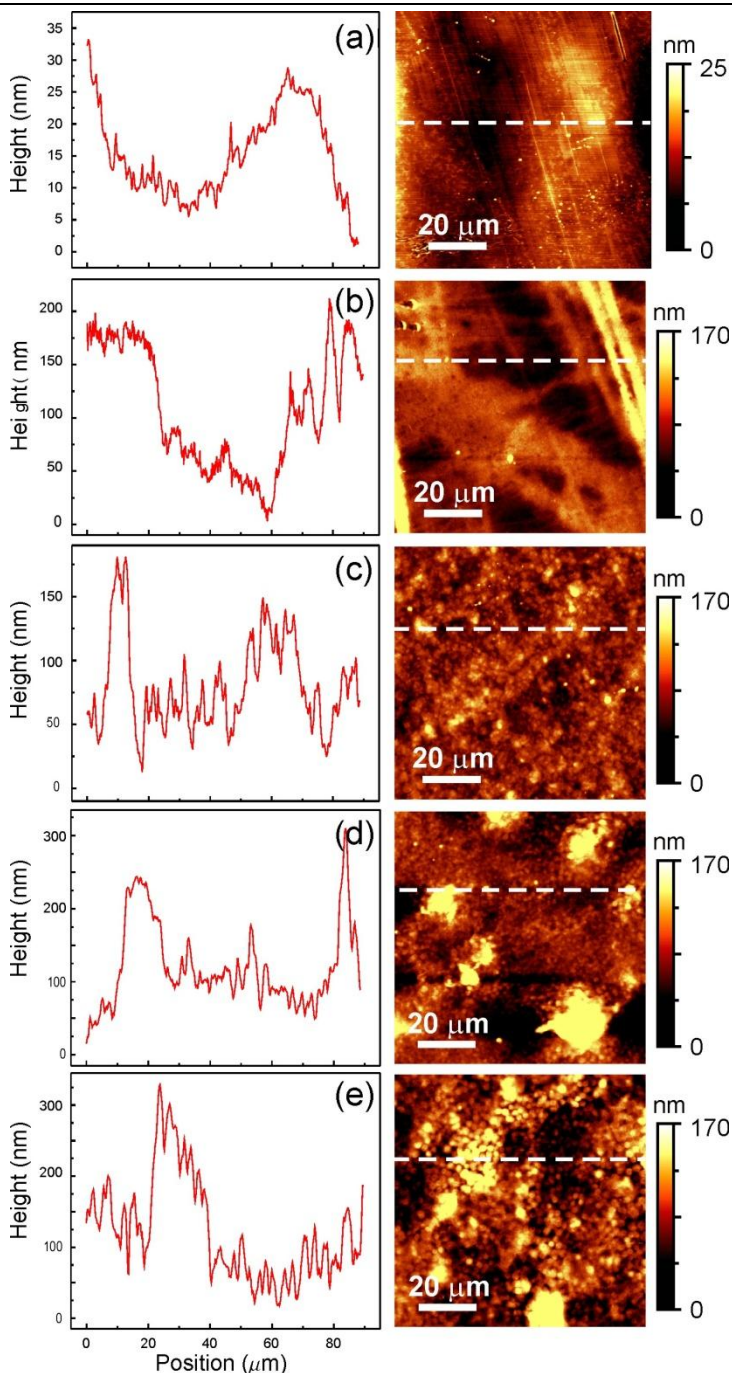


Figure 31 AFM topography images and section lines of a bare A-PET substrate (a), and the same substrate coated with 5 (b), 10 (c), 20 (d), and 30 (e) CS/CNs bilayers. Note the different height scale bars.

The results shown in Figure 32 are also in agreement with the fitting results of the ellipsometry data. Indeed, in order to increase the fitting accuracy, the Bruggeman model of the effective medium approximation was employed (Hoeger et al., 2011). This allowed for the film thickness analysis (see Figure 29) by incorporating air as an integral part of the ultrathin film. For the $(CS_{pH4}/CNs_{pH2})_n$ sample, in particular, we found that the percentage of air voids reduces from 30-40% for the first two bilayers to less than 6% after the fifth bilayer (see Figure 32), denoting an increasing filling of the CS/CNs nanocomposite with increasing thickness. This finding is in good agreement with the oxygen permeability results for the (CS_{pH4}/CNs_{pH2}) sample, which reveal the establishment of good barrier properties only after more than 5 deposited bilayers. Interestingly, similar phenomena have recently been postulated as the reason for the absence of oxygen-barrier properties in a multi-functional LbL coating produced by TEMPO-oxidized cellulose nanofibers and nano-chitin (Qi et al., 2012), where 10 bilayers were deposited with an overall thickness (~ 100 nm) very similar to our 5 bilayers coating. By our analysis, we are, therefore, able to interpret such occurrence by quantifying the pore density by means of ellipsometry measurements. The high porosity of CS_{pH2}/CNs_{pH6} sample is due to the higher rigidity of molecular chains resulting from pH values. According to the ellipsometry results, after 8 deposited bilayers the (CS_{pH2}/CNs_{pH6}) coating was still characterized by more than 15% air voids, which discloses that more LbL cycles are needed to obtain a homogenous nano-coating compared to the (CS_{pH4}/CNs_{pH2}) conditions.

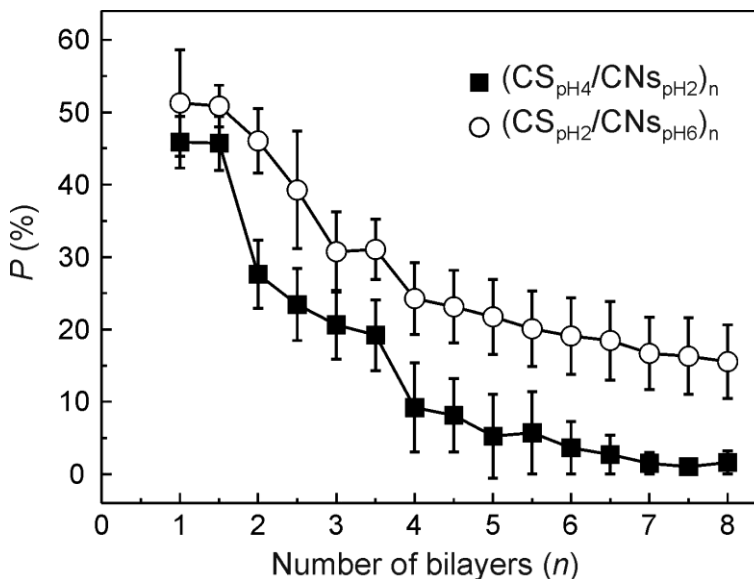


Figure 32 The air void percentage P as a function of the number of bilayers (n), as obtained from the fitting procedure of the ellipsometry data.

In this work, the OTR values were measured only under the dry condition and obtained relatively good performance. Since CS and CNs are both hydrophilic biopolymers, the oxygen barrier will be certainly reduced under high RH. This limitation is common to the currently used synthetic barrier polymers (polyamide (PA), polyvinyl alcohol (PVOH), ethylene vinyl alcohol (EVOH)) and led to the development of multilayer structures, designed in order to protect moisture sensitive polymers with polyolefin such as low-density polyethylene (LDPE), high-density polyethylene (HDPE), and polypropylene (PP).

3.14 Conclusions 3

We demonstrated the use of CS/CNs nanocomposites realized by LbL self-assembly as oxygen barrier under different pH combinations, which has not been systematically reported so far to the best of our knowledge. The oxygen permeability coefficient of CS/CNs nanocomposites is as low as $0.02 \text{ cm}^3 \mu\text{m}^{-2} 24\text{h}^{-1} \text{ kPa}^{-1}$, close to EVOH co-polymers, under dry conditions (Lee et al., 2008). Although the oxygen barrier property of the CS/CNs bio-nanocomposite is still not as outstanding as that of some LbL coatings including inorganic nanoclays (Svagan et al., 2012; Yang et al., 2011), we consider the absence of any potential risks for human beings and the renewable origin of the carbohydrate polymers as significant added values that justify a deeper investigation and exploitation of the LbL process applied to CS/CNs (Kovacs et al., 2010; Lordan et al., 2011). Moreover, the production processes for chitosan and cellulose nanocrystals are both low-energy consuming, especially compared to microfibrillated cellulose (MFC) produced by mechanical processes (Isogai et al., 2011) and the inexpensive use of cotton linters might lead to further promising practical applications. Finally, it deserves to be underlined also the chance of finely tuning the oxygen permeability by means of the pH values and the sharp control of the thickness associated with this process. Therefore, based on the advantages outlined above, the LbL CS/CNs nanocomposite represents a promising oxygen barrier component in transparent flexible packaging materials and semi rigid tridimensional objects (bottles, trays, boxes and etc.).

3.15 References

- Affinito, J. D. et al., 1996, A new method for fabricating transparent barrier layers. *Thin Solid Films* 290–291: 63-67.
- Angles, M. N., Dufresne, A., 2000, Plasticized starch/tunicin whiskers nanocomposites. 1. Structural analysis. *Macromolecules* 33: 8344-8353.
- Chang, J.-H. et al., 2003, Poly(lactic acid) nanocomposites with various organoclays. I. Thermomechanical properties, morphology, and gas permeability. *Journal of Polymer Science Part B: Polymer Physics* 41: 94-103.
- Chung, A. J., Rubner, M. F., 2002, Methods of Loading and Releasing Low Molecular Weight Cationic Molecules in Weak Polyelectrolyte Multilayer Films. *Langmuir* 18: 1176-1183.
- Cooper, M. et al., 2011, Developing the NASA Food System for Long-Duration Missions. *Journal of Food Science* 76: R40-R48.
- Da Róz, A. L. et al., 2010, Adsorption of chitosan on spin-coated cellulose films. *Carbohydrate Polymers* 80: 65-70.
- Daiko, Y. et al., 2008, Proton Conduction in Thickness-Controlled Ultrathin Polycation/Nafion Multilayers Prepared via Layer-by-Layer Assembly. *Chemistry of Materials* 20: 6405-6409.
- Dambies, L. et al., 2000, Characterization of metal ion interactions with chitosan by X-ray photoelectron spectroscopy. *Colloids and Surfaces A: Physicochemical and Engineering Aspects* 177: 203-214.
- de Mesquita, J. P. et al., 2010, Biobased Nanocomposites from Layer-by-Layer Assembly of Cellulose Nanowhiskers with Chitosan. *Biomacromolecules* 11: 473-480.
- Decher, G., 1997, Fuzzy Nanoassemblies: Toward Layered Polymeric Multicomposites. *Science* 277: 1232-1237.
- Donadi, S. et al., 2011, PET/PA Nanocomposite Blends with Improved Gas Barrier Properties: Effect of Processing Conditions. *Journal of Applied Polymer Science* 122: 3290-3297.
- Dong, X. M. et al., 1996, Effects of Ionic Strength on the Isotropic–Chiral Nematic Phase Transition of Suspensions of Cellulose Crystallites. *Langmuir* 12: 2076-2082.
- Dvoracek, C. M. et al., 2009, Antimicrobial Behavior of Polyelectrolyte–Surfactant Thin Film Assemblies. *Langmuir* 25: 10322-10328.
- Eichhorn, S. et al., 2010, Review: current international research into cellulose nanofibres and nanocomposites. *Journal of Materials Science* 45: 1-33.
- Etienne, O. et al., 2005, Antifungal coating by biofunctionalized polyelectrolyte multilayered films. *Biomaterials* 26: 6704-6712.
- Farris, S. et al., 2012, Charge Density Quantification of Polyelectrolyte Polysaccharides by Conductometric Titration: An Analytical Chemistry Experiment. *Journal of Chemical Education* 89: 121-124.
- Frank, C. W. et al., 1996, Structure in Thin and Ultrathin Spin-Cast Polymer Films. *Science* 273:

912-915.

Fukuzumi, H. et al., 2008, Transparent and High Gas Barrier Films of Cellulose Nanofibers Prepared by TEMPO-Mediated Oxidation. *Biomacromolecules* 10: 162-165.

Ghasemi, H. et al., 2012, Properties of PET/clay nanocomposite films. *Polymer Engineering and Science* 52: 420-430.

Hoeger, I. et al., 2011, Ultrathin film coatings of aligned cellulose nanocrystals from a convective-shear assembly system and their surface mechanical properties. *Soft Matter* 7: 1957-1967.

Isogai, A. et al., 2011, TEMPO-oxidized cellulose nanofibers. *Nanoscale* 3: 71-85.

Jang, W.-S. et al., 2008, Layer-by-layer assembly of thin film oxygen barrier. *Thin Solid Films* 516: 4819-4825.

Kasarova, S. N. et al., 2007, Analysis of the dispersion of optical plastic materials. *Optical Materials* 29: 1481-1490.

Kato, Y. et al., 2005, Oxygen Permeability and Biodegradability of Polyuronic Acids Prepared from Polysaccharides by TEMPO-Mediated Oxidation. *Journal of Polymers and the Environment* 13: 261-266.

Kim, B.-S. et al., 2008, Hydrogen-Bonding Layer-by-Layer-Assembled Biodegradable Polymeric Micelles as Drug Delivery Vehicles from Surfaces. *ACS Nano* 2: 386-392.

Kontturi, E. et al., 2007, Cellulose Nanocrystal Submonolayers by Spin Coating. *Langmuir* 23: 9674-9680.

Kovacs, T. et al., 2010, An ecotoxicological characterization of nanocrystalline cellulose (NCC). *Nanotoxicology* 4: 255-270.

Lee, D. S. et al. *Food Packaging Science and Technology*. CRC Press, 2008, 58-59, 86-93.

Leterrier, Y., 2003, Durability of nanosized oxygen-barrier coatings on polymers. *Progress in Materials Science* 48: 1-55.

Li, Q. et al., 2009, Structure and properties of the nanocomposite films of chitosan reinforced with cellulose whiskers. *Journal of Polymer Science Part B: Polymer Physics* 47: 1069-1077.

Ligler, F. S. et al., 2001, Development of Uniform Chitosan Thin-Film Layers on Silicon Chips. *Langmuir* 17: 5082-5084.

Lordan, S. et al., 2011, Cytotoxic effects induced by unmodified and organically modified nanoclays in the human hepatic HepG2 cell line. *Journal of Applied Toxicology* 31: 27-35.

Matienzo, L. J., Winnacker, S. K., 2002, Dry Processes for Surface Modification of a Biopolymer: Chitosan. *Macromolecular Materials and Engineering* 287: 871-880.

Nuraje, N. et al., 2010, Durable Antifog Films from Layer-by-Layer Molecularly Blended Hydrophilic Polysaccharides. *Langmuir* 27: 782-791.

Osman, M. A. et al., 2005, Gas permeation properties of polyethylene-layered silicate nanocomposites. *Journal of Materials Chemistry* 15: 1298-1304.

- Park, Y. T. et al., 2010, High Electrical Conductivity and Transparency in Deoxycholate-Stabilized Carbon Nanotube Thin Films. *The Journal of Physical Chemistry C* 114: 6325-6333.
- Priolo, M. A. et al., 2010, Super Gas Barrier of Transparent Polymer–Clay Multilayer Ultrathin Films. *Nano Letters* 10: 4970-4974.
- Qi, Z.-D. et al., 2012, Multifunctional Coating Films by Layer-by-Layer Deposition of Cellulose and Chitin Nanofibrils. *Biomacromolecules* 13: 553-558.
- Ravi Kumar, M. N. V., 2000, A review of chitin and chitosan applications. *Reactive and Functional Polymers* 46: 1-27.
- Sánchez-Valdes, S. et al., 2006, Effect of Ionomeric Compatibilizer on Clay Dispersion in Polyethylene/Clay Nanocomposites. *Macromolecular Materials and Engineering* 291: 128-136.
- Sanchez-Garcia, M. D. et al., 2010, Natural micro and nanobiocomposites with enhanced barrier properties and novel functionalities for food biopackaging applications. *Trends in Food Science & Technology* 21: 528-536.
- Sei-ichi, M. et al., 2001, Change in Refractive Index of Cellulose Particle with Particle Size. *Bulletin of the Faculty of Human Environmental Science, Fukuoka Women's University* 32: 65-69.
- Siró I., Plackett, D., 2010, Microfibrillated cellulose and new nanocomposite materials: a review. *Cellulose* 17: 459-494.
- Svagan, A. J. et al., 2012, Transparent Films Based on PLA and Montmorillonite with Tunable Oxygen Barrier Properties. *Biomacromolecules* 13: 397-405.
- Yang, Y.-H. et al., 2011, Super Gas Barrier of All-Polymer Multilayer Thin Films. *Macromolecules* 44: 1450-1459.
- Zhai, L. et al., 2004, Stable Superhydrophobic Coatings from Polyelectrolyte Multilayers. *Nano Letters* 4: 1349-1353.
- Zhang, L., Sun, J., 2010, Layer-by-Layer Codeposition of Polyelectrolyte Complexes and Free Polyelectrolytes for the Fabrication of Polymeric Coatings. *Macromolecules* 43: 2413-2420.

APPENDIX I

Gas and water vapor permeability coefficient summary

	KP _{O₂} ^a	Reduction(%)	KP _{H₂O} ^b	Reduction(%)	KP _{N₂} ^a	KP _{CO₂} ^a	References
PLA*	2255±138		1132±9				
PLA (80% RH)	1538±112						(Martinez-Sanz et al., 2012)
1%BCNs FD+PLA	1495±69	34%					
1%BCNs P+PLA (80% RH)	1132±26	26%					
3%BCNs ES			639±4	44%			
A-PET*	36.30						
Coated A-PET	2.34	94%					(Li et al., 2013)
CS/CNs coating	0.02						
Gelation*			5088.00				(George & Siddaramaiah, 2012)
Gelation+4% BCNs			3840.00	25%			
PLA*	305±10		899±156				
PLA/1s-CNs	227±11	26%	596±9	34%			(Fortunati et al., 2012)
PLA/5-CNs	174±14	43%	855±86	4%			
PLA/5s-CNs	158±6	48%	760±112	15%			
CNs	92389±1773				106179±2101	78009±789	(Belbekhouche et al., 2011)
MFC	59±0.7				98±2.6	66±1.3	
Carrageenan*			5927±35				(Sanchez-Garcia et al., 2010)
Carrageenan+3%CNs			1738±320	71%			
MC 0kGy*			6300±200				
MC-50kGy			5800±200				(Khan et al., 2010)
MC-CNs-0kGy			5900±200				
MC-0.25%CNs-50kGy			4200±200	33%			
100% PVOH*			20592				(Paralikara et al., 2008)
10% CNs/10%PAA/80%PVOH			7488	64%			

^a cm³ μm² day⁻¹ kPa⁻¹

^b g μm² day⁻¹ kPa⁻¹

* Controls for reduction calculations

Chitosan XPS plots comparison between the 30 and 60 min

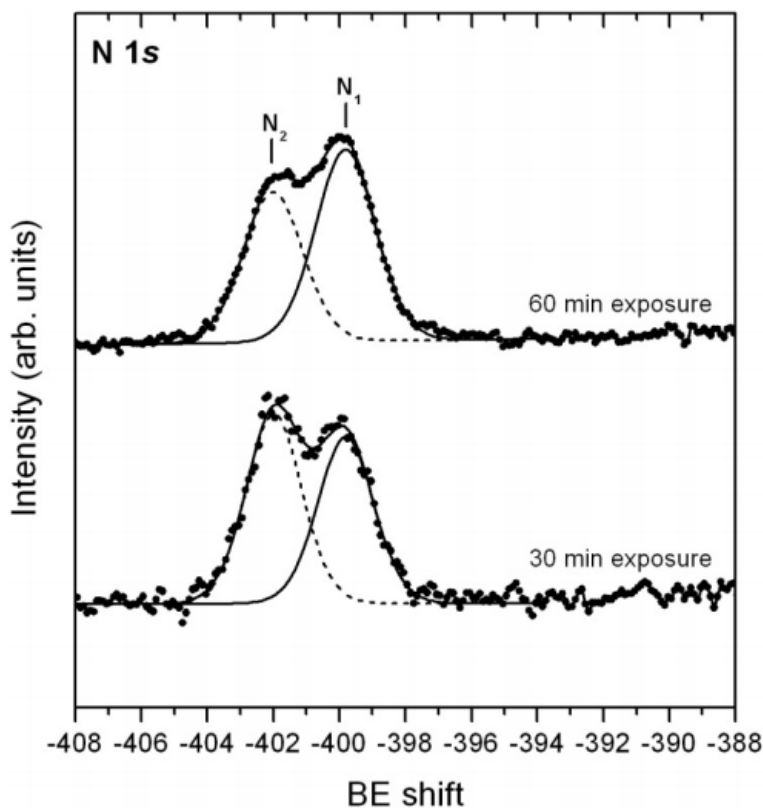


Figure A-1 Chitosan XPS plots comparison between the 30 and 60 min

Table A-2 All analyzed peaks at the two exposures time (30 and 60 min)

Atoms	C 1s [%]					O 1s [%]				N 1s [%]		
	Conc.	C ₁	C ₂	C ₃	C ₄	Conc.	O ₁	O ₂	O ₃	Conc.	N ₁	N ₂
30 min	64±3	10±1	74±2	12±1	3.5±0.5	28.3±0.4	9.7±0.5	88±2	2.6±0.4	7±1	47±6	53±6
60 min	67±3	11±1	72±3	13±1	3.5±0.5	27.7±0.4	9.5±0.7	88±3	2±1	7±1	53±4	47±3.5

The column ‘concentration’ refers to the atomic concentration of the selected element, calculated on the basis of the detailed scans and with the same relative sensitivity factors of those used in Table A-2. The results are normalized only to the signal from oxygen, carbon and nitrogen, and the agreement with the results of Table 11 is good, once the signal from contaminants is discounted. There are no variations in the carbon and oxygen peaks, and also the concentration of nitrogen in the sample does not change with the increase of X-ray exposure. Parts of the protonated or oxidized nitrogen are converted into not protonated, or not oxidized

form.

References

- Belbekhouche, S. et al., 2011, Water sorption behavior and gas barrier properties of cellulose whiskers and microfibrils films. *Carbohydrate Polymers* 83: 1740-1748.
- Fortunati, E. et al., 2012, Effects of modified cellulose nanocrystals on the barrier and migration properties of PLA nano-biocomposites. *Carbohydrate Polymers* 90: 948-956.
- George, J., Siddaramaiah, 2012, High performance edible nanocomposite films containing bacterial cellulose nanocrystals. *Carbohydrate Polymers* 87: 2031-2037.
- Khan, R. A. et al., 2010, Production and Properties of Nanocellulose-Reinforced Methylcellulose-Based Biodegradable Films. *Journal of Agricultural and Food Chemistry* 58: 7878-7885.
- Li, F. et al., 2013, Tunable green oxygen barrier through layer-by-layer self-assembly of chitosan and cellulose nanocrystals. *Carbohydrate Polymers* 92: 2128-2134.
- Martinez-Sanz, M. et al., 2012, On the Optimization of the Dispersion of Unmodified Bacterial Cellulose Nanowhiskers into Polylactide Via Melt Compounding to Significantly Enhance Barrier and Mechanical Properties. *Biomacromolecules*.
- Paralikara, S. A. et al., 2008, Poly(vinyl alcohol)/cellulose nanocrystal barrier membranes. *Journal of Membrane Science* 320: 248-258.
- Sanchez-Garcia, M. D. et al., 2010, Morphology and Water Barrier Properties of Nanobiocomposites of k/i-Hybrid Carrageenan and Cellulose Nanowhiskers. *Journal of Agricultural and Food Chemistry* 58: 12847-12857.

APPENDIX 2

Copies of Extended abstract of papers

Publications

1. Journal: Electroanalysis

Title: Carbon Nanotube-Adsorbed Electrospun Nanofibrous Membranes as Coating for Electrochemical Sensors for Sulfhydryl Compounds Abstract: A new method to modify electrodes with carbon nanotubes (CNT) was developed. Multiwalled carbon nanotubes (MWNT) were adsorbed on the electrospun nylon-6 nanofibrous membranes (Ny-6-NFM) and used as a coating to modify conventional glassy carbon electrodes. The modified electrode was designed for the amperometric detection of sulfhydryl compounds with the potential held at +0.3 V vs. Ag/AgCl. The modified electrode showed a linear response for cysteine up to 0.4 mM ($R^2=0.997$), with a sensitivity of 5.1 mA/mM and a detection limit of 15 mM. Other sulfhydryl compounds showed similar results. After use, the Ny-6-NFM was easily peeled off, leaving the bare electrode surface back to its original electrochemical behavior. This is the first attempt to use a disposable membrane functionalized with MWNT for electroanalytical purposes.

Short Communication**ELECTROANALYSIS****Carbon Nanotube-Adsorbed Electrospun Nanofibrous Membranes as Coating for Electrochemical Sensors for Sulfhydryl Compounds***Fei Li,^a Matteo Scampicchio,^{*b} Saverio Mannino^a*^a Università degli Studi di Milano, Dipartimento di Scienze e Tecnologie Alimentari e Microbiologiche, Via Celoria 2 – 20133 Milano, Italy^b Free University of Bolzano, Faculty of Science and Technology, Piazza Università, 5-39100 Bolzano, Italy
^{*e-mail:} matteo.scampicchio@unibz.it

Received: February 7, 2011

Accepted: March 29, 2011

Abstract

A new method to modify electrodes with carbon nanotubes (CNT) was developed. Multiwalled carbon nanotubes (MWNT) were adsorbed on the electrospun nylon-6 nanofibrous membranes (Ny-6-NFM) and used as a coating to modify conventional glassy carbon electrodes. The modified electrode was designed for the amperometric detection of sulfhydryl compounds with the potential held at +0.3 V vs. Ag/AgCl. The modified electrode showed a linear response for cysteine up to 0.4 mM ($R^2=0.997$), with a sensitivity of 5.1 μ A/mM and a detection limit of 15 μ M. Other sulfhydryl compounds showed similar results. After use, the Ny-6-NFM was easily peeled off, leaving the bare electrode surface back to its original electrochemical behaviour. This is the first attempt to use a disposable membrane functionalized with MWNT for electroanalytical purposes.

Keywords: Cyclic voltammetry (CV), Electrochemistry, Electrospun nanofibrous membranes, Carbon nanotubes (CNT), Sulfhydryl compounds

DOI: 10.1002/elan.201100068

2. Carbohydrate Polymers

Title: Tunable Green Oxygen Barrier through Layer by Layer Self-assembly of Chitosan and Cellulose Nanocrystals

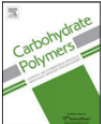
Abstract: We address the oxygen-barrier properties of a nanocomposite created by layer-by-layer assembly of two biopolymers, chitosan (CS) and cellulose, in nanocrystals form (CNs), on an amorphous PET substrate. We systematically investigated the oxygen permeability, morphology, and thickness of the nanocomposite grown under two different pH combinations and with different number of deposition cycles, up to 30 bilayers. Noticeably, the thickness of each deposited bilayer can be largely tuned by the pH value of the solution, from ~7 up to ~26 nm in the tested conditions. By our analysis, it is reliably concluded that such CS/CNs nanocomposite holds promises for gas barrier applications in food and drug packaging as a clear coating on plastic films and tridimensional objects, improving performance and sustainability of the final packages.

Carbohydrate Polymers 92 (2013) 2128–2134

Contents lists available at SciVerse ScienceDirect

Carbohydrate Polymers

journal homepage: www.elsevier.com/locate/carbpol

Tunable green oxygen barrier through layer-by-layer self-assembly of chitosan and cellulose nanocrystals

Fei Li^a, Paolo Biagioni^b, Marco Finazzi^b, Silvia Tavazzi^c, Luciano Piergiovanni^{a,*}

^a DeFENS – Department of Food, Environmental and Nutritional Sciences, Packaging Division, Università degli Studi di Milano, Via Celoria, 2, 20133 Milano, Italy
^b Dipartimento di Fisica and CNISM, Politecnico di Milano, Piazza L. da Vinci, 32, 20133 Milano, Italy
^c Dipartimento di Scienza dei Materiali, Università degli Studi di Milano Bicocca, Via Cozzi, 53, I-20125 Milano, Italy

ARTICLE INFO

Article history:
Received 12 September 2012
Received in revised form 16 November 2012
Accepted 17 November 2012
Available online xxx

Keywords:
Oxygen barrier
Flexible packaging
Layer-by-layer coating
Cellulose nanocrystals
Chitosan
Packaging sustainability

ABSTRACT

We address the oxygen-barrier properties of a nanocomposite created by layer-by-layer assembly of two biopolymers, chitosan (CS) and cellulose, in nanocrystals form (CNs), on an amorphous PET substrate. We systematically investigated the oxygen permeability, morphology, and thickness of the nanocomposite grown under two different pH combinations and with different number of deposition cycles, up to 30 bilayers. Noticeably, the thickness of each deposited bilayer can be largely tuned by the pH value of the solution, from ~7 up to ~26 nm in the tested conditions. By our analysis, it is reliably concluded that such CS/CNs nanocomposite holds promises for gas barrier applications in food and drug packaging as a clear coating on plastic films and tridimensional objects, improving performance and sustainability of the final packages.

© 2012 Elsevier Ltd. All rights reserved.

Posters

1. SLIM 2010 in Zaragoza, Spain (2010)

Title: Moisture effects on water vapor permeability measurements of Polylactide films

Abstract: The moisture barrier properties of polylactide was investigated. The first part of the study focused on the moisture sorption of PLA films. The results showed that it was not linear between the relative humidity (from 10% to 80%) and moisture sorption. The second part of the study investigated the influences of relative humidity on the water vapour transmission rate (WVTR) under the condition of 38 °C by two methods. One was by PLA bags with calcium chloride, another one was using the permeability equipment. According to the results, the WVTR values were linear with relative humidity from 10% to 80% with very high correlation coefficient. Therefore, it concluded that the moisture sorption did not have effect on the WVTR under the different relative humidity.

SLIM (Shelf Life International Meeting)

23rd – 25th June 2010

**PT23 — MOISTURE EFFECTS ON WATER VAPOR PERMEABILITY
MEASUREMENTS OF POLYLACTIDE FILMS**

F. Li, L. Introzzi, S. Farris, L. Piergiovanni

Università degli studi di Milano, Dipartimento di Scienze e Tecnologie Alimentari e Microbiologiche - Packlab, Via
Celoria 2, 20133 Milano – Italia

The water-polymer interactions can affect significantly both the permeability and the mechanical properties of PLA polymers. Even if low amounts of moisture absorbed can be crucial for the general performance of the packaging material, only few investigations have been carried out so far on this topic. The aim of this work was to evaluate the moisture effects on the water vapor transmission rate (WVTR) for a widely used thermo-sealable PLA film. Its moisture sorption was measured at 38 °C, in the range between 11 and 86% of relative humidity and, in the same RH range and at the same temperature, its WVTR was measured using two different methods.

The moisture sorption of the PLA film at 38 °C was quite limited at the lowest RH values (11 – 52%), but increases quickly, reaching the values reported by other Authors (about 6000 ppm), above that range. The amount of water absorbed by PLA film tested, thus, seems strongly affected by the relative humidity of the surrounding environment and the moisture increase is not linearly proportional to the RH values. On the contrary, the values of WVTR obtained both with a gravimetric method and with a isostatic equipment, appear linearly related to the driving force. Therefore, it must be concluded that the different amounts of water absorbed by the PLA film tested at the various relative humidity (demonstrated by the isotherm experiment) do not affect the proportionality of the water transmission to the ΔRH , at least in the RH range considered and at the temperature of 38°C.

2. PhD workshop in Napoli, Italy (2010)

Title: Development of nano-material for food packaging

Abstract: Over the past decades, polymers have replaced conventional materials in packaging applications due to their functionality, lightweight, ease of processing, and low cost. However, despite their huge versatility, a limiting property of these polymers is their inherent permeability to gases and vapors. This has boosted interest in developing new strategies to enhance the general performance and to carry out research aimed to understand the ‘structure-properties’ relationships. The most frequently used strategies to enhance the properties of synthetic polymers are the use of polymer blends, high barrier coatings, and the use of multilayered films. Polymers can also be added with suitable fillers to form composites with enhanced barrier properties. Fibers, platelets and particles have been used to form polymer composites with enhanced mechanical, barrier and thermal properties. Environmental concerns and the need for a sustainable development led to a growing attention towards bio-based materials also in the packaging sector. Hence, the general goal of the project is to achieve better performance of food packaging materials using bio-based nano-materials, mainly obtained from cellulose.

15th Workshop on the *Developments in the Italian PhD Research on Food Science Technology and Biotechnology*,
University of Naples – Federico II, Portici, 15-17 September, 2010

Development of nano-material for food packaging

Fei LI (fei.li@unimi.it)

Department of Food Science, Technology and Microbiology, DiSTAM, University of Milan, Milan, Italy

Tutor: Prof. Luciano Piergiovanni

The aim of this PhD project is to improve the properties of conventional food packaging materials and develop new food packaging concepts. To this purpose, nano-materials as coatings of traditional polymers will be used and composites with nano-materials as functional constituents will be produced, together with the setting up the best technologies to improve the ultimate performance of the package. Particularly, improvement and innovation will be achieved using bio-polymers, especially cellulose, of both bacterial and plant origin. An additional fundamental aim of the research is the understanding of the 'structure→morphology→properties' hierarchical relationship of the obtained nano-materials, in order to control deliberately the ultimate performance.

Studio e sviluppo di nano materiali per migliorare le prestazioni degli imballaggi alimentari

Scopo del presente progetto di dottorato è sviluppare nuovi concetti nel settore dell'imballaggio alimentare, al fine di migliorare le proprietà dei materiali utilizzati nel settore. A questo scopo verranno utilizzati nano-materiali sotto forma di coatings da depositare sui tradizionali polimeri e verranno prodotte strutture composite a base di nano-materiali come costituenti funzionali, contemporaneamente allo sviluppo delle migliori tecnologie per il miglioramento delle performance finali dell'imballaggio. In particolare, miglioramento ed innovazione saranno raggiunti utilizzando bio-polimeri, in particolare cellulosa di origine sia batterica che vegetale. Un ulteriore obiettivo della ricerca è la comprensione della relazione gerarchica 'struttura→morfologia→proprietà' dei nano-materiali ottenuti, allo scopo di poter intervenire deliberatamente nel controllo delle performance finali.

1. State-of-the-Art

Over the past decades, polymers have replaced conventional materials in packaging applications due to their functionality, lightweight, ease of processing, and low cost. Synthetic polymers are world-wide used in food packaging where they provide mechanical, chemical, and microbial protection from the environment and allow product display. Polymers most frequently used in food packaging are polyethylene, polypropylene, polystyrene, polyvinyl chloride, and polyethylene terephthalate (Bureau *et al.*, 1996; Marsh *et al.*, 2007). However, despite their huge versatility, a limiting property of these polymers is their inherent permeability to gases and vapors (e.g. oxygen, carbon dioxide, and organic vapors). This has boosted interest in developing new strategies to enhance the general performance and to carry out research aimed to understand the 'structure-properties' relationship.

The most frequently used strategies to enhance the properties of synthetic polymers are the use of polymer blends, high barrier coatings, and the use of multilayered films. Polymers can also be added with suitable fillers to form composites with enhanced barrier properties (Matthews *et al.*, 1994). Fibers, platelets, and particles have been used for decades to form polymer composites with enhanced mechanical and thermal properties. A recent breakthrough in composite materials is the advancement of nanotechnology. Nanocomposites are materials in which the filler has at least one dimension smaller than 100 nm. Mechanical, thermal, and properties of nanocomposites often differ markedly from those of their component materials. Polymer nanocomposites promise a new crop of stronger, more heat resistant, and high barrier materials (Arora *et al.*, 2010). Moreover, biopolymer nanocomposites from fruit and vegetable purees and cellulose nanofibers (CNF) have been recently studied as film-forming edible materials. Cellulose nanofibers were added to improve tensile properties, water vapor permeability, and glass transition temperature of mango puree films (Azeredo *et al.*, 2009). Environmental concerns and the need for a sustainable development led to a growing attention towards bio-based materials also in the packaging sector. However, biopolymers are exhibit high water vapor permeability and low mechanical properties in comparison with traditional materials. Hence, the general goal of the project: to achieve better performance of food packaging materials using bio-based nanomaterials, mainly obtained from cellulose.

2. PhD Thesis Objectives and Milestones

Within the overall objective mentioned above this PhD thesis project can be subdivided into the following activities according to the Gantt diagram given in Table 1:

- A1) **Determination of the physical and chemical properties of selected biopolymers:**
in the form of nanofibers, including bacterial and wood cellulose nanofibers, obtained by acid hydrolysis or electrospinning under optimized condition (A1.1) and morphology (A1.2).
- A2) **Characterization of plastic films coated with selected nanofibers:** the effects on barrier, optical, surface properties (A2.1), and others (A2.2) of different nanofibers used will be determined.

3. PhD workshop in Lodi, Italy (2011)

Title: Development of nano-material for food packaging

Abstract: The first two activities of the PhD thesis project are described. Firstly, the process of producing cellulose nanocrystals was set up and the morphology of cellulose nanocrystals such as a coating onto a plastic film, were observed by transmission electronic microscopy (TEM) and field-emission scanning electronic microscopy (FE-SEM). Secondly, the coating conditions and properties of cellulose nanocrystals were investigated and optimized by means of an auto-applicator coating device and different techniques of characterization.

16th Workshop on the *Developments in the Italian PhD Research on Food Science Technology and Biotechnology*
University of Milano and Piacenza, Lodi, 21-23 September, 2011

Development of Nano-material for Food Packaging

Fei Li (fei.li@unimi.it)

Dept. Food Science, Technology and Microbiology, DiSTAM, University of Milan, Milan, Italy

Tutor: Prof. Luciano Piergiovanni; Co-tutor: Prof. Saverio Mannino

The first two activities of the PhD thesis project are described. Firstly, the process of producing cellulose nanocrystals was set up and the morphology of cellulose nanocrystals such as a coating onto a plastic film, were observed by transmission electronic microscopy (TEM) and field-emission scanning electronic microscopy (FE-SEM). Secondly, the coating conditions and properties of cellulose nanocrystals were investigated and optimized by means of an auto-applicator coating device and different techniques of characterization.

Studio e sviluppo di nano materiali per migliorare le prestazioni degli imballaggi alimentari

Le prime due attività, previste dal progetto di tesi, sono state condotte nel II anno di Dottorato e vengono qui descritte. Dapprima è stato definito e testato il processo di produzione di nano cristalli di cellulosa e successivamente la loro morfologia, come rivestimento applicato su di un film plastico, è stata osservata con tecniche microscopiche TEM e FE-SEM. In secondo luogo, l'operazione di coating per mezzo di un applicatore automatico ed alcune proprietà fisiche del rivestimento sono state indagate ed ottimizzate.

Key words: Cellulose nanocrystals (CNs), coating, field emission scanning electronic microscope (FE-SEM)

4. MATBIM in Dijon, France (2012)

Titile: Cellulose nanocrystals coating to improve the properties of flexible films for food packaging applications

Abstract: The use of synthetic polymers is common in food packaging applications because they are able to provide mechanical, chemical, and microbial food protection from the environment and good products display. However, despite their enormous versatility, it is not always easy to match the overall needs of a product with the specific properties of the flexible packaging materials available. In the recent years, in particular, the expectations for more sustainable packaging raised significantly. The strategies most frequently used to achieve the required properties for a final flexible packaging material are the application of synthetic coatings, the use of multilayered films, or the blending of polymers with suitable fillers or additives. In this context, the use of nanocomposites or nanostructured materials, promises a new crop of stronger, more heat resistant, and high barrier materials. Among the various nanostructures recently developed for practical applications like hybrid organic-inorganic systems, cellulose nanocrystals (CNs) are promising solutions used in combination with different polymers due to their unique characteristics such as broad availability, low cost, biodegradability, high stiffness and low density. Therefore, the general goal of our work is to use cellulose nanocrystals as coating of common plastic films to modulate and improve their original properties by means of a real sustainable approach.

**Cellulose nanocrystals coating to improve the properties of flexible films
for food packaging applications**

F. LI^a, E. Mascheroni^a and L. Piergiovanni^a

^aDISTAM, Dipartimento di Scienze e Tecnologie Alimentari e Microbiologiche, University of Milan,
via Celoria 2, 20133 Milan, Italy

Introduction

The use of synthetic polymers is common in food packaging applications because they are able to provide mechanical, chemical, and microbial food protection from the environment and good products display. However, despite their enormous versatility, it is not always easy to match the overall needs of a product with the specific properties of the flexible packaging materials available. In the recent years, in particular, the expectations for more sustainable packaging raised significantly^[1].

The strategies most frequently used to achieve the required properties for a final flexible packaging material are the application of synthetic coatings, the use of multilayered films, or the blending of polymers with suitable fillers or additives. In this context, the use of nanocomposites or nanostructured materials, promises a new crop of stronger, more heat resistant, and high barrier materials^[2]. Among the various nanostructures recently developed for practical applications like hybrid organic-inorganic systems^[3-4], cellulose nanocrystals (CNs) are promising solutions used in combination with different polymers due to their unique characteristics such as broad availability, low cost, biodegradability, high stiffness and low density^[5-7].

Therefore, the general goal of our work is to use cellulose nanocrystals as coating of common plastic films to modulate and improve their original properties by means of a real sustainable approach.

5. SLIM 2012 in Changwon, Korea (2012)

Title: Green oxygen barrier of self-assembled bionanocomposites

Abstract: Layer-by-layer (LbL) assembly is commonly used in different research, especially for nano-scale multiple layers on different substrates applied into various fields. Generally speaking, the steps of LbL coating are polycation deposition, rising, drying, other polyanion deposition, and repeated until obtaining the desired thickness and properties.

SLIM (Shelf Life International Meeting)

30th May–1st June 2012

PN58

**GREEN OXYGEN BARRIER OF SELF-ASSEMBLED
BIO-NANOCOMPOSITES**

Fei Li^a, Paolo Biagioni^b, Luciano Piergiovanni^a

^aDeFENS, Department of Food Environmental and Nutritional Sciences, Università degli Studi di Milano, Italy; ^bPhysics Department, Politecnico di Milano, Italy
E-mail: luciano.piergiovanni@unimi.it

Layer-by-layer (LbL) assembly is commonly used in different research, especially for nano-scale multiple layers on different substrates. Shortly, the steps of LbL assembly are polycation deposition, rising, drying, other polyanion deposition, and repeated layering until obtaining the desirable thickness. In our research, the LbL coating is intended for innovative flexible food packaging, as a sustainable oxygen barrier coating. The cellulose nanocrystals (CNs) and chitosan (CS) were coated on A-PET substrate via electrostatic interaction and strong hydrogen bonding. Cellulose and chitosan are the first and second most abundant natural polymers on the earth, respectively. Due to the nontoxicity and biodegradability, chitosan has been widely applied to food packaging and medical fields, whilst cellulose nanocrystals (CNs) were found to have neither genotoxicity nor effects on survival and growth in the ecotoxicological tests; their use, therefore, is safe and sustainable.

The thickness of 30 bilayers reaches $\sim 775 \pm 14$ nm under pH 4 of CS and pH 2 of CNs as measured by ellipsometry on glass slides. Atomic force microscope phase was used to investigate the roughness of the coating onto A-PET film, which is increasing according to the growth of thickness. Roughness and thickness vary from 2 to 14 nm and from 120 to 775 nm for 10 to 30 bilayers nanocomposites, respectively. The linear increases of thickness and roughness prove that CS/CNs LbL self-assembly system is a stable and replicable process in nano-scale. The oxygen barrier properties of CS/CNs bio-nanocomposites onto 180 μm A-PET are related to the increasing thickness of LbL coating. At 30 bilayers, the OTR value of coated A-PET reduced 94%, comparing to uncoated A-PET: from 20 down to 1.29 $\text{cm}^3 \text{m}^{-2} 24\text{h}^{-1} \text{bar}^{-1}$, due to the strong electrostatic interaction and hydrogen bonding between CS and CNs. The oxygen permeability coefficient of CS/CNs nanocomposites is as low as 4.28 $\text{cm}^3 \mu\text{m m}^{-2} 24\text{h}^{-1} \text{bar}^{-1}$, quite similar to EVOH under dry conditions, and resulted very constant in broad range of thickness. Meanwhile, the processes for producing chitosan and cellulose nanocrystals are low energy-consumption. Therefore, the LbL CS/CNs nanocomposites are suitably used as a green oxygen barrier for food packaging applications.

Keywords: Barrier materials, sustainable packaging, layer-by-layer, cellulose nanocrystals

6. PhD workshop in Cesena, Italy (2012)

Title: Development of nano-material for food packaging

Abstract: The aim of PhD project research is to improve the properties of food packaging materials and develop new food packaging materials. To the purpose, we use nano-materials to improve the characteristics of materials, as well as to produce nanocomposite. Particularly, biopolymer, cellulose nanocrystals (CNs), is considered as the main coating material for improving the gas barrier properties of conventional packaging materials. In order to better understand the relationships between nano-coating and its properties, we investigated the oxygen barrier and mechanical properties, morphology and thickness of nanocomposite through advanced instruments.

17th Workshop on the *Developments in the Italian PhD Research on Food Science Technology and Biotechnology*
Alma Mater Studiorum - University of Bologna, Cesena, 19-21 September, 2012

Development of Nano-Material for Food Packaging

Fei Li (fei.li@unimi.it)

DeFENS - Dept. of Food, Environmental and Nutritional Sciences, University of Milan, Italy
Tutor: Prof. Luciano Piergiovanni; Co-tutor: Prof. Saverio Mannino

The aim of PhD project research is to improve the properties of food packaging materials and develop new food packaging materials. To the purpose, we use nano-materials to improve the characteristics of materials, as well as to produce nanocomposite. Particularly, biopolymer, cellulose nanocrystals (CNs), is considered as the main coating material for improving the gas barrier properties of conventional packaging materials. In order to better understand the relationships between nano-coating and its properties, we investigated the oxygen barrier and mechanical properties, morphology and thickness of nanocomposite through advanced instruments.

Studio e sviluppo di nano materiali per migliorare le prestazioni degli imballaggi alimentari

L'obiettivo fondamentale della tesi di dottorato è quello di migliorare le proprietà funzionali di materiali flessibili per il confezionamento alimentare, attraverso lo sviluppo di soluzioni innovative e sostenibili che impieghino nano strutture di materiali di origine naturale. In particolare sono stati studiati i cristalli di nano cellulosa (CNs) con il fine di ottenere componenti a bassa permeabilità ai gas, da impiegare come lacche a base acquosa da applicare su convenzionali, anche in combinazione con Chitosano (CS). Per comprendere le relazioni tra nano strutture biopolimeriche e caratteristiche funzionali, è stata indagata la morfologia dei rivestimenti e le proprietà meccaniche di barriera.

Key words: Cellulose nanocrystals (CNs), layer-by-layer (LbL) coating, oxygen barrier.